รายงานวิจัยฉบับสมบูรณ์

โครงการ การประดิษฐ์ฟิล์มท่อนาโนคาร์บอนเพื่อใช้เป็นขั้วเก็บประจุไฟฟ้าและขั้วเคาเตอร์ของเซลล์แสงอาทิตย์ชนิดสีย้อมไวแสง

Title: Fabrication of carbon nanotube film for the supercapacitor and dye-sensitized solar cell applications

โดย ดร. สมัคร์ พิมานแพง และคณะ

10 กุมภาพันธ์ 2553

สัญญาเลขที่ MRG5080226

รายงานวิจัยฉบับสมบูรณ์

โครงการ การประดิษฐ์ฟิล์มท่อนาโนคาร์บอนเพื่อใช้เป็นขั้วเก็บประจุไฟฟ้าและขั้วเคาเตอร์ของเซลล์แสงอาทิตย์ชนิดสีย้อมไวแสง

Title: Fabrication of carbon nanotube film for the supercapacitor and dye-sensitized solar cell applications

คณะผู้วิจัย	**สังกัด**
1. ดร.สมัคร์ พิมานแพง	ภาควิชาฟิสิกส์ มหาวิทยาลัยขอนแก่น
2. รศ. ดร.สันติ แม้นสิริ	ภาควิชาฟิสิกส์ มหาวิทยาลัยขอนแก่น
3. รศ. ดร.วิทยา อำมรกิจบำรุง	ภาควิชาฟิสิกส์ มหาวิทยาลัยขอนแก่น

สนับสนุนโดยสำนักงานคณะกรรมการการอุดมศึกษา และสำนักงานกองทุนสนับสนุนการวิจัย
(ความเห็นในรายงานนี้เป็นของผู้วิจัย สกอ. และ สกว. ไมจำเป็นต้องเห็นด้วยเสมอไป)

บทคัดย่อ

ในรายงานนี้แบ่งงานวิจัยออกเป็น 2 เรื่อง คือ ศึกษาค่าการเก็บประจุไฟฟ้าของฟิล์มพอลิอะนิลีนผสมท่อนาโนคาร์บอนและศึกษาประสิทธิภาพของเซลล์แสงอาทิตย์ชนิดสีย้อมไวแสง สำหรับเรื่องที่ 1 ฟิล์มพอลิอะนิลีนผสมท่อนาโนคาร์บอนถูกเตรียมด้วยกัน 3 กระบวนการ คือกระบวนการ electrospinning กระบวนการ electrophoretic และ กระบวนการ slurry paste ผลการทดลองพบว่าเราไม่สามารถเตรียมฟิล์มด้วยวิธี electrospinning เพราะว่าไม่สามารถละลายพอลิอะนิลีนได้ ฟิล์มพอลิอะนิลีนผสมท่อนาโนคาร์บอนที่เตรียมด้วยวิธี electrophoretic นั้นสามารทำการอัดและคายประจุได้เพียงแค่ 10 รอบ แต่ฟิล์มพอลิอะนิลีนผสมท่อนาโนคาร์บอนที่เตรียมด้วยวิธี slurry paste สามารถทำการอัดและคายประจุได้มากกว่า 300 รอบ และค่าเก็บประจุที่ได้ด้วยวิธีนี้สูงกว่าเตรียมด้วยวิธี electrophoretic ฟิล์มที่มีส่วนผสมระหว่างพอลิอะนิลีนและท่อนาโนคาร์บอน 0.2 กรัม และ 0.4 กรัม ตามลำดับ จะให้ค่าเก็บประจุไฟฟ้าสูงสุดประมาณ 50 g/F สำหรับเรื่องที่ 2 เราได้ทำการศึกษา 3 หัวข้อ คือการเตรียมฟิล์มไททาเนียมไดออกไซด์ด้วยวิธี electrophoretic เพื่อใช้เป็นขั้วดูดกลืนแสง การเตรียมฟิล์มท่อนาโนคาร์บอนด้วยวิธี electrophoretic เพื่อใช้เป็นขั้วเคาเตอร์และการเตรียมฟิล์มท่อนาโนคาร์บอนด้วยวิธี slurry paste เพื่อใช้เป็นขั้วเคาเตอร์ ผลการทดลองพบว่าฟิล์มไททาเนียมไดออกไซด์ที่ความหนาประมาณ 14 μm ให้ประสิทธิภาพสูงที่สุดประมาณ 3% ฟิล์มคาร์บอนที่เตรียมด้วยวิธี electrophoretic จะมีแมกนีเซียมผสมด้วยแต่ถ้าแมกนีเซียมมากเกินไปจะส่งผลให้ประสิทธิภาพเซลล์แสงอาทิตย์ลดลง และฟิล์มคาร์บอนที่เตรียมด้วยวิธี slurry paste จะให้ประสิทธิภาพที่สูงกว่าเตรียมด้วยวิธี electrophoretic คิดว่าเกิดจากการที่ท่อนาโนคาร์บอนยึดกับกระจกดีกว่าวิธี electrophoretic

Abstract

In this full reported, we summarized all the work done, which can be divided into two different sections: 1) supercapacitor and 2) dye-sensitized solar cell. First section is about fabricating the composite polyaniline/multiwall carbon nanotube (MWCNT) film and testing its electrocapacitance. Three methods are employed for coating the composite polyaniline/MWCNT film on the stainless steel: 1) the electrospinning, 2) the electrophoretic depsotion (EPD) and 3) the slurry paste. We did not succeed in depositing the composite film by the electrospining. This is due the low dissolve ability of polyaniline. The composite films prepared by the electrophoretic deposition have a short life time only ~10 charge-discharge cycles. Whereas, the slurry paste composite polyaniline/MWCNT film provides the longer charge-discharge cycles (over 300 cycles) and the higher specific capacitance than the EPD method. The 0.4 g CNT + 0.2 g MWCNT film delivers the highest specific capacitance of ~50 F/g. The increase of the specific capacitance with the addition of the polyaniline is attributed to the high redox reaction of polyaniline.

In the second section, we had studied the performance of the dye-sensitized solar cell on three different areas: 1) TiO_2 film prepared by the electrophoretic deposition, 2) carbon film prepared by the electrophoretic deposition and 3) carbon film prepared by the slurry paste. It is found that the optimal TiO_2 thickness prepared by the EPD technique is ~ 14 μm, which delivers the highest energy conversion efficiency ~ 3%. The longer deposition duration of the carbon film by EPD is found to induce more magnesium particles formation on the carbon nanotube film, and the incorporation of magnesium particles is found to degrade the solar cell efficiency. The carbon film prepared by the slurry paste generates higher efficiency than the EPD carbon films. This should be attributed to the carbon film prepared by the slurry pasted is better adhering to the substrate than the EPD method.

Content

Section 1: Electrocapacitance of the multiwall carbon nanotube films

Introduction

The increasing of pollution and decreasing of oil reservation have attracted researchers to find an alternative energy resource, which do not affect and cause the pollution to the environment. Various types of non-polluted energy resources have been considered and tested for the alternative future energy resources such as solar cell, fuel cell. In addition to the energy problem, one associated problem to this is the energy storage device in storing energy for the later used. An example, solar cell can generate energy only in the daytime, but at night, it does not be able to do so. Therefore, it is necessary to store this solar cell energy for the nighttime used. The recent study found that the supercapacitor can store a larger amount of energy and have a longer discharge time than the dielectric capacitor. Thus, the supercapacitor could be one of the possible solutions to the energy storage devices.

As present the amount of the portable devices is kept increasing. The portable devices require a fast charging and high-energy storage device, which can be complement by the supercapacitor. The new development of hybrid automobile, which is a combination of gas and electricity as energy resources, also requires the fast charging and high-energy storage device. Here, with the widely applications of supercapacitor, researchers have explored various ways in improving the supercapacitor capability. It is observed that the increase of the electrode surface area will increase the specific capacitance [1]. Thus, by creating the electrode which have large surface, it should increase the specific capacitance of the electrode. There are many techniques, which are currently used in enhancing the electrode surface. For examples, growing in alumina template, using nanotube or nanoparticle. Many types of materials are been tested as the supercaparitor such as metal oxide (RuO_2), conductive polymers (polyaniline or polypyrrol) or carbon nanotube [2,3,4,5,6,7,8]. Although, the RuO_2 electrode provides the highest specific capacitance as compared to other materials, its production coat is very high. Other materials such as the conductive polymer and carbon nanotube are shown a great potential as the supercapacitor electrode. Thus, in this work, we are interested in fabricating the composite conductive polymer (polyaniline, PANi) and multiwall carbon nanotube film for the supercapacitor electrode.

There are many methods in preparing the composite polyaniline/carbon nanotube film such as polymerization of PANi on carbon nanotube, electrodeposition of PANi on carbon, electrohoretic deposition [9,10,11,12]. Here, in this report, we investigated three different techniques in fabricating the composite carbon nanotube/polyaniline film: 1) electrospinning, 2) electrophoretic deposition and 3) slurry pasted. In addition to the fabricating capacitor electrode, we had also built the simple capacitance tester in roughly analyzing the electrode capacitance.

ลูกลบ: 1
ลูกลบ: 2
ลูกลบ: 3
ลูกลบ: 4
ลูกลบ: 5
ลูกลบ: 6
ลูกลบ: 7
ลูกลบ: 8
ลูกลบ: 9
ลูกลบ: 10
ลูกลบ: 11
ลูกลบ: 12

Results and discussion

1) Design a simple capacitance tester (a constant current charge-discharge measurement)

We had built a simple charge-discharge system for estimating the film capacitance. The reason that we had to build this charge-discharge system because

AUTOLAB system is at another university, which is far from Khon Kaen University so it will save our time and money in roughly analyzing the film capacitance. The simple charge-discharge system is illustrated in Fig. 1. Briefly description of this setup is that an interested capacitor is connected to a resistor and a variable voltage supplier. The output voltage will be supplied from a national instrument (NI) card, which is controlled by a homemade program writing with VB 6. During the charge-discharge measurement, the voltage over the resistor (R) and the capacitor are measured. The voltage over R is used to calculate the current flow through the system. Since R and C are connected in series so that the current flow through R and C is equal. During the charging process, the output voltage from the supplier will continually increase in keeping a constant current flow through R and C. Whereas, during the discharge process, the output voltage from the supplier continually reduces in maintaining the constant discharge current through the capacitor.

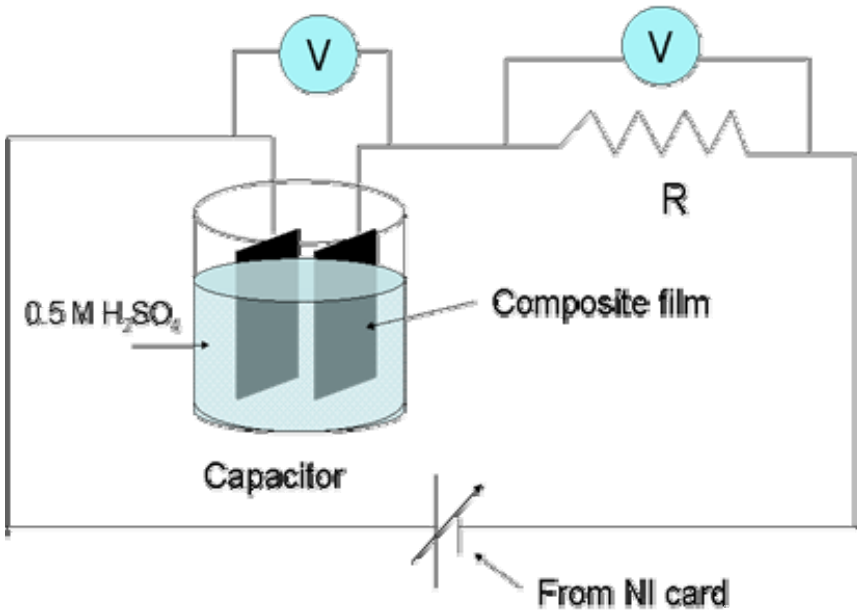

Fig. 1: The schematic of the charge-discharge setup.

2) Fabrication of polyaniline nanofiber

We tried to fabricate the polyaniline nanofibers. However, we did not success in forming the polyaniline nanofibers. We obtained the discontinuous droplet rather than a continuous nanofiber. This believes to be due to a non-well dispersion of polyaniline in solvent (chloroform). We had used the polyaniline emerald base M_w ~5000 and M_w ~300,000 dissolved in chloroform at the polyaniline solution at 1 wt%, 5 wt% and 10 wt% in chloroform, but none of them were able to form fiber.

After the more literature review, we found that the way in generating polyaniline nanofiber have two possible approaches. The first way is by using the easy spun polymer solution such as polystyrene as the main polymer with a small

addition of polyaniline. By this method, the percentage of polystyrene was found to be much greater than polyaniline in order to be able to spin as nanofibers. The large addition of a non-conductive polymer would reduce the film conductivity and lower the electrode specific capacitance. Therefore, the addition of non-conductive polymer may not be a good choice for fabricating the supercapacitor electrode. The second method is by using a highly concentrated H_2SO_4 acid as a polyaniline solvent because polyaniline dissolves well in the high concentrated acid. However, to spin the polyaniline nanofibers from the highly concentrated H_2SO_4 acid solution is a dangerous task, and it may cause the damage to the electrospinning system. Thus, we decided not to continue fabricating the capacitor electrode by electrospinning. We switched to the new method, which is the electrophoretic deposition (EPD).

2) Fabrication of polyaniline/multiwall carbon nanotubes by electrophoretic deposition (EPD)

The EPD setup consists of 1) a conductive substrate, 2) a solution, 3) a counter electrode and 4) power supplied as shown in Fig. 2. The electrophoretic deposition uses an electric field to attract a charged particle from solution to a conductive substrate. Thus, in order to deposit polyaniline and mulltiwall carbon nanotubes (MWCNTs) on the substrate by this EPD technique, the interested particle surfaces must compose of either negative or positive charges. A negative charge can be introduced to MWCNTs surface by an acid modification. To modify carbon nanotubes, MWCNTs will be dipped in the mixed H_2SO_4:H_2NO_3 at ratio volume ratio of 3:1 for 30 min. Then, MWCNTs are filtered and rinsed with DI water for removing acid of the nanotube surface.

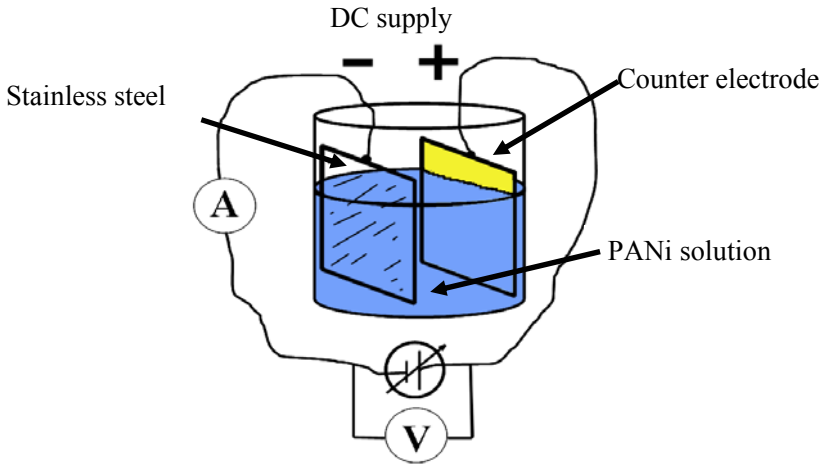

Fig. 2: The schematic of the electrophoretic deposition setup.

After the surface modification process, carboxylic group forms on the CNTs surface. This carboxylic group exhibits a small negative charge, but it is not that strong. Thus, we adding $Mg(NO_3)_2 \cdot 6H_2O$ into the CNTs solution (methanol as solvent) to increase the charge strength. The Mg^{2+} will surround carboxylic groups and enlarge the CNTs charge strength. After the addition of $Mg(NO_3)_2 \cdot 6H_2O$, a lot of

CNTs are deposited on the negative electrode (stainless steel type 304). Since polyaniline exhibits a small positive charge so polyaniline should be attracted to the CNTs carboxylic groups or Mg^{2+}, and be deposited on the stainless steel with CNTs during EPD process. Therefore, by this EPD method, we obtained a composite polyaniline/carbon nanotube film coated on the stainless steel.

The capacitance of the polyaniline/MWCNT films is tested by the cyclic voltamogram (CV) and the constant current charge-discharge measurement. The cyclic voltamogram result is shown in Fig. 3 and the constant charge-discharge result is shown in Fig. 4. The CV and charge-discharge results show that this composite film (polyaniline/MWCNT) could store energy. But, the CV and charge-discharge results show a non-ideal supercapacitor behavior. For the ideal supercapacitor, the CV curve should exhibit a square like shape, and the charge-discharge curve should be a triangle. The non-ideal behavior should be due to a high contact resistance between a polyaniline/carbon nanotube and a stainless steel surface, i.e. the polyaniline/carbon nanotube film is not well attached to the stainless steel

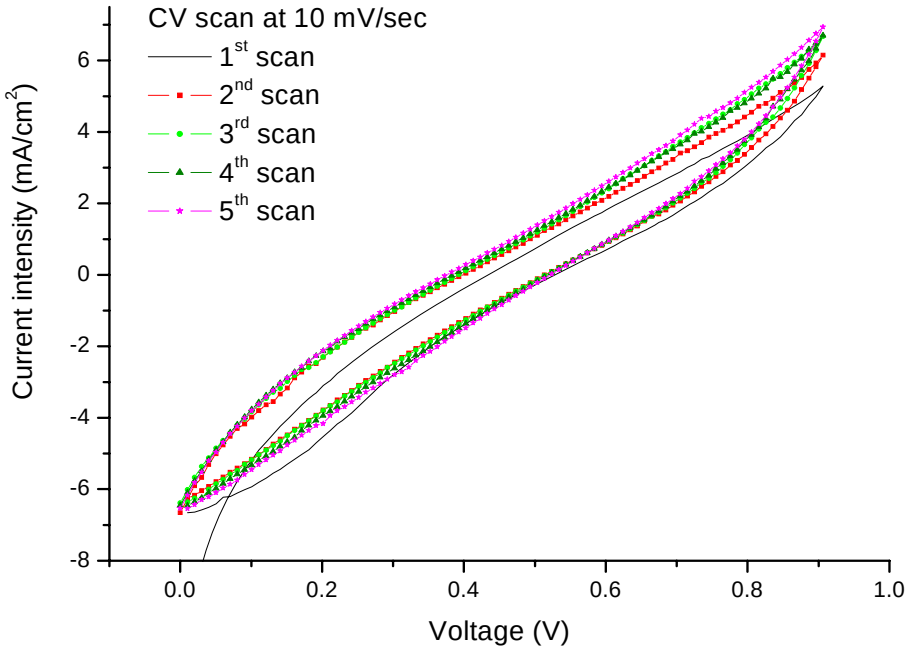

Fig. 3: The CV scans of the composite polyaniline/carbon nanotube film prepared by EPD from a 0.004g polyaniline + 0.04g MWCNTs + 0.005 $Mg(NO_3)_2 \cdot 6H_2O$ in 40 mL methanol.

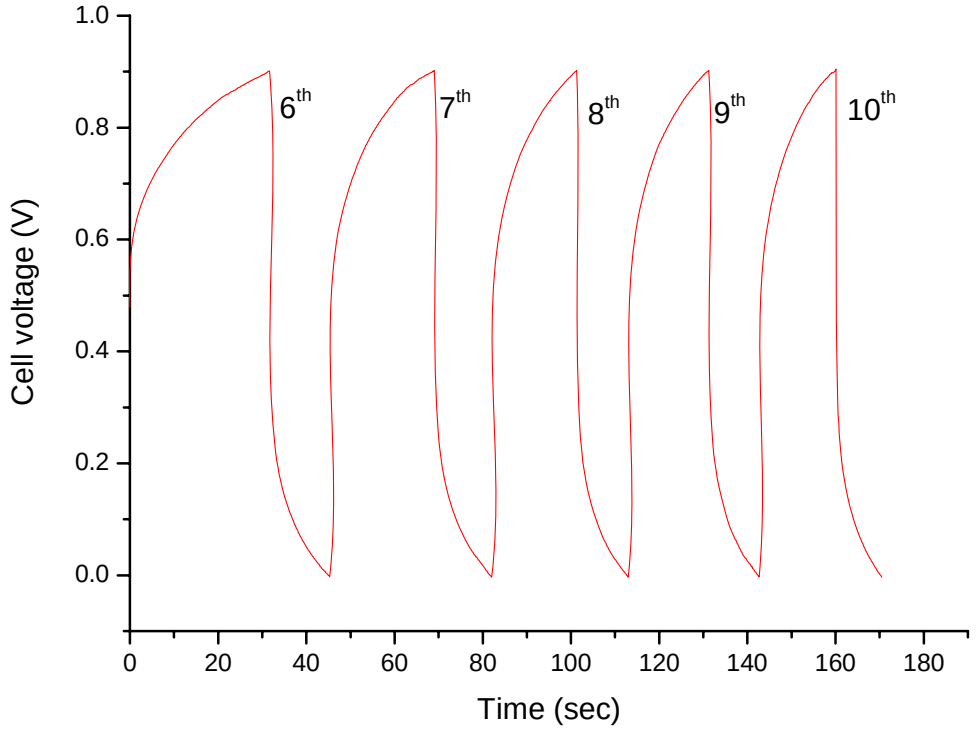

Fig. 4: The charge-discharge curves of the composite polyaniline/carbon nanotube film prepared from a 0.004 g polyaniline + 0.04 g MWCNTs + 0.005 g $Mg(NO_3)_2 \cdot 6H_2O$ in 40 mL methanol at a current density 2 mA/cm^2.

However, we found that this composite polyaniline/MWCNT film prepared by EPD method cannot sustain many charge-discharge cycles. After ~10 cycles, we found a lot of carbon nanotubes falling into the electrolyte (0.5 M H_2SO_4). The short life time of the film should be due to the not well attachment of the film to the stainless surface. Thus, the electrophoretic deposition may not be an appropriated technique for preparing the composite film for using as the capacitor electrode.

3) Fabrication of the composite polyaniline/MWCNT film by the slurry paste

We found that the polyaniline/MWCNT film prepared by the electrophoretic deposition can be sustained a charged-discharged only ~10 cycles. Thus, the other technique should be used to prepare the composite film. The slurry paste is a common used method in preparing the carbon nanotube film. In order to link nanotubes to the substrate, polymers such as PVF or PVDF are mixed with the carbon nanotube slurry for binding nanotubes to the substrate. We observed that the film prepare by this slurry paste technique has a much longer life time than the EPD film.

In this section, we studied the influence of the polyaniline/carbon nanotube ratio to the electrochemical capacitance. Five different ratios between polyaniline and carbon nanotube (0 wt.%, 7 wt.%, 14 wt.%, 21 wt.% and 29 wt.% of PANi) are prepared and tested.

Scanning electron microscopy (SEM)

SEM was used to analyze the surface morphology of the composite films and SEM images are shown in Fig. 5. It sees that the different polyaniline (PANi) concentration films result in a different film structure. The low PANi percentage film has more carbon nanotubes exposed surface than the high PANi percentage films. This should be due to coverage of polymer on the CNTs surface. In addition, the polymer size seems to increase with the PANi concentration.

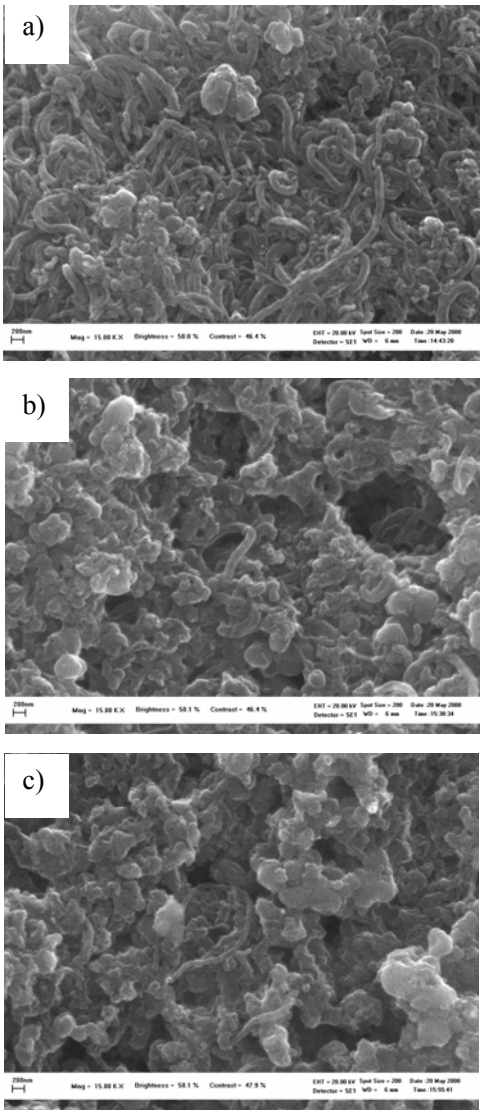

Fig. 5: SEM images of the composite polyaniline (PANi)/carbon nanotube film; a) the 0 wt.% PANi film, b) the 7 wt.% PANi and c) the 14 wt.% PANi.

Cyclic voltamogram (CV) result

The cyclic voltamogram was performed on the composite PANi/carbon nanotube film prepared by the slurry paste. Figure 6 shows the CV result of the composite electrode at a scan rate of 10 mV/s by using the 0.5 M H_2SO_4 as the electrolyte. The Pt plate and the Ag/AgCl electrode are used as the counter electrode and as the reference electrode, respectively. It sees that the current of the composite films is much larger than that of the stainless steel, meaning that the composite film can store energy much greater than the pure stainless steel. The carbon nanotube film stores energy by a double layer mechanism, where PANi stores energy by a redox reaction. The CV curve of the 14% PANi film is more like a rectangular shape than the pure carbon, which implies that the small addition of PANi improves the electrode become more an ideal capacitor. The 14% PANi film exhibits the oxidation peak at ~0.55 V and the reduction peak at ~0.4 V. However, the further increase of the PANi percentage is found to deduct the current respond, as observed in Fig. 6. The 29% PANi film has a lower current and the curve is deviated to the non-ideal capacitor as observed in Fig. 6. The decrease of the current density and the deviation of CV curve should be attributed to the reduction of the film conductivity. This is because PANi has a lower conductivity than the carbon nanotube.

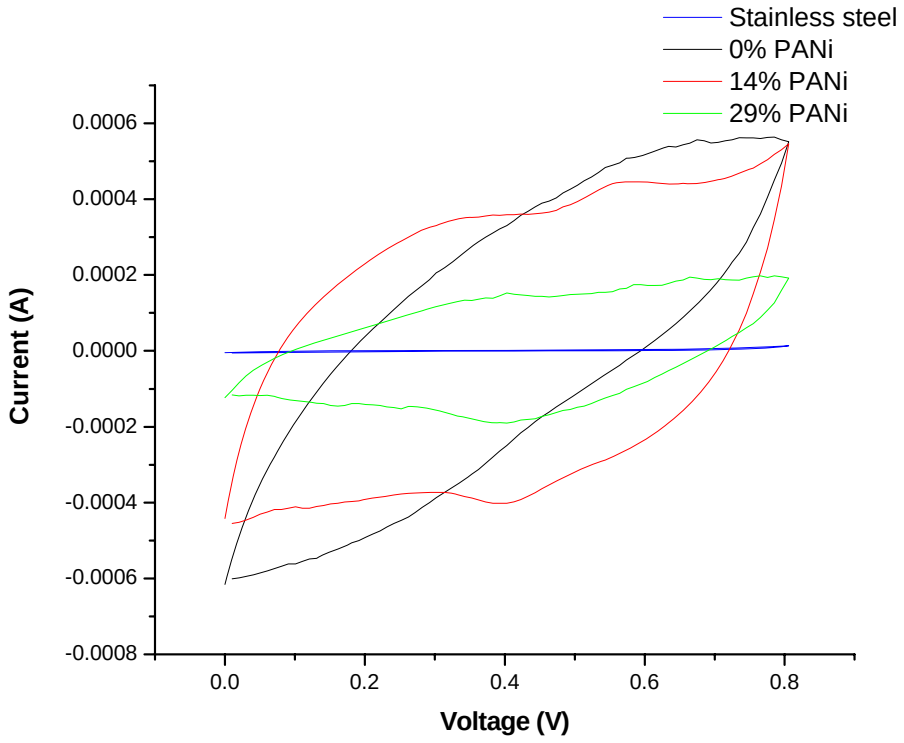

Fig. 6: The cyclic voltamogram of the stainless steel, the 0 wt.% PANi film, the 14 wt.% PANi film and the 29 wt.% PANi film as the working electrode. The Pt plate and the Ag/AgCl electrode are used as the counter electrode and the reference electrode, respectively.

Charge-discharge measurement

Charge-discharge was also performed to estimate the capacitance and the durability of the composite electrodes. The charge-discharge was performed at a constant current 5 mA/cm^2. If the composite film has a high capacitance, then its charging and discharging times should be long. The capacitance of the film is calculated from the following equation:

$$C = I \cdot \Delta t / \Delta V,$$

Where, I is a constant current (A), Δt is a charging or discharging time (s) and ΔV is the different voltage (V). It is observed from Fig. 7 that by adding PANi 14 wt.%, the charging-discharging time has significantly increased as compared to the 0 wt.% film, which means that the capacitance value is also greatly improved. However, too large PANi loading results in a dramatically decrease of the charge-discharge time and a higher IR drop on the charge-discharge curve. An increase in the IR drop suggests the increase of the film resistance. The charge-discharge result is agreed well with the CV result. To identify that the change of the film capacitance is governed by the film resistance, the electrochemical impedance spectroscopy (EIS) was used to analyze the film resistance.

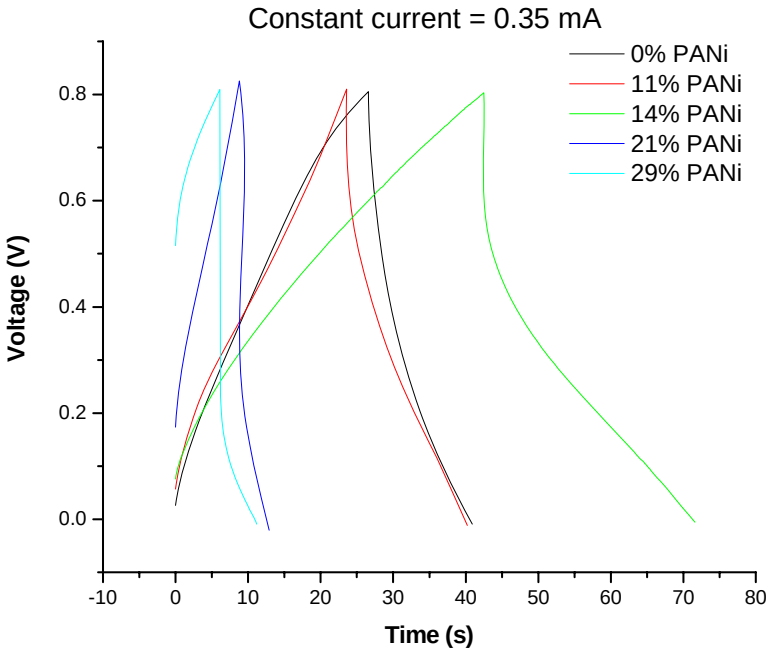

Fig. 7: The charge-discharge curves of the 0 wt.%, 11 wt.%, 14 wt.%, 21 wt.% and 29 wt.% PANi films at a constant current 0.35 mA (or 5 mA/cm^2).

Electrochemical impedance spectroscopy (EIS)

EIS was used to estimate the film resistance from the two symmetry electrodes with the 0.5 M H_2SO_4 as the electrolyte. EIS was operated from the frequency range of 100 kHz to 0.10 Hz. The impedance result (Fig. 8) shows that these films have about the same series resistance (R_s) (~20-25 Ohm), but the charge transfer resistance (R_{ct}) is largely vary from one film to another film. The series resistance should be due to the contact resistance between film and the substrate. The charge transfer resistance (R_{ct}) is the resistance reducing the electrons transferring rate through the film to the electron collector (substrate). It sees in Fig. 8(a), R_{ct} increases with the PANi percentage, meaning that the film resistance increases with the PANi percentage. The 0 wt.% PANi film has the lowest R_{ct} (25 Ohm), but the 29 wt.% PANi film has the highest R_{ct} (~1500 Ohm). The increase of the charge transfer resistance with the amount of PAni is consistence with the decrease of the CV curve and the charge-discharge time.

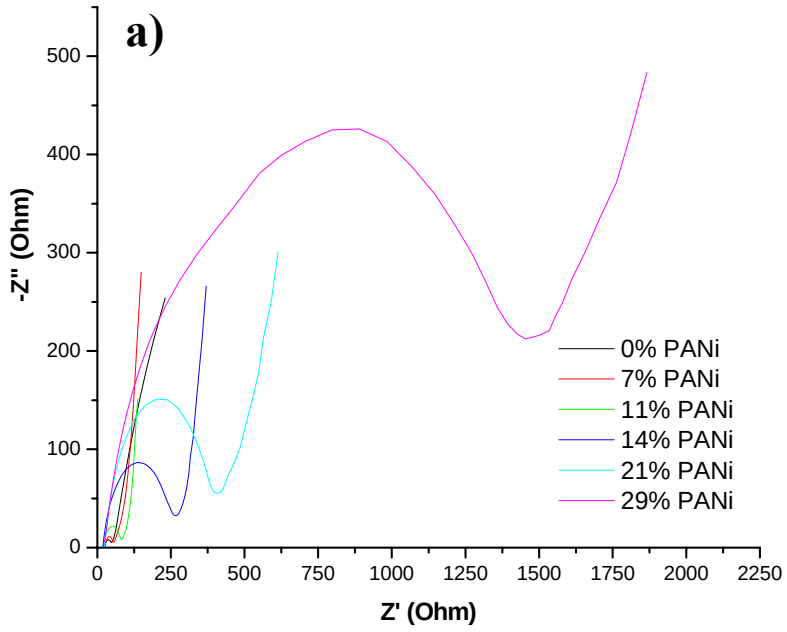

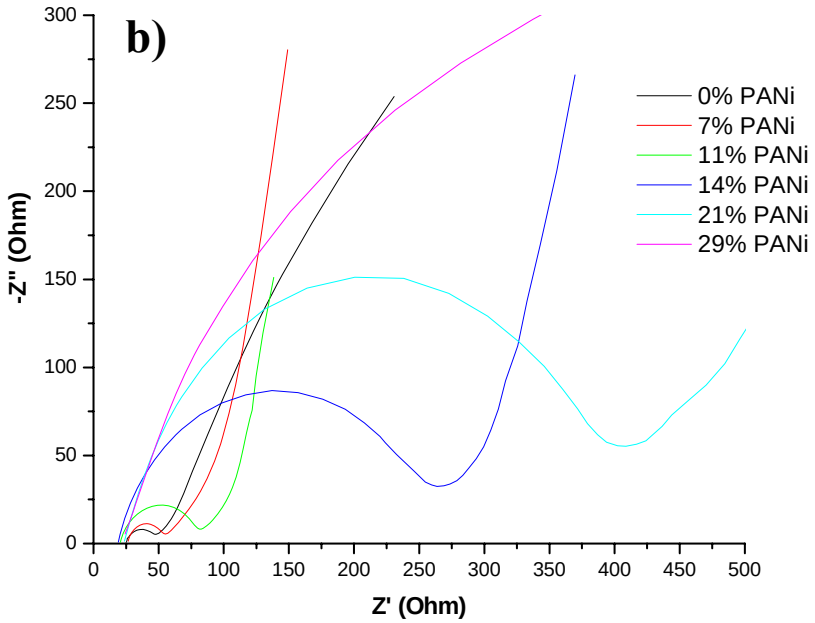

Fig. 8: a) The electrochemical impedance spectroscopy of 0 wt.%, 11 wt.%, 14 wt.%, 21 wt.% and 29 wt.% PANi films scanning from a 100 kHz to 0.1 Hz and b) the zoom-in image of a).

We repeated preparing the composite film by the slurry paste and tested the film capacitance with the constant current charge-discharge measurement, as shown in Fig. 9. The specific capacitance of the electrodes is estimated from the charge-discharge curve with the following equation:

$$C = (I \cdot \Delta t)/(\Delta V \cdot m),$$

Where, m is the mass of the film (g). The similar trend is still observed that is with the small addition of PANi, the specific capacitance is increased, but with the large amount of PANi, the specific capacitance is decreaseed. From Fig. 9, it sees that the 0.4 g CNT + 0.2 g MWCNT film and the 0.5 g CNT + 0.1 g MWCNT film exhibit the specific capacitance ~ 62 F/g and ~ 55 F/g, respectively, at the first discharge cycle. However, the specific capacitance decreases with the number of the discharge cycles. After ~ 100 cycles, the specific capacitance is more stable. Here, we found that the slurry paste composite PANi/carbon nanotube films can stand discharge at least 300 cycles.

Beside, the polyaniline composition, the composite MnO_2/CNTs films were also prepared and examed as the potential use of supercapacitor. It is reported that the metal oxide surface is commonly cover by hydroxyl groups, which is an electroactive group. Thus, by mixing with carbon nanotube, the film specific capacitance should be enhanced. However, we found that the addition of MnO_2 has a small effect on the specific capacitance. The addition of MnO_2 0.05 g increases the specific capacitance to ~15-17 F/g. The low capacitance, the composite MnO_2 film may be due to the low redox reaction or the well particle dispersion.

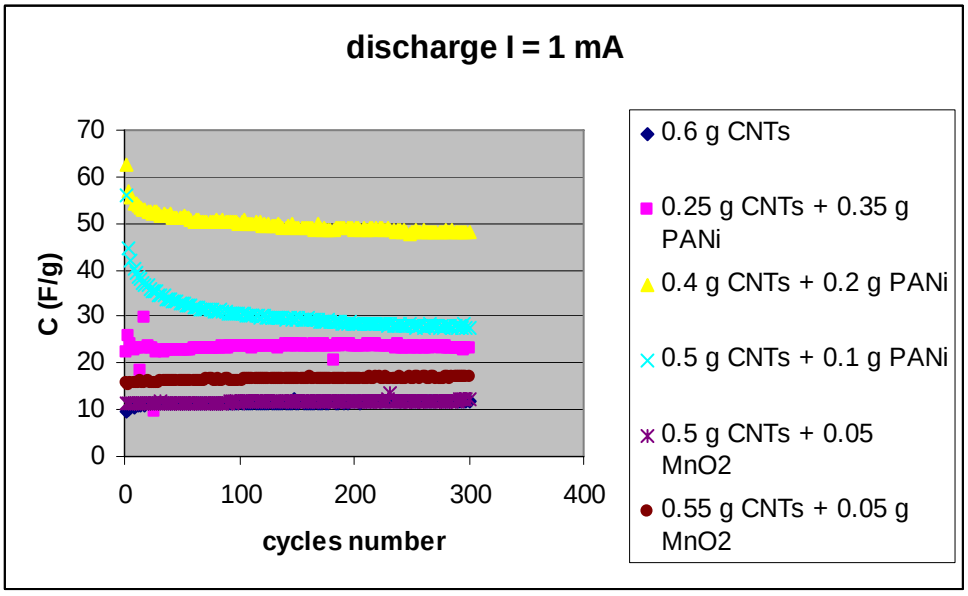

Fig. 9: The plot of the specific capacitance of six different electrodes versus the discharge cycles.

We also repeated analyzing the surface morphology of the composite polyaniline/MWCNT films and the composite MnO_2/MWCNT films by SEM (shown in Fig. 10). It is no CNT detect on the film surface, which may be due to MnO_2 covering the nanotube surface. This may be a reasattributed to the low dispersion of the polymer and MnO_2 with CNTs resulting in the reduction of the specific capacitance.

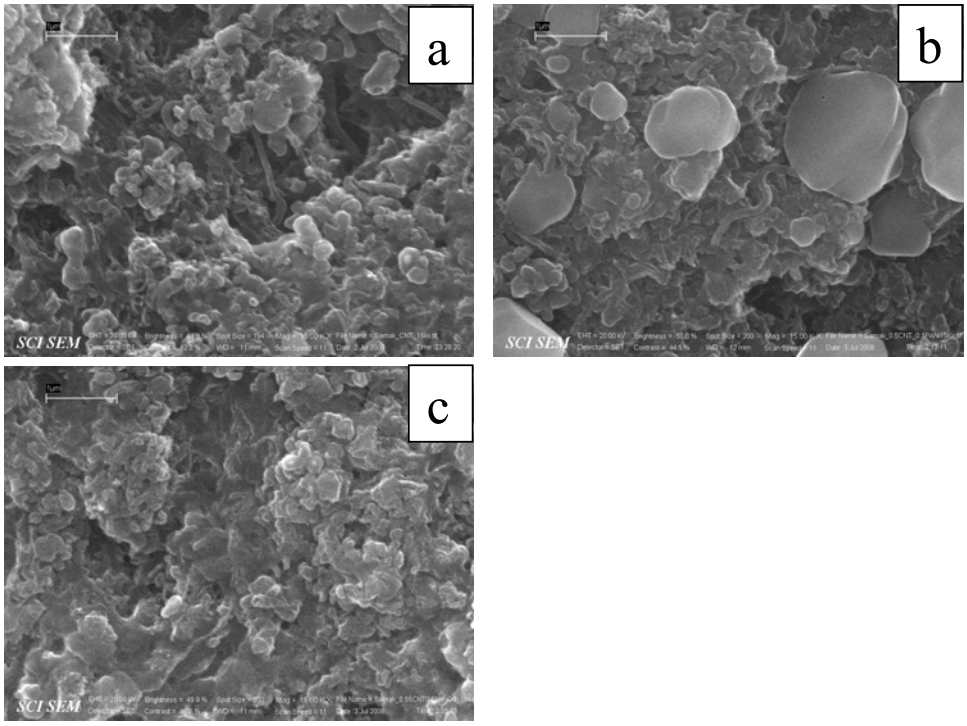

Fig. 10: SEM images of a) the CNT film (0.6 g CNT), b) the polyaniline/CNT film (0.4 g CNT + 0.2 g PANi) and c) the MnO_2/CNT film (0.55 g CNT + 0.05 g MnO_2).

Conclusion

In this section, we tried to fabricate the composite polaniline/MWCNT film by three different methods: 1) the electrospinning, 2) the electrophoretic depsotion and 3) the slurry paste. We could not fabricate film by the electrospining. We could prepared the composite films by the electrophoretic deposition and the slurry paste. The composite film prepared by EPD has a short life time only ~10 cycles. The slurry paste composite polyaniline/MWCNT film provides the long life time (over 300 cycles) and the high specific capacitance. The 0.4 g CNT + 0.2 g MWCNT film delivers the highest specific capacitance of ~50 F/g. The increase of the specific capacitance with the addition of the polyaniline is attributed to the high redox reaction of polyaniline.

Section 2: Dye-sensitized solar cell

Introduction

Dye-sensitize solar cell (DSSC) has been intensively studied because of its simple structure, low fabrication cost, promising light harvesting efficiency and environmental friendliness. DSSC is thought as the next generation solar cell, which exhibits a potential alternative to conventional silicon solar cell. The high energy conversion efficiency of dye-sensitized solar cells is accomplished through the use of a high porous semiconductor film coated with a monolayer dye-sensitizer as the working electrode, which was developed by O'Regan and Grätzel in 1991 [13]. TiO_2 nanoparticle is commonly used semiconductor because it delivers the highest energy conversion efficiency among semiconductors (ZnO, Nb_2O_5, WO_3, In_2O_3, SnO_2) [14,15,16,17]. TiO_2 particles will server as the electron-transporting medium between dye-sensitizers and the electron collector (transparent conductive substrate). Electrons from the electron collector will flow through the external load reaching the counter electrode, and undergo the reduction with tri-iodide ($I_3^- + 2e^- \rightarrow 3I^-$) by help of the catalyst film. The dye-sensitized solar cell consists of three main important parts: the working film, the electrolyte and the catalyst film (counter electrode). Thus, to optimize solar cell efficiency, these all three parts have to be miximized.

There are various ways in preparing TiO_2 electrodes such as sputtering, thermal evaporation, doctor-blade and electrophoretic. Recently, electrophoretic deposition (EPD) has a great deal of attention because it has a fast deposition rate, simple apparatus, no restriction on the substrate shape, and no binder required. Thus, a sample can be prepared from any kind of conductive substrate shape, and the EPD technique can be adapted to mass production processing. In addition, the electrophoretic deposition does not require a high temperature during the deposition process so that it is possible to prepare a thick TiO_2 film on a flexible conducting plastic [18,19,20].

Grinis et al. have used an electrophoretic TiO_2 film as a working electrode of a DSSC [21]. They observed that with the addition of film annealing or film compression, the DSSC performance is further improved. This is because the TiO_2 nanoparticles are more connected to each other resulting in better electron transport to the conductive substrate. However, the effects of the deposition voltage and deposition duration on the film surface morphology and the energy conversion efficiency of a DSSC have not been characterized in details. Therefore, in this section, we first have investigated the effects of the deposition voltage and deposition duration on the film morphology and the solar cell energy conversion efficiency.

Platinum (Pt) film is commonly used as the DSSC counter electrode because of its good catalytic activity, but Pt is an expensive material. Other cheaper materials have been studied as the alternative DSSC catalyst such as carbon black, carbon nanotubes or conductive polymers [22,23,24,25,26]. Carbon nanotubes are considered used as the DSSC counter electrode because of its unique properties such as good catalytic activity, good conductivity, high thermal stability, high aspect ratio and comparatively lower price than Pt. Thus, by switching to carbon nanotube counter electrode, the DSSC production cost should be minimized. Beside the DSSC application, carbon nanotubes have also been tested for many applications such as

ลูกลบ: 13
ลูกลบ: 14
ลูกลบ: 15
ลูกลบ: 16
ลูกลบ: 17
ลูกลบ: 18
ลูกลบ: 19
ลูกลบ: 20
ลูกลบ: 21
ลูกลบ: 22
ลูกลบ: 23
ลูกลบ: 24
ลูกลบ: 25
ลูกลบ: 26

composite material, biosensor, field emission or supercapacitor [27,28,29,30,31,32,33,34].

Carbon nanotube films are fabricated by various methods such as chemical vapor deposition, arc discharge, electrophoretic deposition or slurry paste [29,30,31,32,33,34,35]. The electrophoretic deposition (EPD) and the slurry paste are simple methods in preparing the low temperature carbon film. To coat carbon nanotubes (CNTs) on the conductive glass by EPD, the nanotube surface must have a charge surround the nanotube surface. The acid treatment (H_2SO_4:HNO_3) is commonly used in introducing a negative carboxylic group on the nanotube surface. A small amount of modified carbon nanotubes can be deposited on an anode surface by EPD, but the film quality is not that homogeneous. With a small addition of $Mg(NO_3)_2 \cdot 6H_2O$ into the carbon nanotube solution, the nanotube deposition rate and the film homogeneity are significantly improved. This is because Mg^{2+} ions surround the negative CNT surface and strengthens the electrostatic attraction force between carbon nanotubes and the cathode. The electrophoretic carbon nanotube film has been tested for many applications such as in biosensors, supercapacitors and field emissions [18,19,36,37,38,39]. However, there is no report in using the electrophoretic carbon nanotube film as the DSSC counter electrode. Here, in this section, we secondly explored the possibility of using the electrophoretically MWCNT film as the DSSC counter electrode. The effects of the carbon nanotube film thickness and the amount of magnesium loading on the carbon films to the solar cell performance were exam.

In addition to the electrophoretic deposition of carbon nanotubes film for the DSSC application, the slurry was also employed. The slurry paste is used polymers such as Polyvinyl Fluoride (PVF) or Polyvinylidene Fluoride (PVDF) as binders. Carbon nanotube film is dried at the low temperature (80 ˚C – 100 ˚C) for certain period up to 24 h. However, not many studies characterize the effect of heating duration and acid modification on the DSSC performance. Thus, thirdly, we had tested the possibility of using the slurry pasted carbon nanotube film as the DSSC counter electrode. Additionally, the suitability in applying carbon nanotube films coated on the conductive plastic as the flexible DSSC counter electrode is also investigated.

ลูกลบ: 27
ลูกลบ: 28
ลูกลบ: 29
ลูกลบ: 30
ลูกลบ: 31
ลูกลบ: 32
ลูกลบ: 33
ลูกลบ: 34
ลูกลบ: 29
ลูกลบ: 30
ลูกลบ: 31
ลูกลบ: 32
ลูกลบ: 33
ลูกลบ: 34
ลูกลบ: 35
ลูกลบ: 18
ลูกลบ: 19
ลูกลบ: 36
ลูกลบ: 37
ลูกลบ: 38
ลูกลบ: 39

Results

2.1 Fabrication of TiO_2 films by the electrophoretic deposition for the DSSC working electrode

SEM image of TiO_2 films

TiO_2 film is prepared by the electrophoretic deposition. The setup of the eelctrohoretic system is shown in Fig. 2. The surface morphology of the TiO_2 films was analyzed by SEM, as shown in Fig. 11. SEM analysis reveals that the TiO_2 surface was comprised of a number of cracks. The size of cracks was found to be on the micrometer scale, and the length of cracks seemed to depend on the deposition voltage and deposition duration. The length of cracks on the TiO_2 films prepared at 5 V for 1 min was about 1-5 μm, as observed in Fig. 11(a). However, the length of cracks on the film prepared at 5 V for 2 and 8 min was remarkably long being even greater than 100 μm, as shown in Figs. 11(b) and 11(c), respectively. Many reasons have been proposed for the mechanism of crack formation in the inorganic film such

as a rapid evaporation of the solvents from the film surface during the drying process, a decrease of TiO_2 particle bonding strength as the film thickens, and a mismatch of the thermal expansion between the FTO substrate and the TiO_2 film [40,41,42]. The film prepared at 20 V for 8 min had the largest crack length compared to other films, as observed in Fig. 11(g). Microcracks formed on the TiO_2 film prepared by EPD were also reported by other groups [21,43,44].

ลูกลบ: 40
ลูกลบ: 41
ลูกลบ: 42
ลูกลบ: 21
ลูกลบ: 43
ลูกลบ: 44

It was observed that different deposition conditions would cause a difference on the film surface. An increase in the deposition voltage and deposition duration also significantly increased film thickness as illustrated in Fig. 12(a). The thickness of the TiO_2 film prepared at 20 V for 8 min was ~25.3 μm, whereas the thickness of the TiO_2 film prepared at 5 V for 1 min was only ~5.0 μm. The plot of the deposition rate vs. the deposition voltage (Fig. 12(b)) exhibited an increasing trend with a function of the deposition voltage for all three-deposition times. However, the deposition rate shows a decreasing trend with the deposition duration, as observed in Fig. 12(b). The reduction of the deposition rate with the prolonged deposition duration may be due to an agglomeration of TiO_2 particles in the solvent, which consequently lowered the particle diffusion rate. The reduction of the TiO_2 deposition rate was also due to the formation of an insulating layer on the conducting glass surface as more TiO_2 particles deposited on the substrate.

Solar cell efficiency

The solar cell characteristic of the dye coated TiO_2 films as the working-electrodes were analyzed at an irradiation of a 100 mW/cm^2 under a standard air mass (AM) 1.5 global filter. In Fig. 13, the current density-voltage curves show that the open circuit voltage (V_{oc}) and the short circuit current density (J_{sc}) of the TiO_2 films prepared at the 5 V for 1, 2 and 8 min were 0.70, 0.69 and 0.68 V, and 4.26, 5.70 and 6.93 mA/cm^2, respectively. The fill factor (FF) and energy conversion efficiency (η) of the TiO_2 films prepared at the 5 V for 1, 2 and 8 min were 0.68, 0.66 and 0.65, and 2.03, 2.60 and 3.06%, respectively. Hence, the J_{sc} and η values increased with an increase of the TiO_2 deposition duration. This was because the film thickness of the longer deposition duration was larger than that of the shorter deposition duration, as shown in Fig. 12(a).

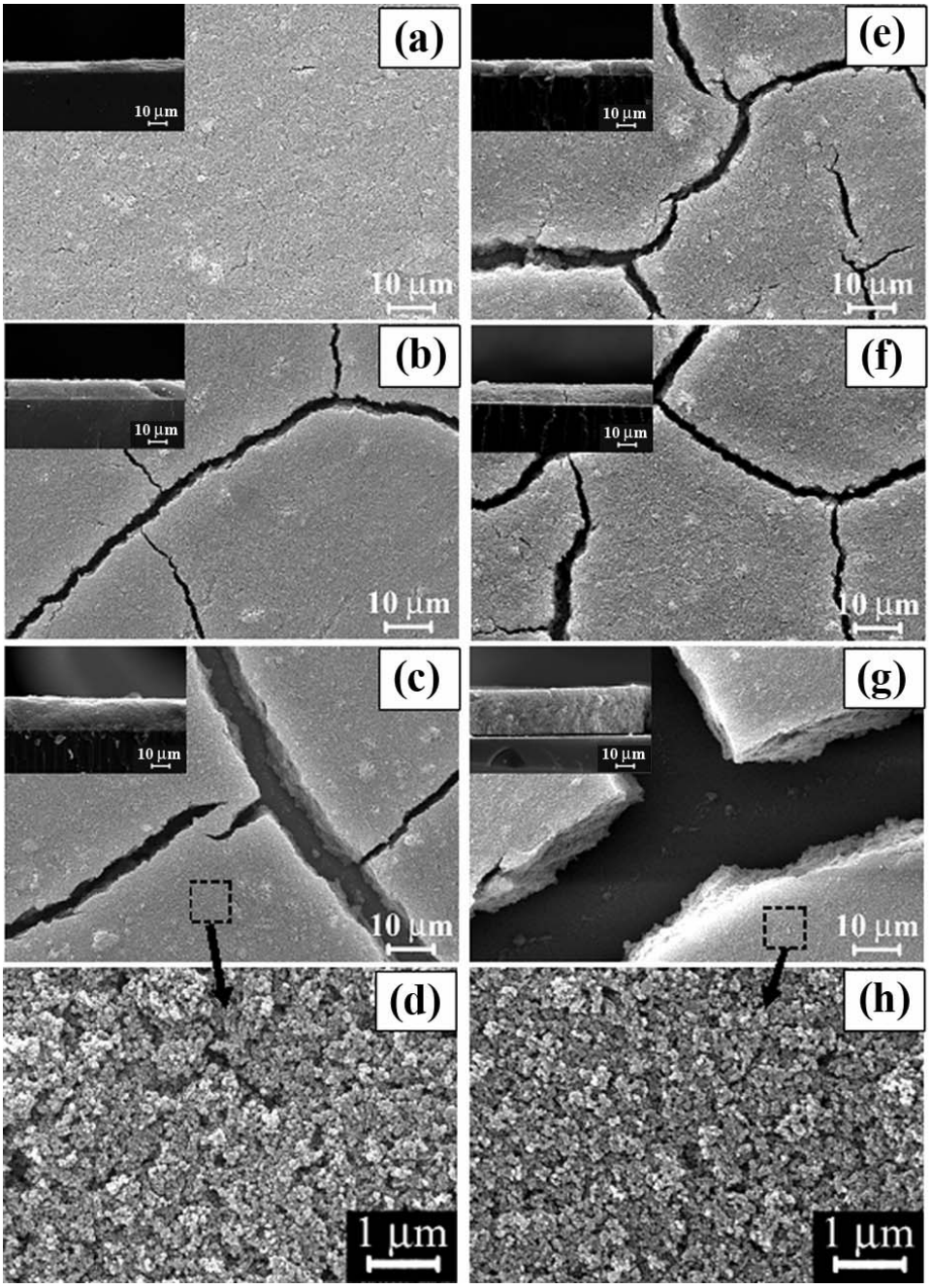

Fig. 11: Top and side view SEM images of the TiO_2 film prepared by the EPD technique at various deposition voltages and duration times: (a) 5 V for 1 min, (b) 5 V for 2 min, (c) 5 V for 8 min, (d) 5 V for 8 min (high magnification), (e) 20 V for 1 min, (f) 20 V for 2 min, (g) 20 V for 8 min, (h) 20 V for 8 min (high magnification).

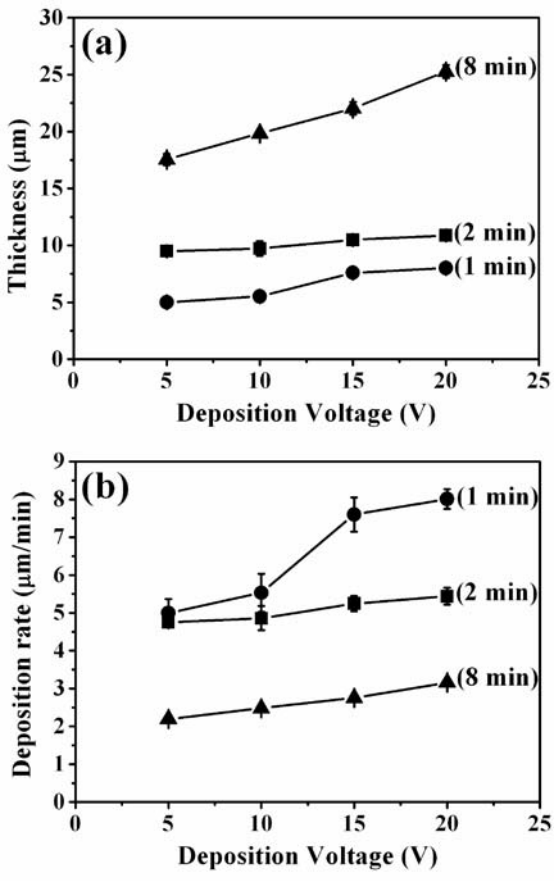

Fig. 12: (a) Plot of the TiO_2 thickness vs. the deposition voltage at various deposition times: 1, 2 and 8 min, (b) plot of the TiO_2 deposition rate vs. the deposition voltage at various deposition times: 1, 2 and 8 min.

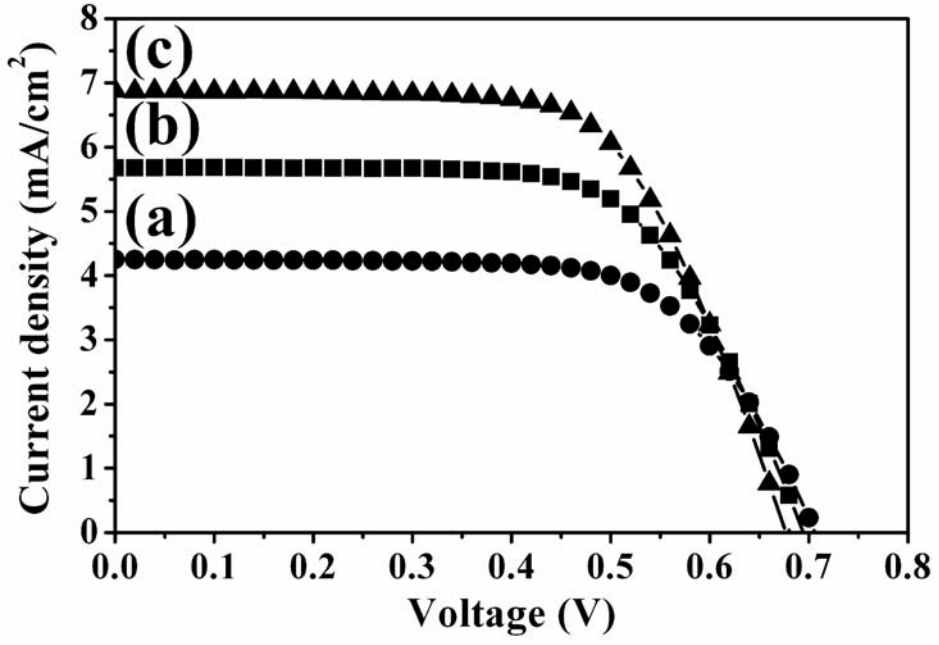

Fig. 13: The J-V characteristics of the DSSC assembled of TiO_2 films deposited at 5 V for three different deposition duration times, (a) 1 min, (b) 2 min, and (c) 8 min as the working-electrode.

The plot of the short circuit current density and the energy conversion efficiency vs. the film thickness (Figs. 14(a) and 14(b)) showed a dependent relationship with the TiO_2 thickness. From Figs. 14(a) and 14(b), the curve fitting of J_{sc} and η vs. the film thickness can be divided into two distinctive regions. The first region is at film thickness below 14 μm and the second region is at film thickness above 14 μm. In the first region (below 14 μm), the J_{sc} and η values increased with the TiO_2 thickness. The increase of J_{sc} and η with the TiO_2 thickness should be due to more TiO_2 nanoparticles being available for dye coating. To confirm this, the amount of absorbed dye on the TiO_2 film was analyzed by a UV-Vis adsorption spectroscopy. Figures 14(a) and 14(b) show a plot of the amount of absorbed dye on the TiO_2 film vs. the film thickness. It was observed that the amount of absorbed dye increases with the TiO_2 thickness; implying that there were more dye molecules absorbed on the thicker film than on the thinner film. This should contribute to the thicker film containing more TiO_2 nanopariticles than the thinner film. However, the J_{sc} and η values in the second region (above 14 μm thick) were reduced as the film became thicker even though the amount of dye loading increases, as observed in Figs. 14(a) and 14(b). The more dye molecules absorbed on the thicker TiO_2 film should generate more free charge carriers resulting in a higher conversion efficiency than the thinner film. In contrast, it was observed that above 14 μm thickness, the J_{sc} and η values decreased with the increase of the TiO_2 thickness and the amount of absorbed

dye. The reduction of J_{sc} with the film thickness suggests the decrease of the amount of free generated electrons reaching the conductive substrate. The degradation of the DSSC conversion efficiency in the second region (above 14 μm) should be due to the high carrier recombination. The decrease of V_{oc} from 0.70 V to 0.65 V (Fig. 14(c)), and FF from 0.68 to 0.66 (Fig. 14(d)) with the increase of the film thickness further supports a higher carrier recombination with TiO_2 thickness.

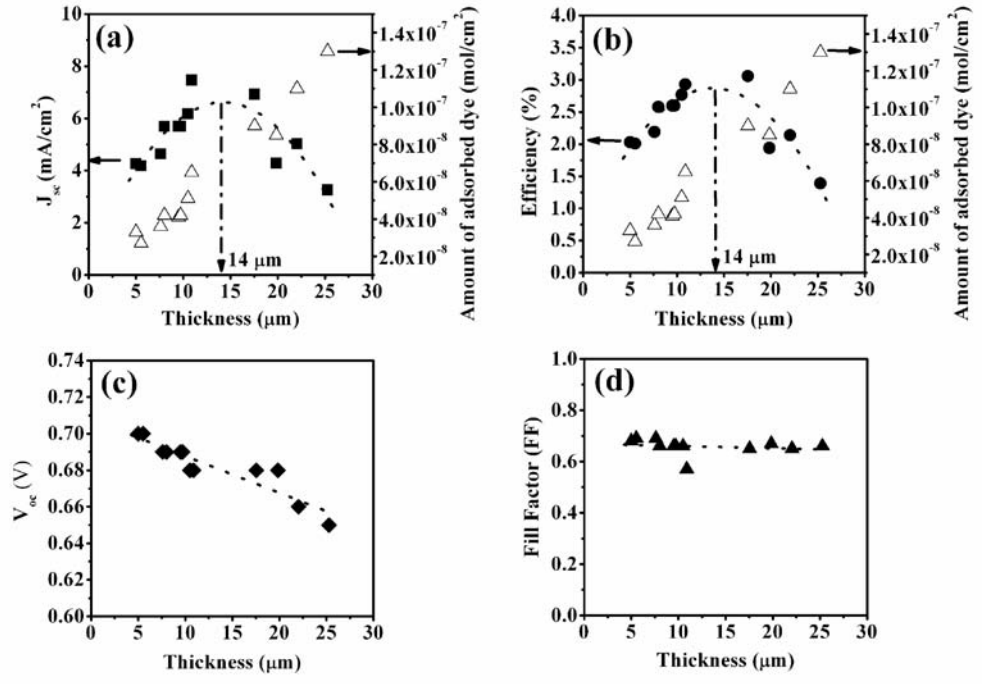

Fig. 14: Plot of (a) the current density (J_{sc}) and the amount of absorbed dye, (b) the energy conversion efficiency (η) and the amount of absorbed dye, (c) the open circuit voltage (V_{oc}) and (d) the fill factor (FF) and the curve fittings vs. the TiO_2 thickness.

2.2 Fabrication of carbon nanotube films by the electrophoretic deposition for the DSSC counter electrode

SEM images of TiO_2 and MWCNT films

TiO_2 and multiwall carbon nanotube films were coated on the FTO substrate by EPD, as shown in Figs. 15 and 16, respectively. The thickness of TiO_2 film estimated from the cross-section SEM image is about 20 μm.

Table 1: The summaries of the film thicknesses, short-circuit photocurrent density (J_{sc}), open-circuit photovoltage (V_{oc}), fill-factor (FF) and efficiency (η) of the dye-sensitized solar cells as using the conductive glass, magnesium film and carbon nanotube (with and without $Mg(NO_3)_2 \cdot 6H_2O$) films as counter electrode.

Sample	Type of counter electrodes	Film thickness (μm)	J_{sc} (mA/cm^2)	V_{oc} (V)	Fill Factor (FF)	Efficiency (η)
Sample 1	Conductive glass	0	0.08	0.59	0.12	0.01%
Sample 2	Magnesium film	N/A	0.23	0.66	0.16	0.02%
Sample 3	WO-Mg-0.02-g-CNT-4- min	N/A	0.42	0.58	0.09	0.02%
Sample 4	WO-Mg-0.04 g CNT-4-min	N/A	0.96	0.61	0.13	0.08%
Sample 5	W-Mg-0.02-g-CNT-1-min	0.5	3.22	0.71	0.31	0.71%
Sample 6	W-Mg-0.02-g-CNT-4-min	5.7	2.20	0.69	0.43	0.65%
Sample 7	W-Mg-0.04-g-CNT-1-min	2.0	3.71	0.67	0.43	1.08%
Sample 8	W-Mg-0.04-g-CNT-4-min	10.1	2.55	0.67	0.48	0.81%

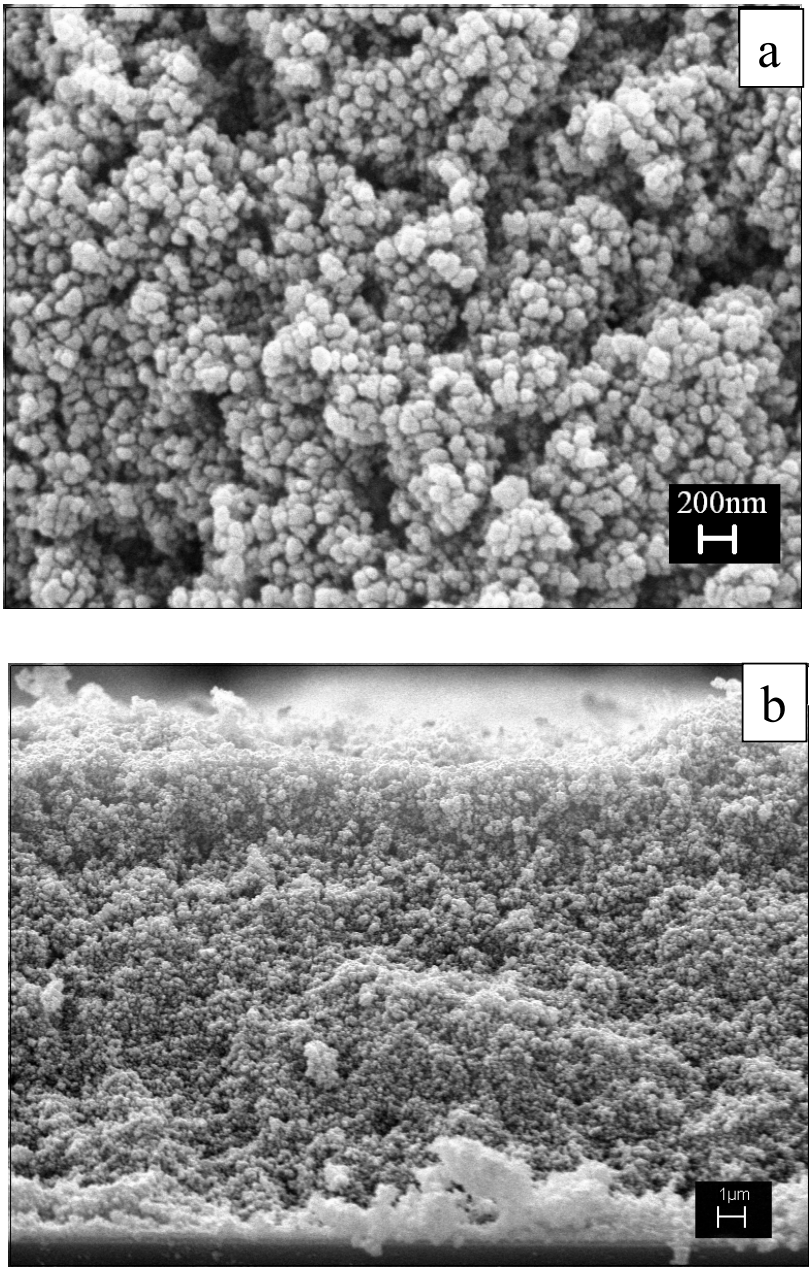

Fig. 15: (a) Top view and (b) cross-section view of TiO_2 film prepared by EPD.

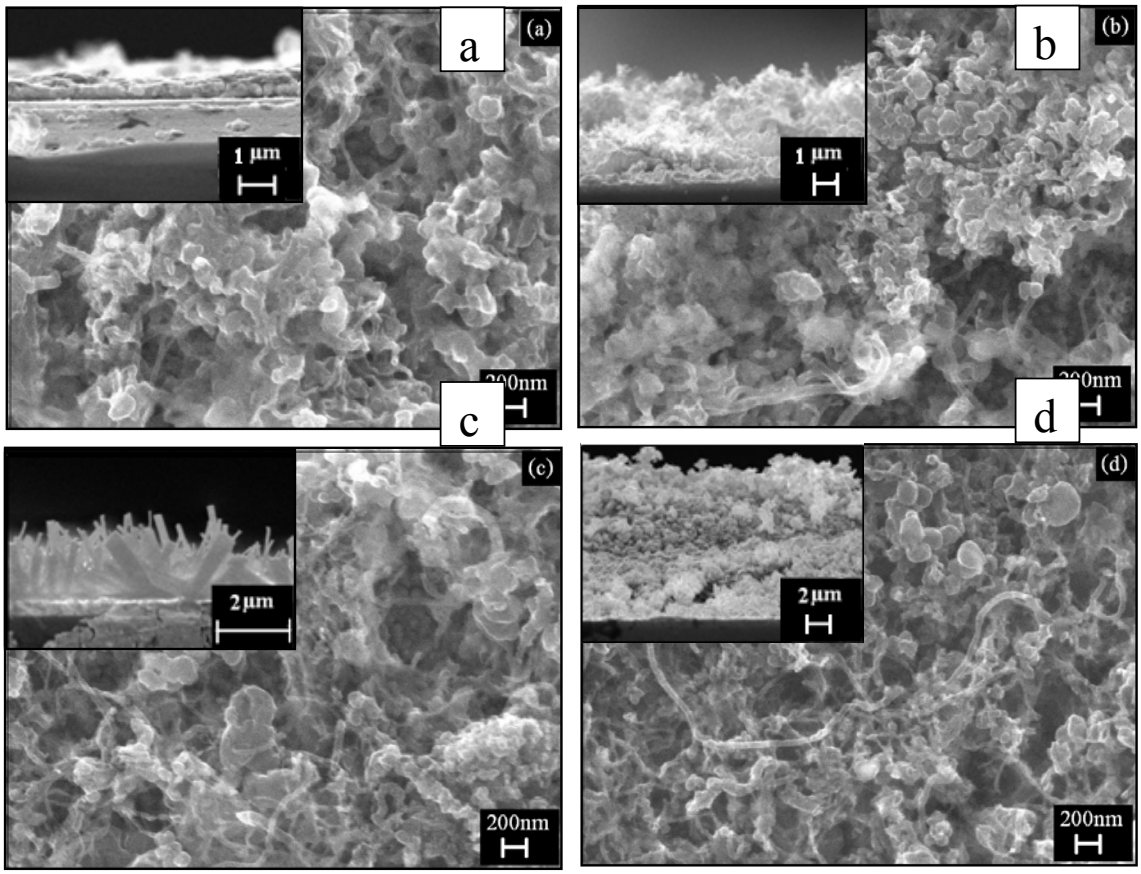

Fig. 16: Top and cross-section SEM images of (a) a W-Mg-0.02-g-CNT-1-min film, (b) a W-Mg-0.02-g-CNT-4-min film, (c) a W-Mg-0.04-g-CNT-1-min film and (d) a W-Mg-0.04-g-CNT-4-min film.

The thickness of W-Mg-CNT films (with $Mg(NO_3)_2 \cdot 6H_2O$ carbon nanotube films), estimated from the cross-section SEM images (Fig. 16(a)-16(d)), is summarized in Table 1. It is observed that at the same carbon nanotube concentration, the 4-min (4 minutes deposition duration) CNT films are thicker than the 1-min films. Similarly, at the same deposition duration, the larger carbon nanotube concentration (0.04 g CNTs) films are thicker than the lower carbon concentration (0.02 g CNTs) films. Hence, the carbon film thickness increases with the deposition duration and the carbon nanotube concentration. Since carbon nanotubes having a high aspect ratio, the surface area of carbon nanotube film should be larger than that of a smooth film. Therefore, the surface area of CNT film and the interfacial area between the electrolyte and the CNT electrode are expected to increase with the film thickness, which would subsequently strengthen the dye-sensitized solar cell performance.

3.2 The performance of DSSCs

The DSSC performance using the conductive glass, magnesium film, WO-Mg-CNT (without $Mg(NO_3)_2 \cdot 6H_2O$ carbon nanotube) films and W-Mg-CNT films as the counter electrode was analyzed with a solar simulator at a light intensity of 100 mW/cm^2, and the photocurrent-photovoltage (J-V) result is presented in Fig. 17. The short-circuit photocurrent density (J_{sc}), open-circuit voltage (V_{oc}), fill factor (FF) and efficiency (η) are calculated from the J-V curves, and they are listed in Table 1. It is found that the conductive glass, magnesium film and WO-Mg-CNT films deliver a very low efficiency as compared to W-Mg-CNT films because the film surfaces contain no catalyst. The efficiency of the WO-Mg-0.04-g-CNT film is larger than the WO-Mg-0.02-g-CNT film and the magnesium film, which may be due to a small amount of CNT deposited on the conductive glass. In case of CNT films prepared from the CNT plus $Mg(NO_3)_2 \cdot 6H_2O$ solution, the trend of the efficiency behaves unexpected because at the same CNT concentration, the longer deposition duration films (thicker CNT films) have a lower efficiency than the shorter deposition duration films (thinner films). However, at the same deposition duration time, the DSSC efficiency of the higher CNT concentration (0.04 g CNT) films is larger than the lower concentration (0.02 g CNT) films. Notice that for the W-Mg-CNT film thickness prepared at the same deposition duration, the 0.04-g CNT concentration films are thicker than the 0.02-g CNT concentration films. Hence, the DSSC efficiency increases with the CNT film thickness through the increased CNT concentration, but decreases with the film thickness through the longer deposition duration. The degradation of the solar cell efficiency with a function of the deposition duration should be caused by particle accumulation on the carbon nanotube surface, as observed in Fig. 16.

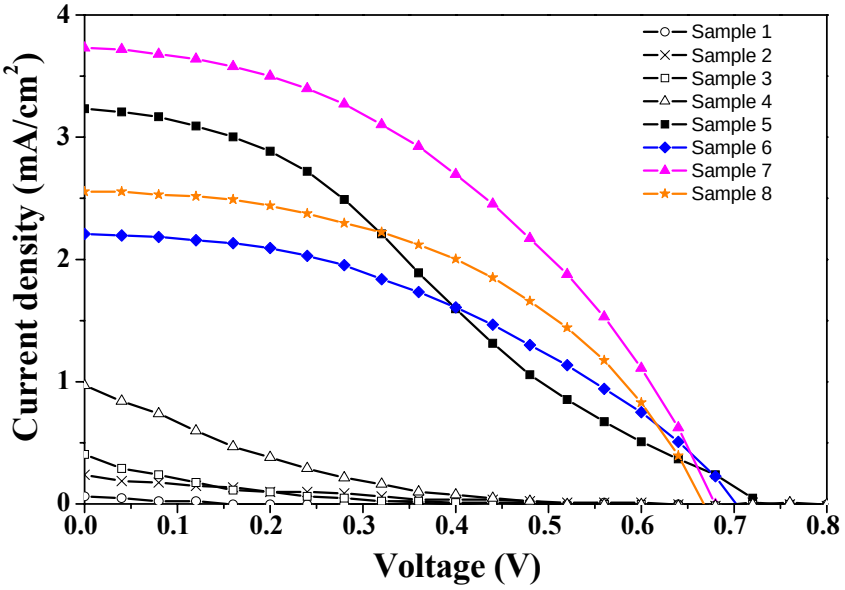

Fig. 17: Plot of the photocurrent density (J) versus the photovoltage (V) of the dye-sensitized solar cells using the conductive glass, the magnesium film and the electrophoretically carbon nanotube films as counter electrode.

EDX result (Fig. 6) detects the existence of magnesium on the W-Mg-CNT films. Therefore, the incorporated particles, which cover the nanotube surface, are magnesium. The increase in magnesium particles' size with the deposition duration should be attributed to an additional deposition of free Mg^{2+} ions. The amount of free Mg^{2+} ions in the low CNT concentration solution should be larger than in the high CNT concentration solution. This is because the lower CNT concentration has less available nanotubes for Mg^{2+} ions to attach to than the higher CNT concentration. This is further supported by the larger magnesium particles on the W-Mg-0.02-g-CNT films than on the W-Mg-0.04-g-CNT films. In addition, EDX also observes a small amount of Ni loaded on carbon nanotube films. This Ni should have adhered to carbon nanotubes during the nanotube fabrication process.

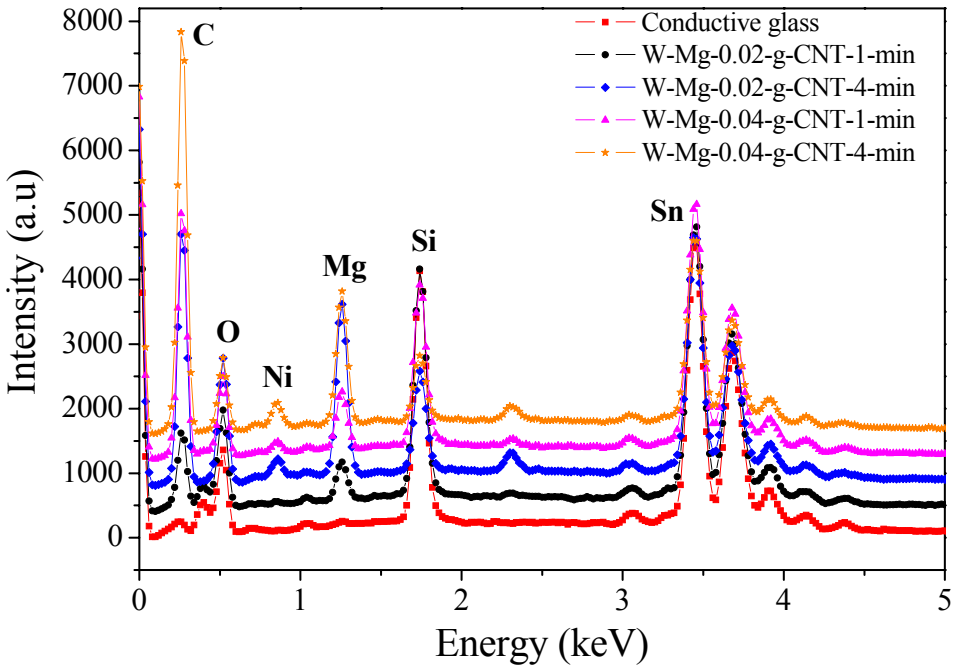

Fig. 19: EDX spectra of the conductive glass and carbon nanotubes films prepared at four different deposition conditions.

The amount of magnesium coated on W-Mg-CNT films is estimated from the integrated ratio of Mg peak (I_{Mg}) over C peak (I_C) of EDX spectra as listed in Table 2. It seems that the I_{Mg}/I_C intensity ratio increases with the deposition duration, but decreases with the carbon nanotube concentration. This means that the percentage of incorporated magnesium on carbon films increases with the deposition duration, but decreases with the carbon concentration. For clarifying the influence of magnesium incorporation on the DSSC performance, the values of the solar cell efficiency (η) and the short-circuit photocurrent density (J_{sc}) are plotted versus the I_{Mg}/I_C intensity ratio, as presented in Fig. 20. Both η and J_{sc} curves show a decreasing trend with a function of the I_{Mg}/I_C intensity ratio, implying that the larger amount of magnesium coated on the W-Mg-CNT films will lower the DSSC efficiency and the photocurrent density. The reduction of η and J_{sc} may be limited by the coverage of magnesium particles on the CNT surface lowering the exposed CNT surface to the electrolyte.

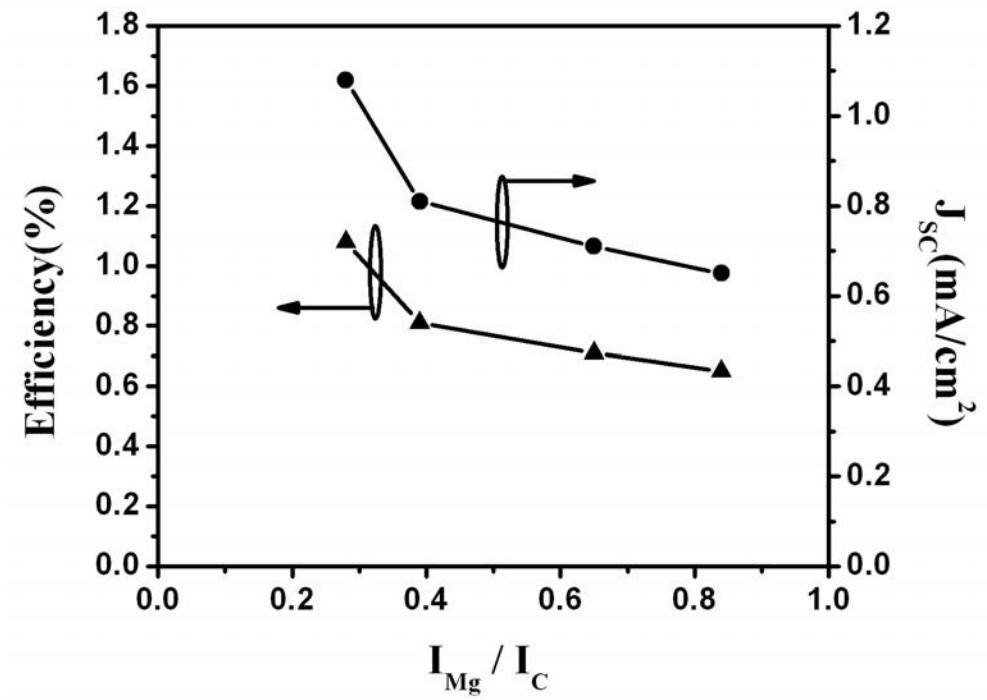

Fig. 20: Plot of the solar cell efficiency (η) and the short-circuit photocurrent density (J_{sc}) versus the I_{Mg}/I_C intensity ratio. The result reveals that η and J_{sc} decrease with the increase in the amount of incorporated magnesium.

Table 2: The summaries of the integrated area of C peak (I_C) and Mg peak (I_{Mg}) of EDX spectra, and the I_{Mg}/I_C intensity ratio of W-Mg-MWCNT films.

MWCNT sample	Integrated area of C peak (I_C)	Integrated area of Mg peak (I_{Mg})	I_{Mg}/I_C intensity ratio
W-Mg-0.02-g-CNT-1 min	77	50	0.65
W-Mg-0.02-g-CNT-4 min	273	230	0.84
W-Mg-0.04-g-CNT-1 min	255	72	0.28
W-Mg-0.04-g-CNT-4 min	429	169	0.39

3.3) Fabrication of carbon nanotube films by the slurry paste for the DSSC counter electrode

In this part, we investigated two different DSSC systems: 1) Glass DSSCs and 2) Flexible DSSCs.

1) Glass DSSCs

The surface morphology of TiO_2 and carbon nanotube films coated on the conductive glass is characterized by SEM, and images are presented in Fig. 21 and 22, respectively. The cross-section image of TiO_2 film (Fig. 21b) clearly shows three different layers; 1) a dense-TiO_2 layer ~0.5 μm, 2) a porous transparent TiO_2 layer ~5.5 μm and 3) a scattered TiO_2 layer is ~3.2 μm. The amount of dye molecules adsorbed on the TiO_2 films, a TiO_2 area of 0.49 cm^2, was analyzed by the UV-visible spectrometer. Figure 23 shows the absorbance spectra of three desorbed dye solutions of TiO_2/FTO samples. All three absorbance spectra exhibit close absorbance value; meaning that the TiO_2 thickness should be close to one another. Hence, it can be inferred that the consistence TiO_2 thickness is possible prepared by the doctor blade technique. The amount of dye loaded on the TiO_2 films is calculated via the following equations:

$$A_\lambda = \varepsilon_\lambda c l, \quad (1)$$

and

$$M = cV. \quad (2)$$

Where, A_λ and ε_λ are the absorbance value and the specific absorbance ($M^{-1}\cdot cm^{-1}$) as a function of wavelength, respectively. c is the desorbed dye concentration (M), l is the thickness of the standard corvette glass (1 cm), V is the volume of the dye solution (10 ml), and M is the amount of dye molecules adsorbed on the TiO_2 films (mol). By using the specific absorbance at λ = 300 nm, $\varepsilon_{300} = 5.7\times10^4$ $M^{-1}cm^{-1}$, the amount of

dye molecules is about 5.32×10^{-8}, 5.25×10^{-8} and 4.86×10^{-8} mol (average $5.14\times10^{-8} \pm 0.25\times10^{-8}$ mol). Here, the amount of dye adsorbed on three TiO_2 films are about the same.

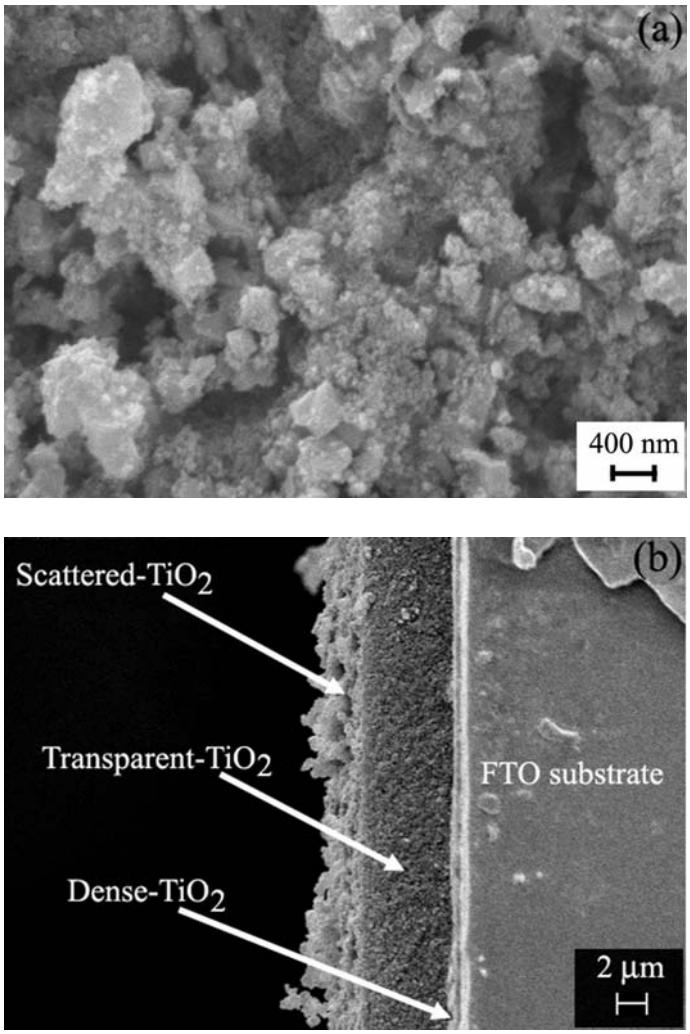

Fig. 21: (a) The top view and (b) the cross-section view SEM images of TiO_2/FTO film.

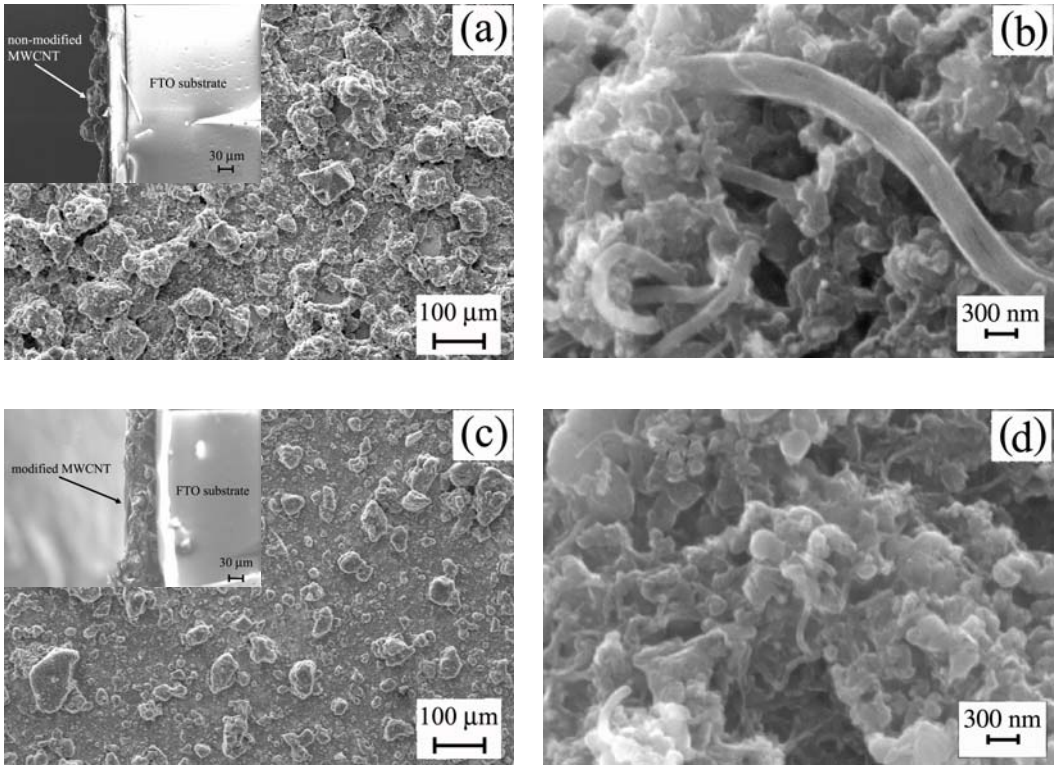

Fig. 22: (a) The low and (b) high magnification SEM images of the non-modified MWCNT/FTO film annealed for 6 h. (c) The low and (d) high magnification SEM images of the modified MWCNT/FTO film annealed for 6 h.

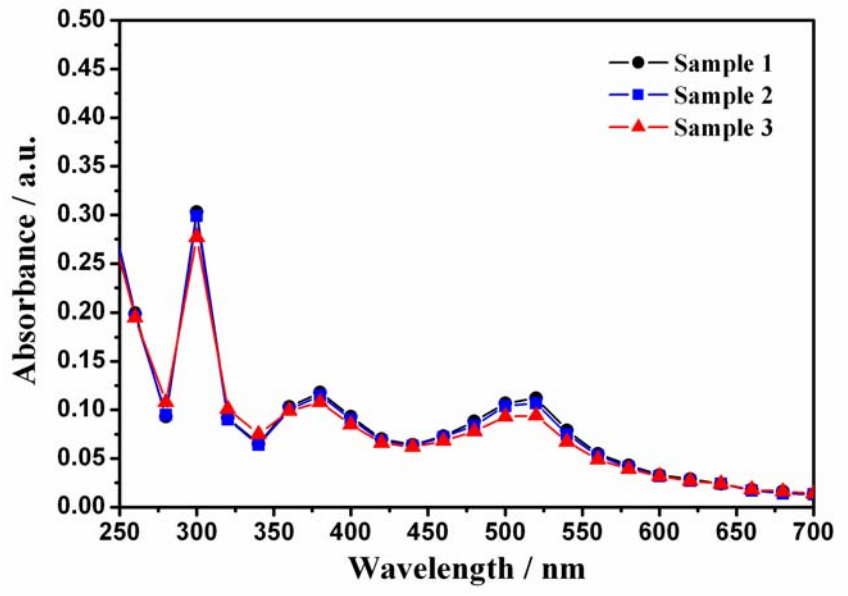

Fig. 23: The absorbance spectra of the desorbed dye solutions of the TiO_2/FTO samples in the 10 ml of 0.1 M NaOH and ethanol at volume ratio of 1:1.

The thickness of the MWCNT film coated on the conductive glass (MWCNT/FTO) estimated from the cross-section SEM images (Fig. 22) is ~33-65 μm. Owing to the high CNT aspect ratio and the high carbon film porosity, the interfacial area between the electrolyte and the counter electrode should increase upon the carbon nanotube film thickness, which subsequently elevating the solar cell efficiency. The DSSC performance was analyzed with the solar simulator, and the photocurrent density (J)-photovoltage (V) curves are presented in Fig. 24(a). The short-circuit current density (J_{sc}), open-circuit voltage (V_{oc}), fill factor (FF) and efficiency (η) are extracted from the J-V curves and are listed in Table 3. As shown in Table 3, the Pt DSSC generates the highest energy conversion efficiency (3.9%) among the counter electrodes. This should be attributed to the better catalytic activity of the Pt film over the carbon nanotube films. To monitor the effects of the acid treatment and the heating duration of MWCNT films on the solar cell performance, the efficiency value is plotted versus the heating duration, as shown in Fig. 24(b). The result reveals that the 6 h annealing duration delivers the maximum efficiency for both the non-modified (2.73%) and modified (3.46%) carbon nanotube DSSCs. However, further annealing time is found to suppress the solar cell efficiency. The degradation of the cell efficiency upon the increase annealing period could be attributed to the deformation of polymer binder causing the deduction of the nanotube connectivity and the carbon film conductivity. Consequently, this will moderate the electron-transferring rate to tri-iodide and the solar cell efficiency.

Treatment conditions	Counter electrode	Heating time (h)	Active area (cm^2)	V_{oc} (V)	J_{sc} (mA/cm^2)	FF	η (%)
Non-modified CNTs	N-2h-CNT/FTO	2	0.49	0.58	7.29	0.41	1.73
	N-4h-CNT/FTO	4	0.49	0.68	7.06	0.49	2.38
	N-6h-CNT/FTO	6	0.49	0.72	7.92	0.48	2.73
	N-8h-CNT/FTO	8	0.49	0.70	8.31	0.44	2.58
	N-12h-CNT/FTO	12	0.49	0.71	7.67	0.48	2.63
Modified CNTs	M-2h-CNT/FTO	2	0.49	0.68	7.56	0.61	3.15
	M-4h-CNT/FTO	4	0.49	0.72	8.57	0.53	3.31
	M-6h-CNT/FTO	6	0.49	0.73	9.34	0.51	3.46
	M-8h-CNT/FTO	8	0.49	0.75	9.78	0.44	3.21
	M-12h-CNT/FTO	12	0.49	0.72	7.39	0.54	2.86
-	Pt/FTO	-	0.49	0.67	9.82	0.59	3.90

Table 3: Summary of the open-circuit (V_{oc}), short-circuit (J_{sc}), fill-factor (FF) and efficiency (η) of the DSSCs as using the Pt, non-modified and modified CNT/FTO films as the cell counter electrode.

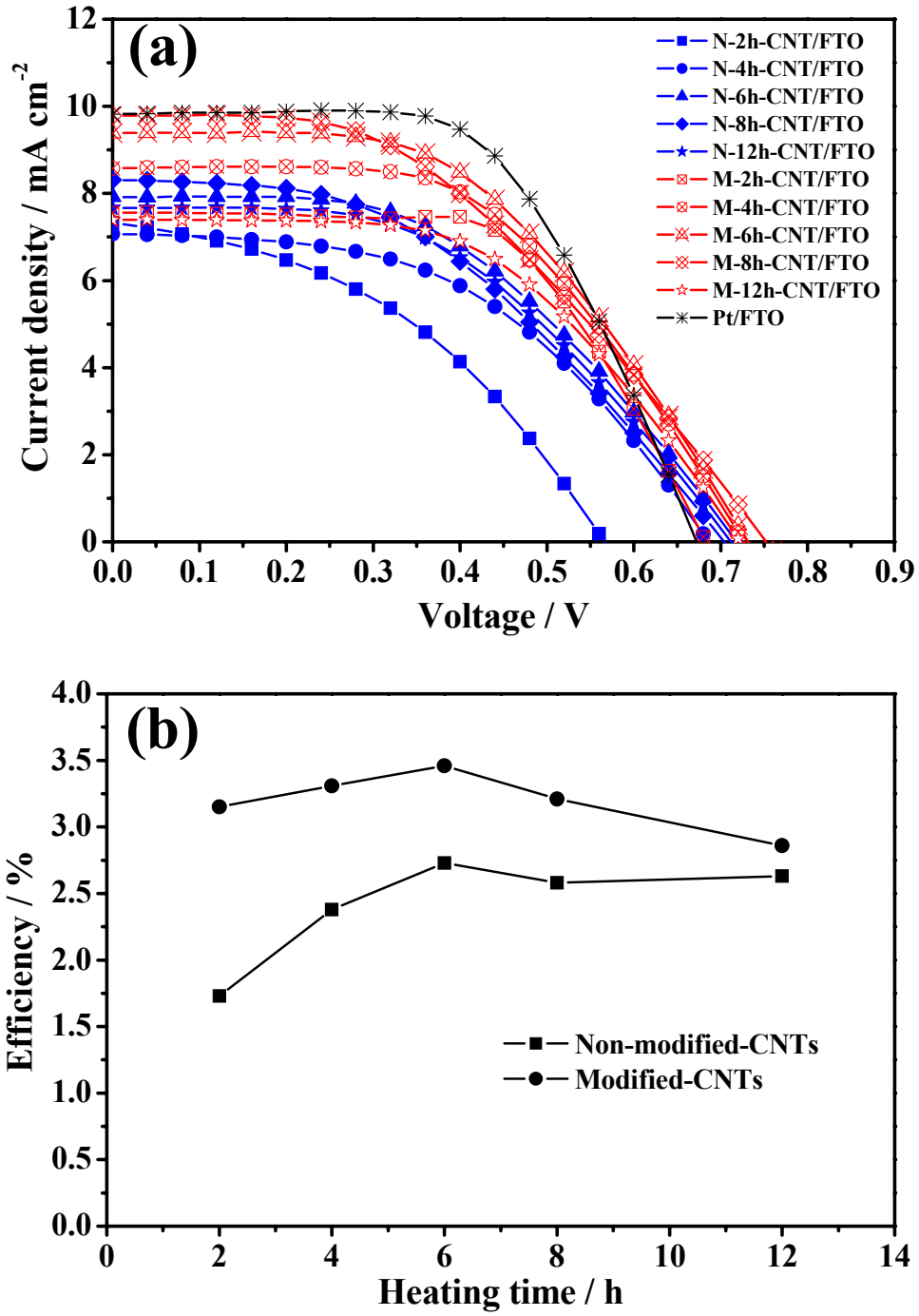

Fig. 24: (a) Plot of the photocurrent density (J) versus the photovoltage (V) and (b) plot of the DSSC efficiency versus the heating time of the non-modified and modified MWCNT/FTO samples.

3.2 Flexible DSSCs

In previous section, we are successfully employing the low temperature carbon nanotube films coated on the conductive glass (MWCNT/FTO) as the DSSC counter electrode. Thus, it should be possible to apply the carbon nanotube film coated on the conductive plastic (MWCNT/ITO/PEN) as the counter electrode. By altering the substrate to the plastic type, the lower production cost, the lighter weight and the flexibility DSSCs should be gained. However, the TiO_2 paste (PST-18NR and PST-400C) is not appropriated in coating the TiO_2 film on the plastic substrate because it contains polymers, which have to be removed at high annealing temperature (400 °C – 500 °C). But, the plastic cannot sustain such a high temperature. Grinis et. al. reported that by compressing TiO_2 film under a high compression pressure, the TiO_2 nanoparticle connectivity is improved resulting in the low TiO_2 film resistance and the high DSSC performance without a high temperature annealing [21]. Fredin et. al. simulation indicates the increase of the electron diffusion coefficient and the photocurrent upon the decrease of the TiO_2 film porosity [45]. Hence, the compression technique may be a suitable approach in depositing TiO_2 film on the conductive plastic substrate. The free polymer TiO_2 slurry, consisted of 5 g TiO_2 (P25) in 20 ml isopropanol, is pasted on the conductive plastic and pressed by the hydraulic pressure at the pressure ~510 MPa.

ลูกลบ: 21

ลูกลบ: 45

Figure 25(a) and 25(b) show the optical images of the un-pressed and pressed TiO_2 films, respectively. It observes that the pressed TiO_2 film is clearer than the un-pressed film, which should be contributed to the denser of TiO_2 nanoparticles. The top and cross-section morphologies of the pressed TiO_2 films are shown in Fig. 25(c) and 25(d), respectively. The thickness of the pressed TiO_2 film estimated from the cross-section SEM is ~1.6 μm.

The amount of dye loaded on the pressed films is analyzed by UV-visible spectrometer, and the result is presented in Fig. 26. Three absorbance spectra in Fig. 26 show the close absorbance value; meaning that the thickness of three TiO_2/ITO/PEN samples are about the same. Hence, with a carefully pasting, the consistence TiO_2 thickness is possible prepared. Note that the solution volume in desorbing dye of the TiO_2/ITO/PEN films is 5 ml, which is a half of a volume of the TiO_2/FTO films (10 ml). By using eqs. (1) and (2), and $\varepsilon_{300} = 5.7\times10^4\ M^{-1}cm^{-1}$, the average amount of dye coated on the pressed TiO_2/ITO/PEN films is $\sim 2.79 \times 10^{-8} \pm 0.20 \times 10^{-8}$ mol. As expected, the amount of dye loaded on the TiO_2/ITO/PEN films is less than the TiO_2/FTO films by ~46% because of the thinner TiO_2 film, as seen in Fig. 25 and 21.

In case of the MWCNT/ITO/PEN films, there are prepared by same method as the MWCNT/FTO films. The carbon film morphologies are characterized and shown in Fig. 27. Interestingly, the low magnification images, Fig. 27(a) and 27(c), indicate the very different structures between the non-modified and modified carbon nanotube films. The modified CNTs is well spread on the ITO/PEN surface, whereas the non-modified CNTs form the island-like structures on the ITO/PEN surface. The well depositing of the modified CNTs on the ITO/PEN surface should be attributed to the strong interaction between functional groups on nanotubes' surface and the functional groups on the ITO/PEN surface [32,46].

ลูกลบ: 32

ลูกลบ: 46

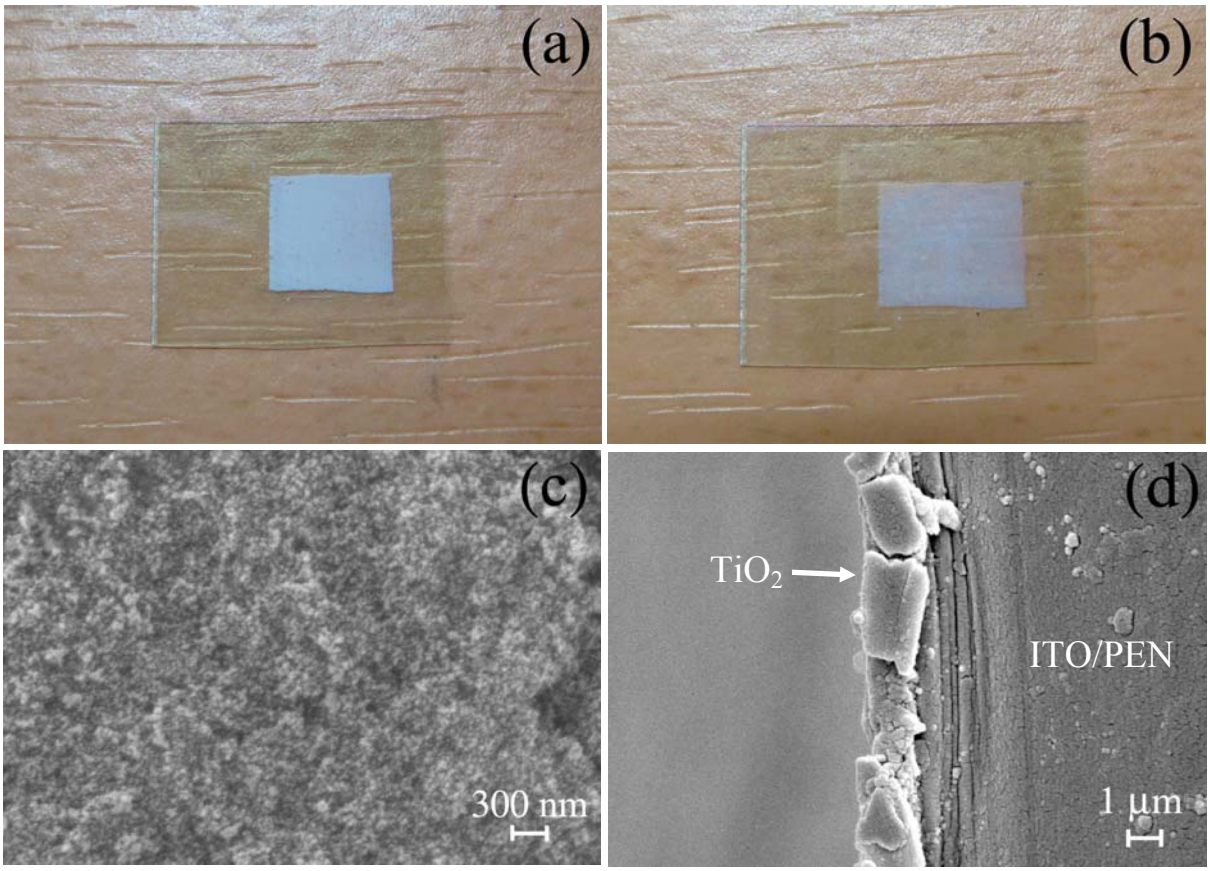

Fig. 25: (a) the optical image of the un-compressed TiO_2 film on ITO/PEN conducting plastic substrate, (b) compressed TiO_2 film on ITO/PEN conducting plastic substrate, (c) top view and (d) the cross-section view of the compressed TiO_2/ ITO/PEN film.

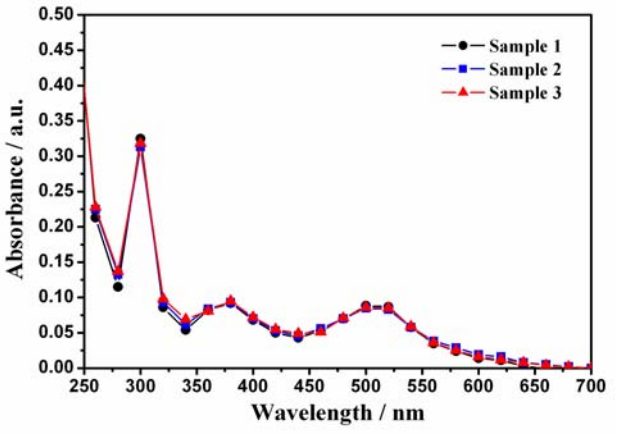

Fig. 26: The absorbance spectra of the desorbed dye solutions of the TiO_2/ITO/PEN plastic samples in the mixture of 5 ml of 0.1 M NaOH and ethanol at volume ratio of 1:1.

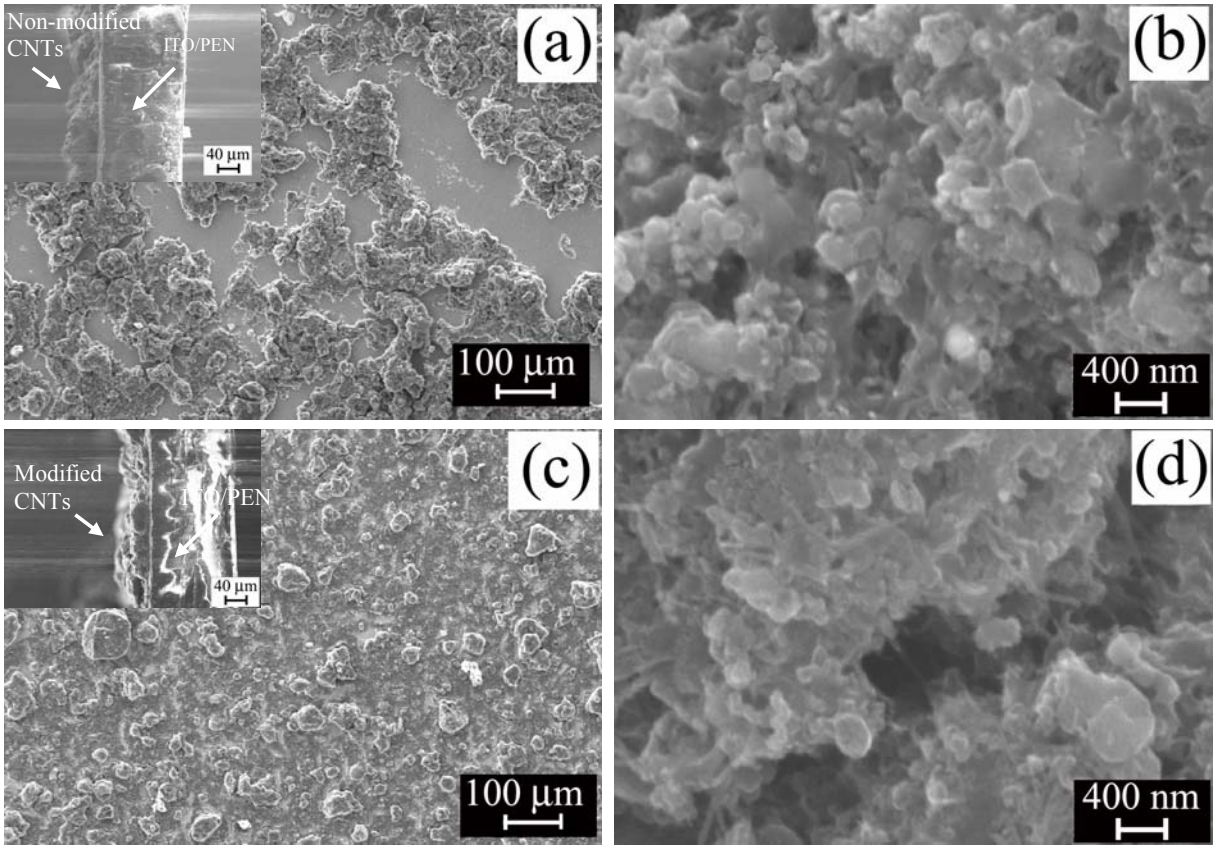

Fig. 27: (a) The low and (b) high magnification images of the non-modified MWCNT/ITO/PEN plastic film annealed for 6 h. (c) The low and (d) high magnification images of the modified MWCNT/ ITO/PEN plastic film annealed for 6 h.

The performance of the flexible DSSCs, using dye/pressed-TiO_2/ITO/PEN film as the working electrode and MWCNT/ITO/PEN film as the counter electrode, are tested, and the result is shown in Fig. 28. J_{sc}, V_{oc}, FF and η are analyzed and summarized in Table 4. Similar behavior to the glass solar cell, the efficiency of the Pt cell is larger than the CNT cells, which further supports the better Pt catalytic activity over the carbon nanotube catalytic activity. The plot of the cell efficiency versus the heating time, Fig. 28(b), exhibits the increasing trend up to six hours and the decreasing trend upon the heating duration similarly to the glass DSSCs. The degradation of the performance above the 6 h heating period may be deducted by the deformation of PVF binder. The efficiency of the flexible solar cells is lower than the glass DSSCs for both the modified and non-mondified carbon nanotube DSSCs. Three reasonable factors in limiting the flexible DSSC performance are: 1) the higher sheet resistance of the conductive plastic (60 Ω/sq) than the conductive glass (15 Ω/sq), 2) the thinner TiO_2/ITO/PEN film (~1.6 μm) than the TiO_2/FTO film (~5.5 μm) and 3) the less amount of dye adsorbed on the TiO_2/ITO/PEN film (2.79×10^{-8} mol) than the TiO_2/FTO film (5.14×10^{-8} mol).

Treatment conditions	Counter electrode	Heating time (h)	Active area (cm^2)	V_{oc} (V)	J_{sc} (mA/cm^2)	FF	η (%)
Non-modified CNTs	N-2h-CNT/ITO/PEN	2	0.49	0.78	2.23	0.16	0.28
	N-4h-CNT/ ITO/PEN	4	0.49	0.77	3.12	0.14	0.34
	N-6h-CNT/ ITO/PEN	6	0.49	0.79	4.07	0.25	0.80
	N-8h-CNT/ ITO/PEN	8	0.49	0.78	3.41	0.20	0.52
	N-12h-CNT/ ITO/PEN	12	0.49	0.79	2.73	0.19	0.40
Modified CNTs	M-2h-CNT/ ITO/PEN	2	0.49	0.79	3.97	0.50	1.16
	M-4h-CNT/ ITO/PEN	4	0.49	0.78	4.64	0.37	1.35
	M-6h-CNT/ ITO/PEN	6	0.49	0.81	4.60	0.57	2.11
	M-8h-CNT/ ITO/PEN	8	0.49	0.81	4.59	0.46	1.70
	M-12h-CNT ITO/PEN	12	0.49	0.80	3.62	0.50	1.44
-	Pt/ ITO/PEN	-	0.49	0.79	5.10	0.61	2.47

Table 2: Summary of the open-circuit (V_{oc}), short-circuit (J_{sc}), fill-factor (FF) and efficiency (η) of the DSSCs as using the Pt, non-modified and modified CNT/ITO/PEN films as the cell counter electrode.

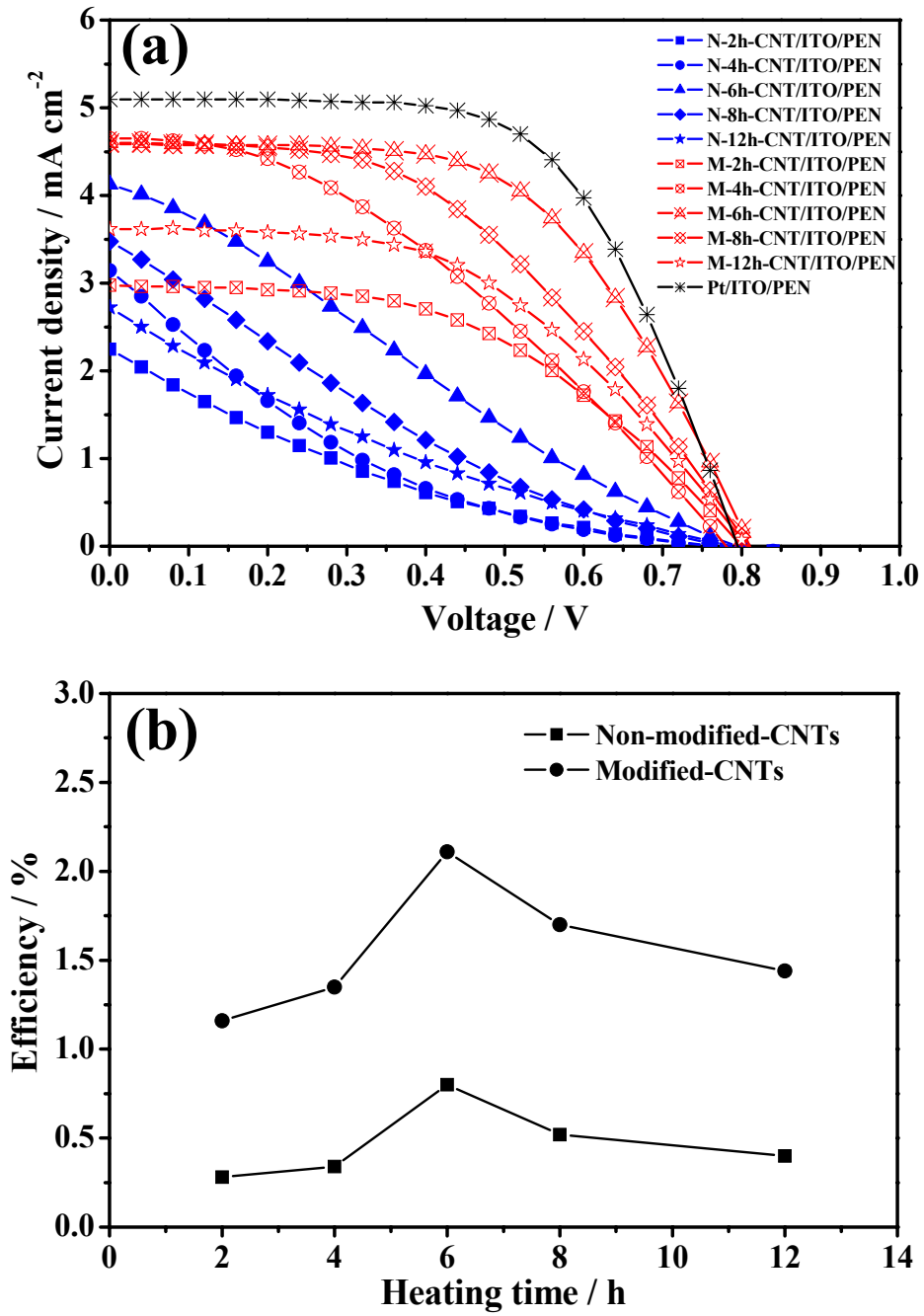

Fig. 28: (a) Plot of the photocurrent density (J) versus the photovoltage (V) and (b) plot of the DSSC efficiency versus the heating time of the non-modified and modified MWCNT/ITO/PEN plastic samples.

Conclusion

In this section, we had studied three different parts: 1) TiO_2 film prepared by the electrophoretic deposition, 2) Carbon film prepared by the electrophoretic deposition and 3) Carbon film prepared by the slurry paste. We found that the longer deposition of TiO_2 films by EPD will induce cracks on TiO_2 film, and the optimum TiO2 thickness for the DSSC application is about 14 um. The longer deposition of the carbon film by EPD also induces more magnesium particles form on the carbon nanotube film, and the magnesium particles low the solar cell efficiency. The carbon film prepared by the slurry paste is found to produce high solar cell efficiency than the carbon film prepared by EPD.

Future work

It sees that the composite polyaniline/carbon nanotube films exhibit a great potential for both supercapacitor and the dye-sensitized solar cell applications. By using polymer, PVF, as a binder, the performance of the supercapacitor and the solar cell is highest as compared to the other preparation techniques. However, PVF is not a conducting polymer so that it may retard the film conductivity resulting in the still low performance of the supercapacitor and the dye-sensitized solar cell. PEDOT:PSS is a conductive polymer, which exhibits strong potential for the supercapacitor and the dye-sensitized solar cell. Therefore, one interest future work is to apply PEDOT:PSS as the polymer binder. The ratio of PEDOT:PSS and nanotube should be investigated in detail in order to obtain the optimum condition for both supercapacitor and dye-sensitized solar cell appllications. One other interesting work is to deposit the thin polyailine film on the carbon nanotube film by the electrochemical and test it as the supecapacotor electrode and the dye sensitized solar cell counter electrode.

Acknowledgement

Author would like to thank mentors for their constructive comments and Wirat Jareenpon, Wasan Miaaugree, Narapon Mumme and Sumarin Inthejun for help with the lab works. Authors would like to thank Associate Professor Werasak Surareungchai for the Autolab system and Intergrated Nanotechnology Research Center (INRC), Khon Kaen University for supplying the conductive glass and the conductive plastic. This work is supported by Thai Research Fund (TRF, grant number MRG5080226).

References

1. H. Shimoda, S.J. Oh, H.Z. Geng, R.J. Walker, X.B. Zhang, L.E. McNeil, and O. Zhou, Adv. Mater. 14 (2002) 899
2. J. P Zheng, P.J. Cygan, and T.R. Jow, *J. Electrochem. Soc.*, 1995; 142(8) 2699.
3. J. P Zheng and T.R. Jow, *J. Electrochem. Soc.*, 1995; 142(1) L6.
4. T.R. Jow and J. P Zheng, *J. Electrochem. Soc.*, 1998; 145(1) 49.
5. Julien Vaillant, Monica Lira-Cantu, Karina Cuentas-Gallegos, Nieves Casan-Pastor, Pedro Gomez-romero, *Progress in Solid State Chemistry*, 2006; 34 147.
6. L. Diederich, E. Barbotini, P. Piseri, A. Podesta, P. Milani, A. Schneuwly, and R. Gallay, *Appl. Phys. Lett.*, 1999; 75(17) 2662.
7. Jian-Shan Ye, Hui Fang Cui, Xiao Liu, Tit Meng Lim, Wei-De Zhang, and Fwu-Shan Sheu, *Small*, 2005; 1(5) 560.
8. E. Frackowiak, V. Khomenko, K. Jurewicz, K. Lota, and F. Beguuin, *J. Power Source*, 2006; 153 413.
9. W. Qin, J.-L. Li, G. Fei, W.-S. Li, K.-Z. Wu, X.-D. Wang, New Carbon Materials, 23(3) (2008) 275.
10. W.-C. Chen, T.-C. Wen and H. Teng, Electrochimica Acta 48 (2003) 641-649.
11. C. Peng, S. Zhang, D. Jewell and G. Z. Chen, Progress in Natural Science 18 (2008) 777.
12. C. Du and N. Pan, Journal of Power Sources 160 (2006) 1487.
13. B. O'Regan, M. Grätzel, Nature 353 (1991) 737.
14. M. Grätzel, J. Photochem. Photobiol. A 164 (2004) 3.
15. K. Tennakone, G.R.R. Kumara, I.R.M. Kottegoda, V.S.P. Perera, Chem. Commun. 1 (1999) 15.
16. K. Sayama, H. Sugihara, H. Arakawa, Chem. Mater. 10 (1998) 3825.
17. Y. Fukai, Y. Kondo, S. Mori, E. Suzuki, Electrochem. Commun. 9 (2007) 1439.
18. T. Miyasaka, Y. Kijitori, T.N. Murakami, M. Kimura, S. Uegusa, Chem. Lett. 12 (2002) 1250.
19. T. Miyasaka, Y. Kijitori, J. Electrochem. Soc. 151 (2004) 1767.
20. J.H. Yum, S.S. Kim, D.Y. Kim, Y.E. Sung, J. Photochem. Photobiol. A 173 (2005) 1.
21. L. Grinis, S. Dor, A. Ofir, A. Zaban, J. Photochem. Photobiol. A 198 (2008) 52.
22. A. Kay, M. Grätzel, Sol. Energy. Mater. Sol. Cell 44 (1996) 99.
23. K. Imoto, K. Takahashi, T. Yamaguchi, T. Komura, J. Nakamura, K. Murata, Sol. Energy Mater. Sol. Cell 79 (2003) 459.
24. T.N. Murakami, M. Grätzel, Inorg. Chim. Acta 361 (2008) 572.
25. K. Suzuki, M. Yamamoto, M. Kumagai, S. Yanagida, Chem. Lett. 32 (2003) 28.
26. P. Balraju, M. Kumar, M.S. Roy, G.D. Sharma, Synthetic Metals 159 (2009) 1325.
27. H.-C. Kuan, C.-C. M. Ma, W.-P. Chang, S.-M. Yuen, H.-H. Wu, T.-M. Lee, Composites Science and Technology 65 (2005) 1703.
28. W. Chen, X. Tao, P. Xue, X. Cheng, Appl. Surf. Sci. 252 (2005) 1404.
29. C. Dhand, S.K. Arya, S.P. Singh, B.P. Singh, M. Datta, B.D. Malhotra, Carbon 46 (2008) 1727.

30. H. Ma, L. Zhang, J. Zhang, L. Zhang, N. Yao, B. Zhang, Appl. Surf. Sci. 251 (2005) 258.
31. C. Du, N. Pan, J. Power Sources 160 (2006) 1487.
32. S.J. Oh, J. Zhang, Y. Cheng, H. Shimoda, O. Zhou, Appl. Phys. Lett. 84 (2004) 3738.
33. B. Gao, G. Guozhen, Z. Yue, Q. Qiu, Y. Cheng, H. Shimoda, L. Fleming, O. Zhou, Adv. Mater. 13 (2001) 1770.
34. A.R. Boccaccini, J. Cho, J.A. Roether, B.J.C. Thomas, E.J. Minay, M.S.P. Shaffer, Carbon 44 (2006) 3149.
35. S. Yang, X. Li, W. Zhu, J. Wang, C. Descorme, Carbon 46 (2008) 445.
36. H. Lindstrőm, A. Holmberg, E. Magnusson, S.-E. Lindquist, L. Malmqvist, A. Hagfeldt, Nano Lett. 1 (2001) 97.
37. H. Lindstrőm, A. Hormberg, E. Magnusson, L. Malmqvist, A. Hagfeldt, J. Photochem. Photobiol. A 145 (2001) 107.
38. T. Miyasaka, Y. Kijitori, J. Electrochem. Soc. 151 (2004) 1767.
39. J.H. Yum, S.S. Kim, D.Y. Kim, Y.E. Sung, J. Photochem. Photobiol. A 173 (2005) 1.
40. G.W. Scherer, J. Am. Ceram. Soc. 73 (1990) 3.
41. R.C. Chiu, T.J. Garino, M.J. Cima, J. Am. Ceram. Soc. 76 (1993) 2257.
42. R.C. Chiu, M.J. Cima, J. Am. Ceram. Soc. 76 (1993) 2769.
43. C. Kaya, F. Kaya, B. Su, B. Thomas, A. R. Boccaccini, Surf. Coat. Technol. 191 (2005) 303.
44. T. Moskalewicz, A. Czyrska-Filemonowicz, A.R. Boccaccini, Surf. Coat. Technol. 201 (2007) 7467.
45. K. Fredin, J. Nissfolk, A. Hagfeldt, Sol. Energy. Mater. Sol. Cell 86 (2005) 283.
46. H. Shimoda, S.J. Oh, H.Z. Geng, R.J. Walker, X.B. Zhang, L.E. McNeil, and O. Zhou, Adv. Mater. 14 (2002) 899.

Appendix I

(Published in **Thin Solid Films**)

Thin Solid Films 517 (2009) 4663–4667

Contents lists available at ScienceDirect

Thin Solid Films

journal homepage: www.elsevier.com/locate/tsf

Optimization of titanium dioxide film prepared by electrophoretic deposition for dye-sensitized solar cell application

Wirat Jarernboon, Samuk Pimanpang *, Santi Maensiri, Ekaphan Swatsitang, Vittaya Amornkitbamrung

Integrated Nanotechnology Research Center, Department of Physics, Faculty of Science, Khon Kaen University, Khon Kaen, 40002, Thailand

ARTICLE INFO

Article history:
Received 17 December 2007
Received in revised form 10 February 2009
Accepted 17 February 2009
Available online 5 March 2009

Keywords:
Electrophoretic deposition
Titanium dioxide
Dye-sensitized solar cell

ABSTRACT

Nanocrystalline TiO_2 films were deposited on a conducting glass substrate by the electrophoretic deposition technique. It was found that the thickness of TiO_2 film increased proportionally with an increase in deposition time and deposition voltage. However, as the deposition duration or deposition voltage increased, the film surface was more discontinuous, and microcracks became more evident. The characteristic of the dye-sensitized solar cell using TiO_2 film as a working electrode was analyzed. The results of the energy conversion efficiency and the photocurrent density exhibited a relationship dependent on the TiO_2 thickness. Curve fitting of energy conversion efficiency vs. TiO_2 thickness revealed the optimum solar cell efficiency ~2.8% at the film thickness of ~14 μm.

1. Introduction

Dye-sensitized solar cells (DSSC) have been an intensive research topic due to their promising light conversion efficiency and low production cost. Since O'Regan and Grätzel [1] discovered the dye-sensitized solar cell in 1991, the efficiency of the dye-sensitized solar cell has much improved compared to those first reported in O'Regan and Grätzel's work. The recent highest efficiency reported in the literature is more than 10% [2]. At present, various wide band gap materials are used for fabricating the working electrode such as TiO_2, ZnO, SnO_2 and Nb_2O_5 [1–6]. TiO_2 is one of the widely used materials for preparing the DSSC working electrode because it provides a high energy conversion efficiency [7–12].

There are various ways in preparing TiO_2 electrodes such as sputtering, thermal evaporation, doctor-blade and electrophoretic. Recently, electrophoretic deposition (EPD) has a great deal of attention because it has a fast deposition rate, simple apparatus, no restriction on the substrate shape, and no binder required. Thus, a sample can be prepared from any kind of conductive substrate shape, and the EPD technique can be adapted to mass production processing. In addition, the electrophoretic deposition does not require a high temperature during the deposition process so that it is possible to prepare a thick TiO_2 film on a flexible conducting plastic [13–15].

It has been reported that TiO_2 nanoparticles can be deposited on a conducting substrate by electrophoretic deposition [15,19–23]. Grinis et al. have used an electrophoretic TiO_2 film as a working electrode of a DSSC [20]. They observed that with the addition of film annealing or film compression, the DSSC performance is further improved. This is because the TiO_2 nanoparticles are more connected to each other resulting in better electron transport to the conductive substrate. However, the effects of the deposition voltage and deposition duration on the film surface morphology and the energy conversion efficiency of a DSSC have not been characterized in details. Therefore, in this work, we have further investigated the effects of the deposition voltage and deposition duration on the film morphology and the solar cell energy conversion efficiency. Possible causes are discussed in this work.

2. Experimental details

In this experiment, an FTO (F-SnO_2 coated glass, sheet resistance 15 Ω/□, Solaronix SA) was used as a conducting substrate for both the working electrode and counter electrode. The TiO_2 films were prepared on the conducting substrate by EPD. The schematic setup of EPD is shown in Fig. 1. The TiO_2 suspension consists of 0.5 g nanocrystalline

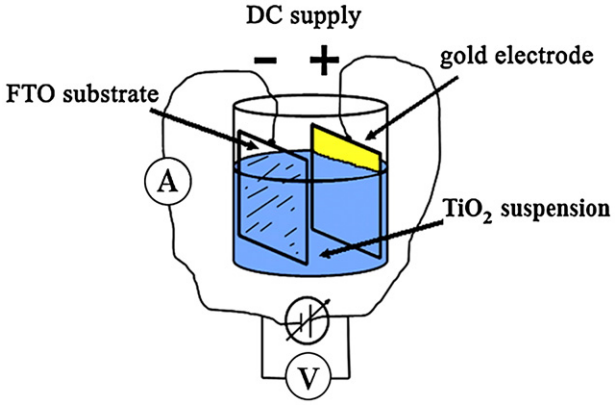

Fig. 1. Schematic of the electrophoretic deposition (EPD) setup.

* Corresponding author. Tel.: +66 43 202222 39x2248; fax: +66 43 202374.
E-mail address: samukpi@kku.ac.th (S. Pimanpang).

0040-6090/$ – see front matter © 2009 Elsevier B.V. All rights reserved.
doi:10.1016/j.tsf.2009.02.129

TiO_2 powder (P25, 20 nm, Degussa,Germany) and 0.04 g Iodine (I_2) (Aldrich, 99.8%) in 50 mL of Acetylacetone (Aldrich, 99.5%). The TiO_2 solution was sonicated for 30 min before the deposition. Gold sheet was used as an anode, and the distance between the FTO substrate and the anode was fixed at 1 cm. Various conditions such as deposition voltage at 5, 10, 15 and 20 V and deposition duration of 1, 2 and 8 min were used to prepare the TiO_2 films. After EPD, the films were heated at 450 °C for 1 h in ambient conditions to improve TiO_2 nanoparticle connection.

The post heated electrodes were immersed in the dye solution, *cis*–bis(isothiocyanato)bis(2,2′-bipyridyl-4,4′-dicarboxylato)-ruthenium (II)-bis-tetrabutylammonium (N719 dye, 5×10^{-4} M in ethanol, Solaronix SA), for 24 h at room temperature. The sputtered Pt on FTO substrate was used as the counter electrode. The working electrode and counter electrode were sandwiched and filled with the liquid electrolyte, which consisted of 0.5 M LiI, 0.1 M I_2, and 0.5 M *tert*-butylpyridine (TBP) in 3-methoxypropionitrile. A 60 μm thick polymer film (Solaronix

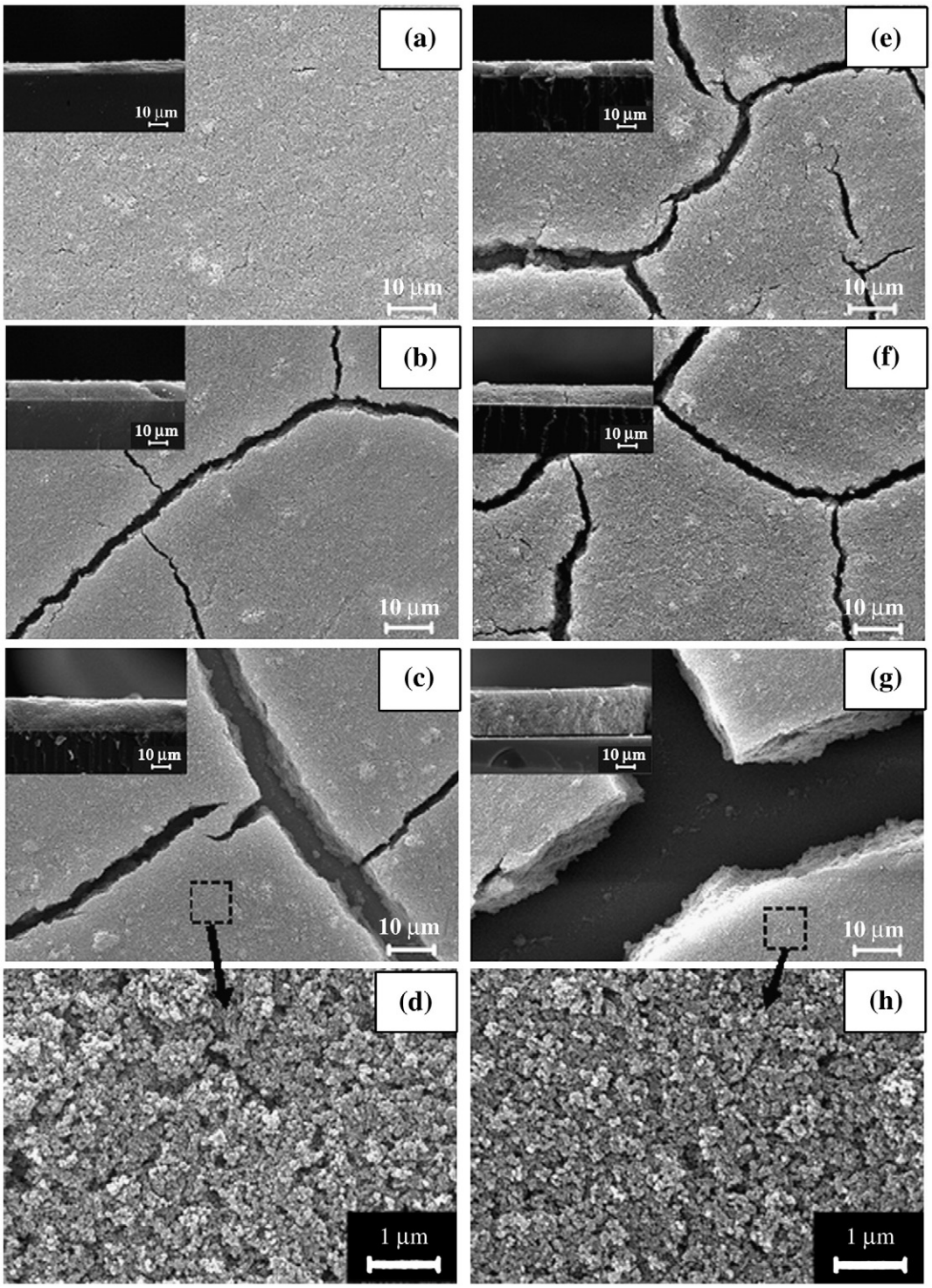

Fig. 2. Top and side view SEM images of the TiO_2 film prepared by the EPD technique at various deposition voltages and duration times: (a) 5 V for 1 min, (b) 5 V for 2 min, (c) 5 V for 8 min, (d) 5 V for 8 min (high magnification), (e) 20 V for 1 min, (f) 20 V for 2 min, (g) 20 V for 8 min, (h) 20 V for 8 min (high magnification).

SA) were used as a spacer and a sealant between the working and counter electrodes. The active area of the solar cell was 1.0 cm^2.

The photocurrent–voltage of these samples was measured with a super solar simulator (WACOM, Class A) system under 1 sun at an air mass (AM) 1.5 global filter (100 mW/cm^2). The surface morphologies and film thickness were characterized by scanning electron microscopy (SEM, LEO, SEM 1450VP, UK) with operating at 20.0 kV. The amount of absorbed dye on the electrophoretically TiO_2 film was estimated by UV–Vis absorption measurement (UV-160A, SHIMADZU). The absorbed dye was desorbed from the TiO_2 samples by soaking in 15 mL of a mixed solution of 0.1 M NaOH and ethanol at a volume ratio 1:1.

3. Results and discussion

3.1. TiO_2 surface morphology

The surface morphology of the TiO_2 films was analyzed by SEM, as shown in Fig. 2. SEM analysis reveals that the TiO_2 surface was comprised of a number of cracks. The size of cracks was found to be on the micrometer scale, and the length of cracks seemed to depend on the deposition voltage and deposition duration. The length of cracks on the TiO_2 films prepared at 5 V for 1 min was about 1–5 μm, as observed in Fig. 2(a). However, the length of cracks on the film prepared at 5 V for 2 and 8 min was remarkably long being even greater than 100 μm, as shown in Fig. 2(b) and (c), respectively. Many reasons have been proposed for the mechanism of crack formation in the inorganic film such as a rapid evaporation of the solvents from the film surface during the drying process, a decrease of TiO_2 particle bonding strength as the film thickens, and a mismatch of the thermal expansion between the FTO substrate and the TiO_2 film [16–18]. The film prepared at 20 V for 8 min had the largest crack length compared to other films, as observed in Fig. 2(g). Microcracks formed on the TiO_2 film prepared by EPD were also reported by other groups [19,21–22].

Beside the formation of microcracks on the sample surface, the TiO_2 surface was covered with nanopores, which were uniformly distributed on the surface as observed with a high magnification SEM images (Fig. 2(d) and (h)). The presence of nanopores on the film should have a huge advantage to a dye-sensitized solar cell

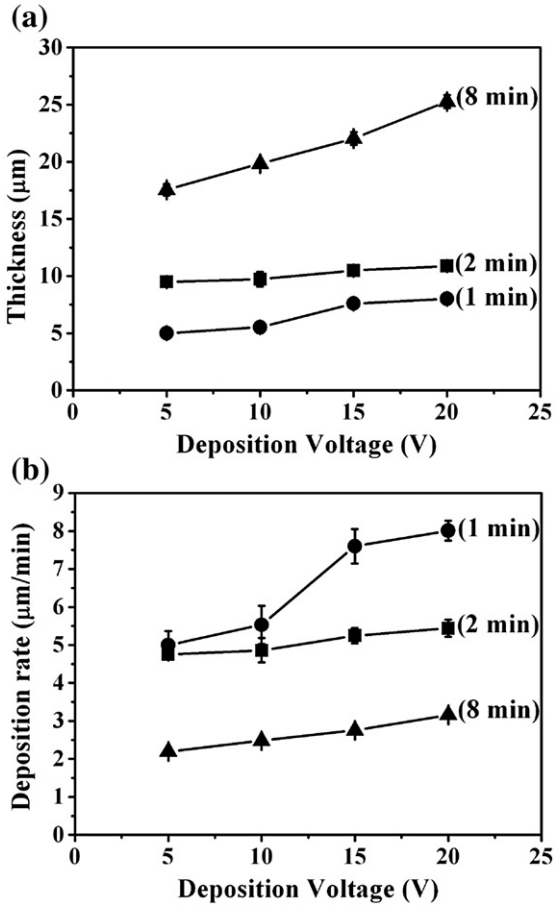

Fig. 3. (a) Plot of the TiO_2 thickness vs. the deposition voltage at various deposition times: 1, 2 and 8 min, (b) plot of the TiO_2 deposition rate vs. the deposition voltage at various deposition times: 1, 2 and 8 min.

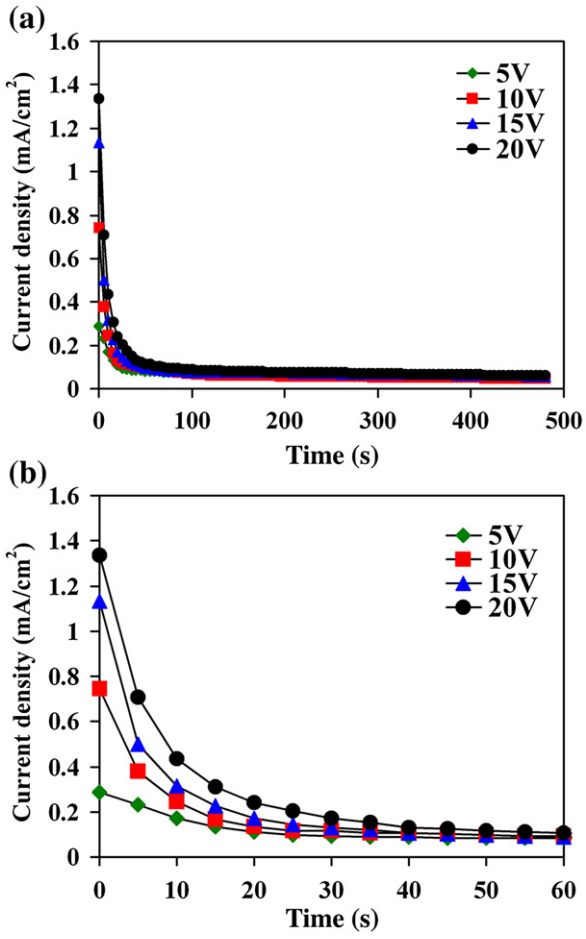

Fig. 4. Plot of the current density vs. the deposition time at 5, 10, 15 and 20 V for 8 min samples: (a) the current density curves of whole 8 min deposition duration time, and (b) the zoom-in current density curves of the first 60 s deposition duration time.

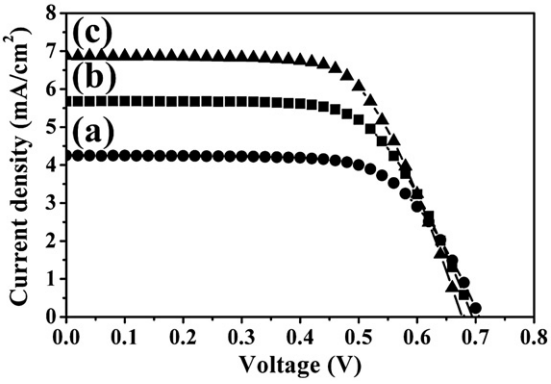

Fig. 5. The *J–V* characteristics of the DSSC assembled of TiO_2 films deposited at 5 V for three different deposition duration times, (a) 1 min, (b) 2 min, and (c) 8 min as the working electrode.

application. This is because nanopores would allow dye molecules to penetrate deeply into the TiO_2 film resulting in more dye absorbed on the TiO_2 film and a larger interfacial area between the working electrode and the electrolyte.

It was observed that different deposition conditions would cause a difference on the film surface. An increase in the deposition voltage and deposition duration also significantly increased film thickness as illustrated in Fig. 3(a). The thickness of the TiO_2 film prepared at 20 V for 8 min was ~25.3 μm, whereas the thickness of the TiO_2 film prepared at 5 V for 1 min was only ~5.0 μm. The plot of the deposition rate vs. the deposition voltage (Fig. 3(b)) exhibited an increasing trend with a function of the deposition voltage for all three-deposition times. However, the deposition rate shows a decreasing trend with the deposition duration, as observed in Fig. 3(b). The reduction of the deposition rate with the prolonged deposition duration may be due to an agglomeration of TiO_2 particles in the solvent, which consequently lowered the particle diffusion rate.

The reduction of the TiO_2 deposition rate was also due to the formation of an insulating layer on the conducting glass surface as more TiO_2 particles deposited on the substrate [24]. The rising of the film resistance as the TiO_2 film gets thicker accompanies a decreasing deposition current density as shown in Fig. 4. Fig. 4 reveals that the current density of the 20 V deposition voltage was higher than that of the 5, 10 and 15 V deposition voltages. This implies that the high deposition voltage promotes more TiO_2 particles deposited on the substrate. Hence, the current density result (Fig. 4) agrees well with the film thickness result (Fig. 3(a)). Basu et al. [25] similarly observed decreasing deposition rate of Zirconia particles with the deposition time at a fixed applied voltage.

3.2. Solar cell efficiency

The solar cell characteristic of the dye coated TiO_2 films as the working electrodes were analyzed at an irradiation of a 100 mW/cm^2 under a standard air mass (AM) 1.5 global filter. In Fig. 5, the current density–voltage curves show that the open circuit voltage (V_{oc}) and the short circuit current density (J_{sc}) of the TiO_2 films prepared at the 5 V for 1, 2 and 8 min were 0.70, 0.69 and 0.68 V, and 4.26, 5.70 and 6.93 mA/cm^2, respectively. The fill factor (FF) and energy conversion efficiency (η) of the TiO_2 films prepared at the 5 V for 1, 2 and 8 min were 0.68, 0.66 and 0.65, and 2.03, 2.60 and 3.06%, respectively. Hence, the J_{sc} and η values increased with an increase of the TiO_2 deposition duration. This was because the film thickness of the longer deposition duration was larger than that of the shorter deposition duration, as shown in Fig. 3(a).

The plot of the short circuit current density and the energy conversion efficiency vs. the film thickness (Fig. 6(a) and (b)) showed a dependent relationship with the TiO_2 thickness. From Fig. 6(a) and (b), the curve fitting of J_{sc} and η vs. the film thickness can be divided into two distinctive regions. The first region is at film thickness below 14 μm and the second region is at film thickness above 14 μm. In the first region (below 14 μm), the J_{sc} and η values increased with the TiO_2 thickness. The increase of J_{sc} and η with the TiO_2 thickness should be due to more TiO_2 nanoparticles being available for dye coating. To confirm this, the amount of absorbed dye on the TiO_2 film was analyzed by a UV–Vis adsorption spectroscopy. Fig. 6(a) and (b) shows a plot of the amount of absorbed dye on the TiO_2 film vs. the film thickness. It was observed that the amount of absorbed dye increases with the TiO_2 thickness; implying that there were more dye molecules absorbed on the thicker film than on the thinner film. This should contribute to the thicker film containing more TiO_2 nanoparticles than the thinner film. However, the J_{sc} and η values in the second region (above 14 μm thick) were reduced as the film became thicker even though the amount of dye loading increases, as observed in Fig. 6(a) and (b). The more dye molecules absorbed on the thicker TiO_2 film should generate more free charge carriers resulting in a higher conversion efficiency than the thinner film. In contrast, it was observed that above 14 μm thickness, the J_{sc} and η values decreased with the increase of the TiO_2 thickness and the amount of absorbed dye. The

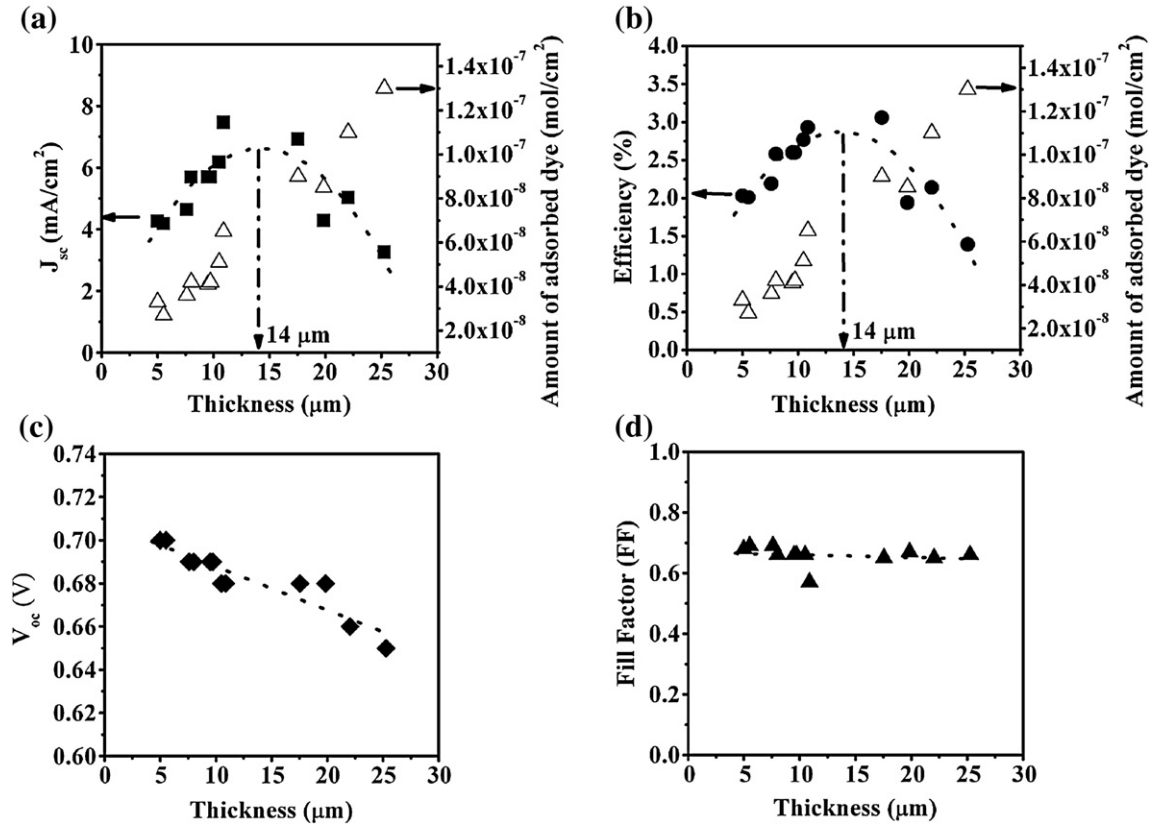

Fig. 6. Plot of (a) the current density (J_{sc}) and the amount of absorbed dye, (b) the energy conversion efficiency (η) and the amount of absorbed dye, (c) the open circuit voltage (V_{oc}) and (d) the fill factor (FF) and the curve fittings vs. the TiO_2 thickness.

reduction of J_{sc} with the film thickness suggests the decrease of the amount of free generated electrons reaching the conductive substrate. Hara et al. observed that the thick TiO_2 film contains more defects than the thin film [26]. These defects would cause carrier recombination, and subsequently lower the current density and the energy conversion efficiency. Therefore, the degradation of the DSSC conversion efficiency in the second region (above 14 μm) should be due to the high carrier recombination. The decrease of V_{oc} from 0.70 V to 0.65 V (Fig. 6(c)), and FF from 0.68 to 0.66 (Fig. 6(d)) with the increase of the film thickness further supports a higher carrier recombination with TiO_2 thickness.

The curve fittings of the current density and the energy conversion efficiency vs. the film thickness, Fig. 6(a) and (b), respectively, suggest that the optimum TiO_2 thickness should be ~14 μm, which will yield a highest solar cell efficiency of ~2.8%. This means that to obtain the highest energy conversion efficiency from this system, the thickness of the TiO_2 film should be about 14 μm. It is worth noticing that our observation of the optimum TiO_2 thickness of 14 μm was close to the optimum thickness (~15 μm) reported by Kim et al. where their TiO_2 films were prepared by a laser direct-write (LDW) technique [27].

4. Conclusion

Nanocrystalline TiO_2 films were prepared on FTO substrates by the EPD technique. The film thickness correlated with increase of the deposition voltage and deposition time. It was observed that the amount and size of microcracks increased with an increase in film thickness. The film deposited at 20 V for 8 min had the largest crack size and the largest empty space compared to other samples. The amount of absorbed dye was found to increase with the TiO_2 thickness. The decrease of J_{sc} and η at above 14 μm TiO_2 thickness may be due to an increase in carrier recombination. In this work, through curve fitting of the DSSC efficiency vs. the film thickness, we found that the optimum TiO_2 film thickness was ~14 μm with the highest DSSC efficiency of ~2.8%.

Acknowledgments

Authors would like to thank the Department of Biology for providing the SEM facility and the National Science and Technology Development Agency (NSTDA) of Thailand for providing Super Solar Simulator facility. This work is supported by the Thailand Research Fund (MRG5080226), The Integrated Nanotechnology Center, Khon Kaen University, and PED project (Physics), The Commission on Higher Education, The Ministry of Education, Thailand.

References

[1] B. O'Regan, M. Grätzel, Nature 353 (1991) 737.
[2] M. Grätzel, J. Photochem. Photobiol. A 164 (2004) 3.
[3] T.N. Rao, L. Bahadur, J. Electrochem. Soc. 144 (1997) 179.
[4] B. O'Regan, V. Sklover, M. Grätzel, J. Electrochem. Soc. 148 (2001) 498.
[5] Y. Fukai, Y. Kondo, S. Mori, E. Suzuki, Electrochem. Commun. 9 (2007) 1439.
[6] P. Guo, M.A. Aegerter, Thin Solid Films 351 (1999) 290.
[7] F. Pichot, J.R. Pitts, B.A. Gregg, Langmuir 16 (2000) 5626.
[8] M.-A. De Paoli, A.F. Nogueira, D.A. Machado, C. Longo, Electrochim. Acta 46 (2001) 4243.
[9] C. Longo, A.F. Nogueira, M.-A. De Paoli, H. Cachet, J. Phys. Chem. B 106 (2002) 5925.
[10] H. Lindstrőm, A. Holmberg, E. Magnusson, S.-E. Lindquist, L. Malmqvist, A. Hagfeldt, Nano Lett. 1 (2001) 97.
[11] H. Lindstrőm, A. Hormberg, E. Magnusson, L. Malmqvist, A. Hagfeldt, J. Photochem. Photobiol. A 145 (2001) 107.
[12] T. Miyasaka, M. Ikegami, Y. Kijitori, J. Electrochem. Soc. 154 (2007) 455.
[13] T. Miyasaka, Y. Kijitori, T.N. Murakami, M. Kimura, S. Uegusa, Chem. Lett. 12 (2002) 1250.
[14] T. Miyasaka, Y. Kijitori, J. Electrochem. Soc. 151 (2004) 1767.
[15] J.H. Yum, S.S. Kim, D.Y. Kim, Y.E. Sung, J. Photochem. Photobiol. A 173 (2005) 1.
[16] G.W. Scherer, J. Am. Ceram. Soc. 73 (1990) 3.
[17] R.C. Chiu, T.J. Garino, M.J. Cima, J. Am. Ceram. Soc. 76 (1993) 2257.
[18] R.C. Chiu, M.J. Cima, J. Am. Ceram. Soc. 76 (1993) 2769.
[19] C. Kaya, F. Kaya, B. Su, B. Thomas, A.R. Boccaccini, Surf. Coat. Technol. 191 (2005) 303.
[20] L. Grinis, S. Dor, A. Ofir, A. Zaban, J. Photochem. Photobiol. A 198 (2008) 52.
[21] T. Moskalewicz, A. Czyrska-Filemonowicz, A.R. Boccaccini, Surf. Coat. Technol. 201 (2007) 7467.
[22] C.K. Lin, T.J. Yang, Y.C. Feng, T.T. Tsung, C.Y. Su, Surf. Coat. Technol. 200 (2006) 3184.
[23] Q.T. Vu, M. Pavlik, N. Hebestreit, J. Pfleger, U. Rammelt, W. Plieth, Electrochim. Acta 51 (2005) 1117.
[24] L. Besra, M. Liu, Prog. Mater. Sci. 52 (2007) 1.
[25] R.N. Basu, C.A. Randall, M.J. Mayo, J. Am. Ceram. Soc. 84 (2001) 33.
[26] K. Hara, T. Horiguchi, T. Kinoshita, K. Sayama, H. Sugihara, H. Arakawa, Sol. Energy Mater. Sol. Cells 64 (2000) 115.
[27] H. Kim, G.P. Kushto, C.B. Arnold, Z.H. Kafafi, A. Piqué, Appl. Phys. Lett. 85 (2004) 464.

Appendix II

(Published in **Synthetic Metals**)

Synthetic Metals 159 (2009) 1996–2000

Contents lists available at ScienceDirect

Synthetic Metals

journal homepage: www.elsevier.com/locate/synmet

Influences of magnesium particles incorporated on electrophoretically multiwall carbon nanotube film on dye-sensitized solar cell performance

Samuk Pimanpang[a,*], Wasan Maiaugree[a], Wirat Jarernboon[b], Santi Maensiri[a], Vittaya Amornkitbamrung[a]

[a] Department of Physics, Faculty of Science, Khon Kaen University, Khon Kaen 40002, Thailand
[b] College of Nanotechnology, Faculty of Science, King Mongkut's Institute of Technology Ladkrabang, Bangkok 10520, Thailand

ARTICLE INFO

Article history:
Received 6 January 2009
Received in revised form 13 June 2009
Accepted 6 July 2009
Available online 15 August 2009

Keywords:
Dye-sensitized solar cell
Multiwall carbon nanotube
Electrophoretic deposition

ABSTRACT

Multiwall carbon nanotube (MWCNT) films are prepared on a conductive substrate by electrophoretic deposition. The thickness of MWCNT films is found to increase with the carbon nanotube concentration and the deposition duration. Scanning electron microscopy and energy dispersive X-ray measurements detect magnesium particles incorporated on the MWCNT films. The performance of dye-sensitized solar cell using the electrophoretically MWCNT films as a counter electrode shows a relationship dependent on the film thickness and the amount of magnesium loading. The increase in the magnesium loading on carbon films diminishes the solar cell efficiency. This is because magnesium particles cover the carbon nanotube surface reducing the nanotube catalytic sites and blocking electron transfer to tri-iodide (I_3^-) ions.

1. Introduction

Since the discovery of dye-sensitized solar cell (DSSC) by O'Regan and Grätzel in 1991 [1], the efficiency of DSSC has been continuously improved. The highest DSSC efficiency reported in the literature is ~10% [2]. With its promising efficiency, low production cost and environmental friendliness, DSSC has received a great attention as a possible alternative energy source. The liquid dye-sensitized solar cell consists of three main parts which are a working electrode, a liquid electrolyte and a counter electrode. The working electrode is commonly fabricated of titanium dioxide (TiO_2) nanoparticles because TiO_2 nanoparticle provides the highest energy conversion efficiency among other semiconductors (ZnO, NiO, SnO_2). The higher light adsorption coefficient of the working electrode can be achieved through an introduction of dye molecules onto the TiO_2 surface via monolayer chemisorption [2]. The liquid electrolyte consists of iodide (I^-) and tri-iodide (I_3^-) as a redox couple. In the case of the counter electrode, a platinum (Pt) film is usually used as the DSSC counter electrode because Pt is a very good catalyst. Beside Pt, other materials have also been tested for a potential DSSC counter electrode such as carbon black and carbon nanotubes (CNTs) [3–5].

Carbon nanotube is considered for use as the DSSC counter electrode because of its unique properties such as good catalytic activity, good conductivity, high aspect ratio, stability in ambient conditions and being relatively cheaper than Pt. Therefore, by using carbon nanotubes as the DSSC counter electrode, the DSSC production cost should be minimized. There are several methods in preparing carbon nanotube and TiO_2 films such as screen-printing, doctor blade, sputtering, chemical vapor deposition or electrophoretic deposition. Electrophoretic deposition (EPD) is one technique that can prepare both TiO_2 and carbon nanotube films on a conductive substrate. EPD uses an electrostatic force between a particle and a substrate in attracting a particle of interest to the substrate; implying that the surface of the particles of interest must be enclosed by either positive or negative charges. The surface of TiO_2 nanoparticles comprises of a negative hydroxyl group so that it can establish the electrostatic attraction force with the substrate and be deposited onto the substrate by the EPD method. The electrophoretic TiO_2 film had been successfully applied as the DSSC working electrode by many groups [6–9]. Grinis et al. observed that with a multilayer deposition of TiO_2 film prepared by EPD combined with high pressure compression, an efficiency of ~8% could be accomplished [6].

In the case of carbon nanotubes (CNTs), its surface is not covered by any charge so it needs to be modified prior to use in electrophoretic deposition. The acid treatment (H_2SO_4:HNO_3) is commonly used in introducing a negative carboxylic group on the nanotube surface. A small amount of modified carbon nanotubes can be deposited on an anode surface by EPD, but the film quality is not that homogeneous. With a small addition of $Mg(NO_3)_2{\cdot}6H_2O$ into the carbon nanotube solution, the nanotube deposition rate

* Corresponding author. Tel.: +66 84 980 5339.
E-mail address: samukpi@kku.ac.th (S. Pimanpang).

0379-6779/$ – see front matter © 2009 Elsevier B.V. All rights reserved.
doi:10.1016/j.synthmet.2009.07.008

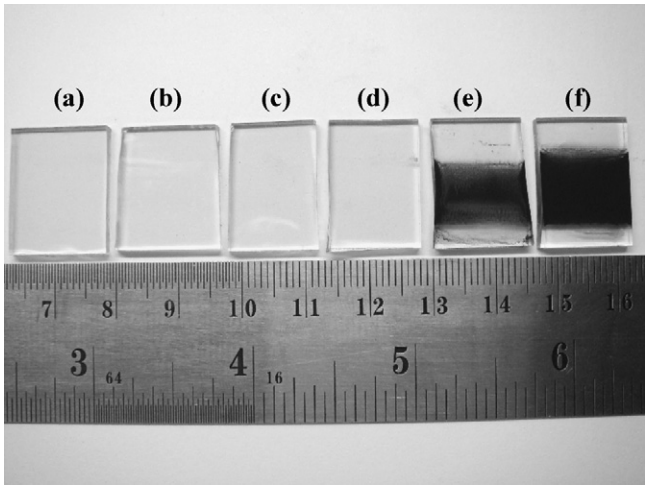

Fig. 1. The optical images of (a) the conductive glass, (b) the magnesium film (EPD in the $Mg(NO_3)_2{\cdot}6H_2O$ solution for 4 min, (c) the WO-Mg-0.02-g-CNT-4-min film (EPD in the without $Mg(NO_3)_2{\cdot}6H_2O$ + 0.02 g CNT solution for 4 min), (d) the WO-Mg-0.04-g-CNT-4-min film, (e) the W-Mg-0.02-g-CNT-4-min film (EPD in the with $Mg(NO_3)_2{\cdot}6H_2O$ + 0.02 g CNT solution for 4 min), (f) the W-Mg-0.02-g-CNT-4-min film.

and the film homogeneity are significantly improved as seen in Fig. 1. This is because Mg^{2+} ions surround the negative CNT surface and strengthen the electrostatic attraction force between carbon nanotubes and the cathode. The electrophoretic carbon nanotube film has been tested for many applications such as in biosensors, supercapacitors and field emissions [10–16]. However, there is no report in using the electrophoretic carbon nanotube film as the DSSC counter electrode. Thus, in this work, we explored the possibility of using the electrophoretically MWCNT film as the DSSC counter electrode. The effects of the carbon nanotube film thickness and the amount of magnesium loading on the carbon films to the solar cell performance were analyzed and discussed in detail.

2. Experimental

2.1. Modification of MWCNTs

Multiwall carbon nanotubes (MWCNTs) were purchased from Chiang Mai University, Thailand. MWCNTs were modified by the mixed acids (H_2SO_4:HNO_3 at a volume ratio of 3:1) for 30 min at room temperature prior to use in order to generate a carboxylic group on the nanotube surface. Then, the carbon solution was diluted with deionized water and filtered with filter paper. The modified carbon nanotubes were rinsed with deionized water three times and dried at 80 °C at the ambient conditions.

2.2. Preparation of TiO_2 and MWCNT films

The FTO (F-SnO_2 coated glass, sheet resistance of 15 Ω/□, Solaronix) was used as a substrate for coating both TiO_2 and MWCNT films by EPD. The TiO_2 solution consists of 0.25 g nanocrystalline TiO_2 powder (P25, 20 nm, Degussa, Germany) and 0.0025 g $Mg(NO_3)_2{\cdot}6H_2O$ in 50 ml of methanol. The TiO_2 suspension was sonicated in an ultrasonic bath for 20 min before EPD deposition. A stainless steel plate was used as an anode electrode, and the distance between the anode and the FTO substrate was fixed at 1 cm. The TiO_2 films were prepared at 10 V for 30 s, and then films were annealed at 550 °C for 1 h at the ambient conditions. The post-annealed TiO_2 films were immersed in the dye solution, *cis*-bis(isothiocyanato)bis(2,2′-bipyridyl-4,4′-dicarboxylato)-ruthenium(II)-bis-tetrabutylammonium (N719, Solaronix, 5×10^{-4} M in ethanol) for 24 h at room temperature.

MWCNT films were prepared from two different carbon nanotube concentrations: (1) 0.02 g MWCNTs + 0.005 g $Mg(NO_3)_2{\cdot}6H_2O$ in 60 ml of methanol (called W-Mg-0.02-g-CNT film) and 0.02 g MWCNTs in 60 ml of methanol (called WO-Mg-0.02-g-CNT film), and (2) 0.04 g MWCNTs + 0.005 g $Mg(NO_3)_2{\cdot}6H_2O$ in 60 ml of methanol (called W-Mg-0.04-g-CNT film) and 0.04 g MWCNTs in 60 ml of methanol (called WO-Mg-0.04-g-CNT film). MWCNT films were deposited at 30 V for two different deposition durations (1 and 4 min), and annealed at 450 °C for 1 h. Magnesium film was prepared from the 0.005 g $Mg(NO_3)_2{\cdot}6H_2O$ in 60 ml of methanol solution at 30 V for 4 min, and also annealed at 450 °C for 1 h.

The dye-sensitized solar cell was assembled using TiO_2 film as the working electrode and the conductive glass, magnesium film, MWCNT film as the counter electrode with an active area of 1 cm × 1 cm. These two films were sandwiched together with a 60-μm thick Surlyn polymer film (Solaronix). A liquid electrolyte was filled into the cell by capillary action through the plastic holes. After electrolyte filling, holes were sealed for preventing electrolyte evaporation. The liquid electrolyte was a mixture of 0.5 M LiI, 0.1 M I_2, 0.5 M *tert*-butylpyridine (TBP) in 3-methoxypropionitrile solvent.

2.3. Film characterization

The optical camera (Sony, DSC-T20) was used to take an image of the conductive glass, magnesium film and CNT films. The surface morphology and thickness of TiO_2 and MWCNT films were characterized by scanning electron microscopy (SEM, LEO, SEM 1450VP, UK). The incorporated elements and chemical bonding on carbon

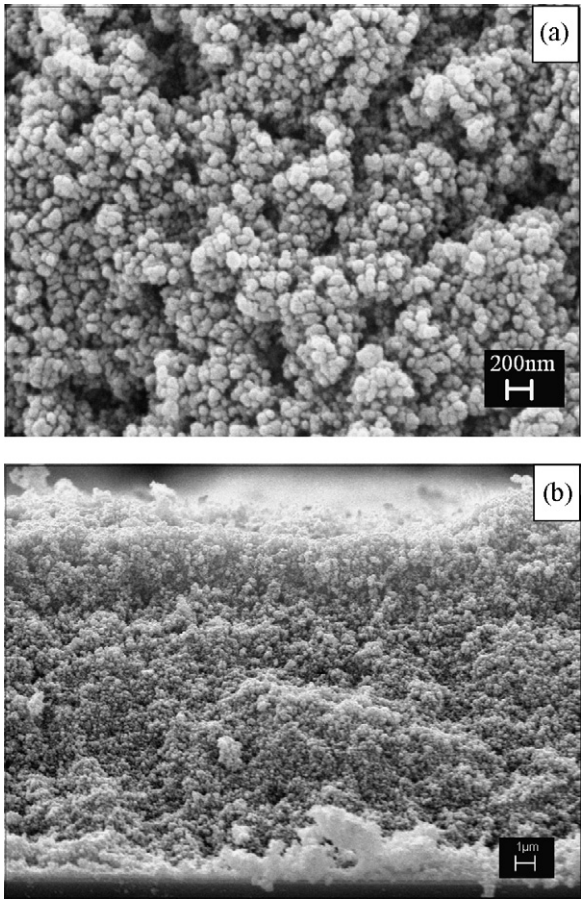

Fig. 2. (a) Top view and (b) cross-section view of TiO_2 film prepared by EPD.

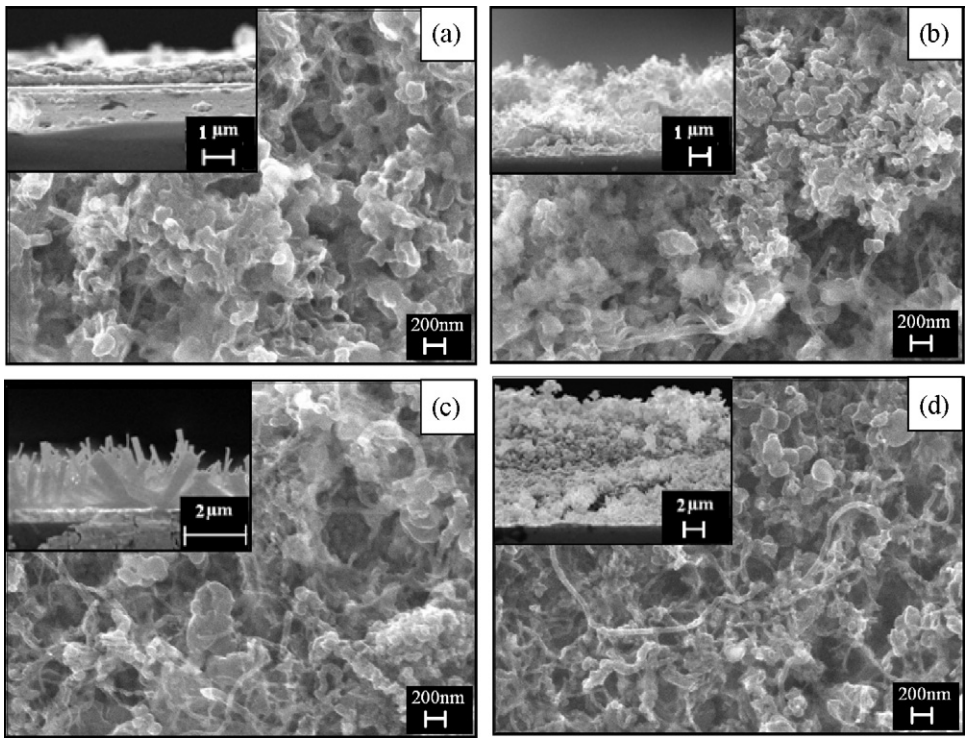

Fig. 3. Top and cross-section SEM images of (a) a W-Mg-0.02-g-CNT-1-min film, (b) a W-Mg-0.02-g-CNT-4-min film, (c) a W-Mg-0.04-g-CNT-1-min film and (d) a W-Mg-0.04-g-CNT-4-min film.

nanotube films were analyzed by energy dispersive X-ray (EDX) and Fourier transform infrared spectroscopy (FTIR, PerkinElmer Spectrum GX FT-IR/FT-Raman spectrometer). The integrated area of C and Mg peaks of EDX spectra was estimated by Gaussian curve fitting. The photocurrent–photovoltage of DSSCs was measured with a super solar simulator (WACOM, Class A) system under 1 sun at an air mass (AM) of 1.5 and a light intensity of 100 mW/cm^2.

3. Results and discussions

3.1. TiO_2 and MWCNT films characterization

TiO_2 and multiwall carbon nanotube films were coated on the FTO substrate by EPD, as shown in Figs. 2 and 3, respectively. The reason that TiO_2 particles and modified nanotubes were deposited on the cathode is because their surfaces are surrounded by Mg^{2+} ions, which are generated from $Mg(NO_3)_2{\cdot}6H_2O$. The positive Mg^{2+} ions attach to the TiO_2 and CNT surfaces at the negative hydroxyl and carboxylic groups, respectively. The thickness of TiO_2 film estimated from the cross-section SEM image is about 20 μm. As observed from the top and cross-section SEM images (Fig. 2(a) and (b)) the TiO_2 film is highly porous. The porosity structure of the TiO_2 film should favor the DSSC application because dye molecules would deeply penetrate into the TiO_2 film resulting in more dye absorbed on the TiO_2 film.

The optical image in Fig. 1(c) and (d) reveals that no nanotubes are deposited on the conductive glass without adding $Mg(NO_3)_2{\cdot}6H_2O$ into the carbon solution. After the addition of $Mg(NO_3)_2{\cdot}6H_2O$, there are a lot of CNTs deposited on the glass, as observed in Fig. 1(e) and (f). This should be due to the increase of the attraction force between nanotubes and the conductive glass. The thickness of W-Mg-CNT films (with $Mg(NO_3)_2{\cdot}6H_2O$ carbon nanotube films), estimated from the cross-section SEM images (Fig. 3(a)–(d)), is summarized in Table 1. It is observed that at the same carbon nanotube concentration, the 4-min (4 min deposition duration) CNT films are thicker than the 1-min films. Similarly, at the same deposition duration, the larger carbon nanotube concentration (0.04 g CNTs) films are thicker than the lower carbon concentration (0.02 g CNTs) films. Hence, the carbon film thickness increases with the deposition duration and the carbon nanotube concentration. Since carbon nanotubes having a high aspect ratio, the film surface area should be larger than that of a smooth film. Therefore, the CNT film surface area and the interfacial area between the electrolyte and the CNT electrode are expected to increase with the film thickness, which would subsequently strengthen the dye-sensitized solar cell performance.

3.2. The performance of DSSCs

The DSSC performance using the conductive glass, magnesium film, WO-Mg-CNT (without $Mg(NO_3)_2{\cdot}6H_2O$ carbon nanotube) films and W-Mg-CNT films as the counter electrode was analyzed with a solar simulator at a light intensity of 100 mW/cm^2, and the photocurrent–photovoltage (J–V) result is presented in Fig. 4. The short-circuit photocurrent density (J_{sc}), open-circuit voltage (V_{oc}), fill factor (FF) and efficiency (η) are calculated from the J–V curves, and they are listed in Table 1. It is found that the conductive glass, magnesium film and WO-Mg-CNT films deliver a very low efficiency as compared to W-Mg-CNT films because the film surfaces contain no catalyst. The efficiency of the WO-Mg-0.04-g-CNT film is larger than the WO-Mg-0.02-g-CNT film and the magnesium film, which may be due to a small amount of CNT deposited on the conductive glass. But, it is too low to be detected by the optical image. In case of CNT films prepared from the CNT plus $Mg(NO_3)_2{\cdot}6H_2O$ solution, the trend of the efficiency behaves unexpected because at the same CNT concentration, the longer deposition duration films (thicker CNT films) have a lower efficiency than the shorter deposition duration films (thinner films). However, at the same deposition duration time, the DSSC efficiency of the higher CNT concentration (0.04 g CNT) films is larger than the lower concentration (0.02 g CNT) films. Notice that for the W-Mg-CNT film thickness prepared at the same deposition duration, the 0.04-g CNT concentration films

Table 1
Summaries of the film thicknesses, short-circuit photocurrent density (J_{sc}), open-circuit photovoltage (V_{oc}), fill factor (FF) and efficiency (η) of the dye-sensitized solar cells as using the conductive glass, magnesium film and carbon nanotube (with and without $Mg(NO_3)_2{\cdot}6H_2O$) films as counter electrode.

Sample	Type of counter electrodes	Film thickness (μm)	J_{sc} (mA/cm^2)	V_{oc} (V)	Fill factor (FF)	Efficiency, η
Sample 1	Conductive glass	0	0.08	0.59	0.12	0.01%
Sample 2	Magnesium film	N/A	0.23	0.66	0.16	0.02%
Sample 3	WO-Mg-0.02-g-CNT-4-min	N/A	0.42	0.58	0.09	0.02%
Sample 4	WO-Mg-0.04-g-CNT-4-min	N/A	0.96	0.61	0.13	0.08%
Sample 5	W-Mg-0.02-g-CNT-1-min	0.5	3.22	0.71	0.31	0.71%
Sample 6	W-Mg-0.02-g-CNT-4-min	5.7	2.20	0.69	0.43	0.65%
Sample 7	W-Mg-0.04-g-CNT-1-min	2.0	3.71	0.67	0.43	1.08%
Sample 8	W-Mg-0.04-g-CNT-4-min	10.1	2.55	0.67	0.48	0.81%

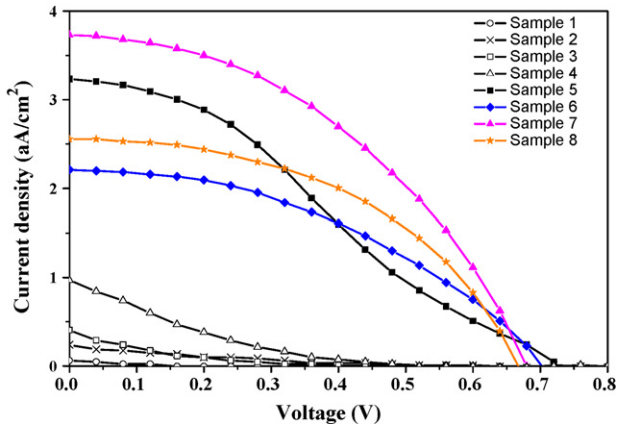

Fig. 4. Plot of the photocurrent density (J) versus the photovoltage (V) of the dye-sensitized solar cells using the conductive glass, the magnesium film and the electrophoretically carbon nanotube films as counter electrode.

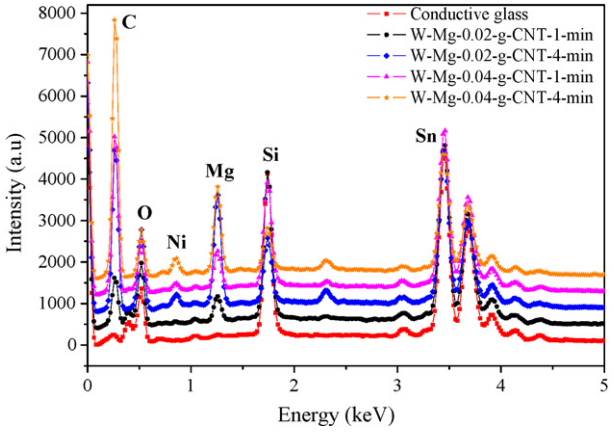

Fig. 6. EDX spectra of the conductive glass and carbon nanotubes films prepared at four different deposition conditions.

are thicker than the 0.02-g CNT concentration films. Hence, the DSSC efficiency increases with the CNT film thickness through the increased CNT concentration, but decreases with the film thickness through the longer deposition duration. The degradation of the solar cell efficiency with a function of the deposition duration should be caused by particle accumulation on the carbon nanotube surface, as observed in Fig. 3.

SEM images (Fig. 3) reveal that number and size of additional particles increase with the deposition duration. To identify the chemistry of these particles, FTIR and EDX measurements are performed on carbon films and the results are illustrated in Figs. 5 and 6, respectively. The FTIR spectrum of the conductive glass shows no significant absorbance peak. However, after electrophoretic deposition of the conductive glass in the $Mg(NO_3)_2{\cdot}6H_2O$ solution for 4 min, two absorbance peaks appear around 1441 and 1614 cm^{-1}. The appearance of these peaks suggests the formation of magnesium on the glass. The spectrum of the WO-Mg-0.04-g-CNT film has no absorbance peak, which is similar to the conductive glass spectrum. However, the spectrum of the W-Mg-0.04-g–CNT sample (Fig. 5(d)) shows two absorbance peaks around 1441 and 1614 cm^{-1}. This indicates that magnesium should also have been deposited on the substrate along with carbon nanotubes. However, the absorbance peaks on the W-Mg-0.04-g-CNT film are not as prominent as the magnesium film; i.e. a lower amount of magnesium on the carbon film than on the magnesium film. It may be limited by the attachment of Mg^{2+} ions onto non-deposited carbon nanotubes. EDX result (Fig. 6) also detects the existence of magnesium on the W-Mg-CNT films. Therefore, it is justifiable to state that the incorporated particles, which cover the nanotube surface, are magnesium. The increase in magnesium particles' size with the deposition duration should be attributed to an additional deposition of free Mg^{2+} ions. The amount of free Mg^{2+} ions in the low CNT concentration solution should be larger than in the high CNT concentration solution. This is because the lower CNT concentration has less available nanotubes for Mg^{2+} ions to attach to than the higher CNT concentration. This is further supported by the larger magnesium particles on the W-Mg-0.02-g-CNT films than on the W-Mg-0.04-g-CNT films and the FTIR result. In addition, EDX also observes a small amount of Ni loaded on carbon nanotube films. This Ni should have adhered to carbon nanotubes during the nanotube fabrication process.

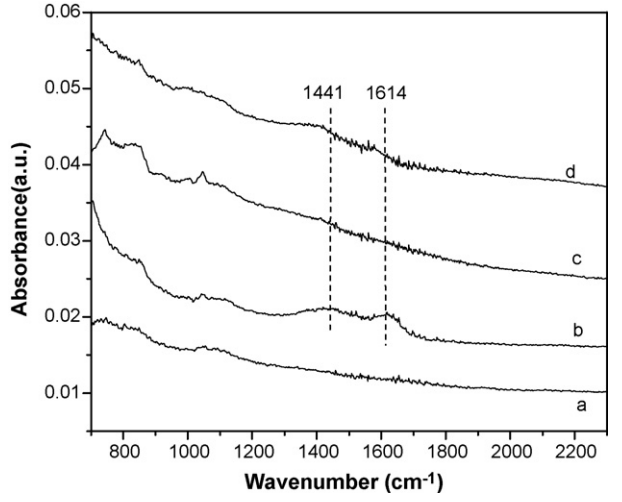

Fig. 5. FTIR spectra of (a) the conductive glass, (b) the magnesium film, (c) the WO-Mg-0.04-g-CNT-4-min film and (d) the W-Mg-0.04-g-CNT-4-min film.

The amount of magnesium coated on W-Mg-CNT films is estimated from the integrated ratio of Mg peak (I_{Mg}) over C peak (I_C) of EDX spectra as listed in Table 2. It seems that the I_{Mg}/I_C intensity ratio increases with the deposition duration, but decreases with the carbon nanotube concentration. This means that the percent-

Table 2
Summaries of the integrated area of C peak (I_C) and Mg peak (I_{Mg}) of EDX spectra, and the I_{Mg}/I_C intensity ratio of W-Mg-MWCNT films.

MWCNT sample	Integrated area of C peak (I_C)	Integrated area of Mg peak (I_{Mg})	I_{Mg}/I_C intensity ratio
W-Mg-0.02-g-CNT-1-min	77	50	0.65
W-Mg-0.02-g-CNT-4-min	273	230	0.84
W-Mg-0.04-g-CNT-1-min	255	72	0.28
W-Mg-0.04-g-CNT-4-min	429	169	0.39

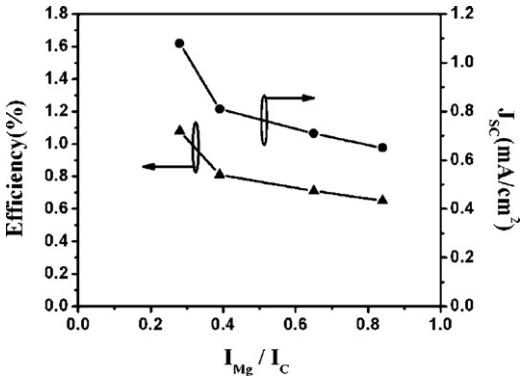

Fig. 7. Plot of the solar cell efficiency (η) and the short-circuit photocurrent density (J_{sc}) versus the I_{Mg}/I_C intensity ratio. The result reveals that η and J_{sc} decrease with the increase in the amount of incorporated magnesium.

age of incorporated magnesium on carbon films increases with the deposition duration, but decreases with the carbon concentration. For clarifying the influence of magnesium incorporation on the DSSC performance, the values of the solar cell efficiency (η) and the short-circuit photocurrent density (J_{sc}) are plotted versus the I_{Mg}/I_C intensity ratio, as presented in Fig. 7. Both η and J_{sc} curves show a decreasing trend with a function of the I_{Mg}/I_C intensity ratio, implying that the larger amount of magnesium coated on the W-Mg-CNT films will lower the DSSC efficiency and the photocurrent density. The reduction of η and J_{sc} may be limited by the coverage of magnesium particles on the CNT surface lowering the exposed CNT surface to the electrolyte.

Yoon et al. observed that the reduction/oxidation of iodide and tri-iodide increases with the increase of the Pt surface area [17]. Thus, in analogy, the decrease of the CNT surface through the magnesium particle coverage should minimize the CNT catalytic sites and the reduction of I_3^- ($I_3^- + 2e^- \rightarrow 3I^-$). Bandara et al. and Kumara et al. found that a coated of a thin MgO layer on the TiO_2 nanoparticles delays the electron recombination between TiO_2 and the electrolyte because the MgO layer acts as an electron transfer barrier [18,19]. Senevirathna et al. also observed that the thin MgO layer coated on SnO_2 nanoparticles significantly reduces the electron recombination and greatly improves the DSSC efficiency from 1.74% to 7.21% [20]. Thus, it can be inferred that the coverage of magnesium particles on the carbon nanotube surface should decrease the CNT surface and block the electron transfer from carbon nanotubes to the electrolyte resulting in a diminishing of the DSSC performance. Here, it is worth mentioning that the DSSC efficiency increases with the CNT thickness if no particles coated the carbon nanotube surface. Therefore, the higher solar cell efficiency should be possibly obtained if the surface of carbon nanotubes films is not much covered by other particles.

4. Conclusion

Multiwall carbon nanotube films have been prepared on the F-SnO_2 substrate by electrophoretic deposition. SEM, FTIR and EDX measurements confirm the incorporation of magnesium particles on MWCNT films. The performance of dye-sensitized solar cell using carbon films as counter electrode shows a decreasing trend with the amount of incorporated magnesium on the MWCNT film. This is because magnesium particles cover the nanotube surface limiting its catalytic sites and the electron transfer from CNTs to the electrolyte.

Acknowledgements

Authors would like to thank Thai Research Fund (TRF grant #MRG5080226) and Integrated Nanotechnology Research Center, Khon Kean University for the supports.

References

[1] B. O'Regan, M. Grätzel, Nature 353 (1991) 737.
[2] M. Grätzel, J. Photochem. Photobiol. A 164 (2004) 3.
[3] A. Kay, M. Grätzel, Sol. Energy. Mater. Sol. Cell 44 (1996) 99.
[4] K. Imoto, K. Takahashi, T. Yamaguchi, T. Komura, J. Nakamura, K. Murata, Sol. Energy Mater. Sol. Cell 79 (2003) 459.
[5] T.N. Murakami, M. Grätzel, Inorg. Chim. Acta 361 (2008) 572.
[6] L. Grinis, S. Dor, A. Ofir, A. Zaban, J. Photochem. Photobiol. A 198 (2008) 52.
[7] J.H. Yum, S.S. Kim, D.Y. Kim, Y.E. Sung, J. Photochem. Photobiol. A 173 (2005) 1.
[8] G.S. Kim, H.K. Seo, V.P. Godble, Y.S. Kim, O.-B. Yang, H.S. Shin, Electrochem. Commun. 8 (2006) 961.
[9] W. Jarernboon, S. Pimanpang, S. Maensiri, E. Swatsitung, V. Amornkitbamrung, Thin Solid Films 517 (2009) 4663.
[10] C. Dhand, S.K. Arya, S.P. Singh, B.P. Singh, M. Datta, B.D. Malhotra, Carbon 46 (2008) 1727.
[11] C. Du, N. Pan, J. Power Sources 160 (2006) 1487.
[12] H. Ma, L. Zhang, J. Zhang, L. Zhang, N. Yao, B. Zhang, Appl. Surf. Sci. 251 (2005) 258.
[13] S.J. Oh, J. Zhang, Y. Cheng, H. Shimoda, O. Zhou, Appl. Phys. Lett. 84 (2004) 3738.
[14] B. Gao, Z. Yue, Q. Qiu, Y. Cheng, H. Shimoda, L. Fleming, O. Zhou, Adv. Mater. 13 (2001) 1770.
[15] O. Zhou, H. Shimoda, B. Gao, S. Oh, L. Fleming, G. Yue, Acc. Chem. Res. 35 (2002) 1045.
[16] H. Zhao, H. Song, Z. Li, G. Yuan, Y. Jin, Appl. Surf. Sci. 251 (2005) 242.
[17] C.H. Yoon, R. Vittal, J. Lee, W.-S. Chae, K.-J. Kim, Electrochim. Acta 53 (2008) 2890.
[18] J. Bandara, S.S. Kuruppu, U.W. Pradeep, Colloids Surf. A 276 (2006) 197.
[19] G.R.A. Kumara, M. Okuya, K. Murakami, S. Kaneko, V.V. Jayaweera, K. Tennakone, J. Photochem. Photobiol. A 164 (2004) 183.
[20] M.K.I. Senevirathna, P.K.D.D.P. Pitigala, E.V.A. Premalal, K. Tennakone, G.R.A. Kumara, A. Konno, Sol. Energy Mater. Sol. Cell 91 (2007) 544.

Appendix III

(อยู่ระหว่างการพิจารณา ตีพิมพ์ ใน**วารสารวิทยาศาสตร์ มหาวิทยาลัยขอนแก่น**)

สมบัติการเก็บประจุไฟฟ้าของฟิล์มท่อนาโนคาร์บอนและฟิล์มท่อนาโนคาร์บอนผสมพอลีเอนิลีน

The capacitance behavior of the multiwall carbon nanotube films and the polyaniline/multiwall carbon nanotube films

สมัคร์ พิมานแพง*

ภาควิชาฟิสิกส์ คณะวิทยาศาสตร์ มหาวิทยาลัยขอนแก่น ขอนแก่น 40002

บทคัดย่อ

งานวิจัยนี้ได้สร้างขั้วเก็บประจุไฟฟ้าความจุสูง (supercapacitor) จากท่อนาโนคาร์บอนและท่อนาโนคาร์บอนผสมกับพอลิเอนิลีนบนแผ่นสแตนเลส ค่าความจุไฟฟ้า (C) ของแต่ละฟิล์มถูกวิเคราะห์ด้วยเทคนิคการอัดประจุและคายประจุที่กระแสไฟฟ้าคงที่ 1 mA โดยมีกรดซัลฟิวริกเจือจาง (0.5 M H_2SO_4) เป็นสารละลายอิเล็กโทรไลต์ ผลการทดลองพบว่าฟิล์มที่มีส่วนผสมของพอลิเอนิลีนจะให้ค่าความจุไฟฟ้าจำเพาะที่สูงกว่าฟิล์มท่อนาโนคาร์บอน ทั้งนี้เป็นเพราะว่าฟิล์มที่มีส่วนผสมของพอลิเอนิลีนจะใช้สองกระบวนการในการเก็บประจุคือ double layer effect กับท่อนาโนคาร์บอนและ redox reaction กับพอลิเอนิลีน แต่ฟิล์มท่อนาโนคาร์บอนจะใช้แค่กระบวนการ double layer effect เท่านั้น

Abstract

The supercapacitor electrodes were fabricated from multiwall carbon nanotubes (MWCNTs) and composite MWCNTs-polyaniline on a stainless steel. The capacitance of each electrode was measured by the constant current charge-discharge measurement with the diluted sulfuric acid (0.5 M H_2SO_4) as the electrolyte. It is found that the specific capacitance of the polyaniline/multi-walled carborn nanotubes films (0.2 g Polyaniline + 0.4g MWCNTs) provides the highest specific capacitance (47 F/g). This is because the composite films use two mechanisms, a double layer effect with MWCNTs and a redox reaction with polyaniline, in storing energy.

คำสำคัญ: ตัวเก็บประจุไฟฟ้าความจุสูง ท่อนาโนคาร์บอน พอลิเอนิลีน

Key words: Supercapacitors; Multiwall carbon nanotubes; Polyaniline

*Coresponding Author: samukpi@kku.ac.th

1. บทนำ

Electrochemical capacitors หรือ supercapacitors เป็นตัวเก็บประจุชนิดหนึ่งที่มีค่าความจุไฟฟ้าสูงกว่าตัวเก็บประจุทั่วไป ซึ่งมีค่าความจุสูงถึงหลักแสนไมโครฟารัด เป็นแหล่งเก็บพลังงานที่สามารถทำการอัดและคายประจุไฟฟ้าซ้ำๆได้เป็นจำนวนหลายพันรอบ โครงสร้างทั่วไปของตัวเก็บประจุความจุสูงจะประกอบด้วยขั้วไฟฟ้าสองแผ่นแช่อยู่ในสารละลายอิเล็กโทรไลต์ ซึ่งจะมีลักษณะโครงสร้างคล้ายโครงสร้างของแบตเตอรี่ ตัวเก็บประจุความจุสูงแตกต่างจากตัวเก็บประจุทั่วไปตรงที่ตัวเก็บประจุทั่วไปจะใช้ฉนวนในการแยกประจุ แต่ตัวเก็บประจุความจุสูงนั้นจะถูกแยกประจุจากสารละลายอิเล็กโทรไลต์ เนื่องจากตัวเก็บประจุความจุสูงมีค่าความหนาแน่นพลังงานมากและสามารถคายประจุได้เร็วจึงถูกนำไปประยุกต์ใช้งานร่วมกับแบตเตอรี่เพื่อเพิ่มประสิทธิภาพในการจ่ายไฟของระบบ

การเก็บประจุไฟฟ้าของตัวเก็บประจุความจุสูงโดยหลักการ double layer effect พบว่ามีขีดจำกัด กลุ่มนักวิจัยหลายกลุ่มค้นพบว่าการผสมพอลิเมอร์ที่สามารถเกิดปฏิกิริยา redox reaction กับอิเล็กโตรไลต์จะทำให้ค่าความจุไฟฟ้าของฟิล์มเพิ่มขึ้นถึงหลายร้อยฟารัดต่อกรัม [1-6] พอลิเมอร์ที่ใช้ในการเพิ่มค่าความจุไฟฟ้ามีอยู่ด้วยกันหลายชนิดเช่น พอลิเอนิลีน (polyaniline) polypyrrole หรือ Poly(3,4-ethylenedioxythiophene) (PEDOT) พอลิเอนิลีนเป็นพอลิเมอร์ที่ได้รับการศึกษาอย่างกว้างขวางเพราะให้ค่าความจุไฟฟ้าที่สูงและมีกระบวนการผลิตที่ง่าย ในงานวิจัยนี้ได้ทำการศึกษาเปรียบเทียบผลการเก็บประจุไฟฟ้าของฟิล์มท่อนาโนคาร์บอนและฟิล์มท่อนาโนคาร์บอนผสมพอลิเอนิลีนและผลของอัตราส่วนระหว่างท่อนาโนคาร์บอนกับพอลิเอนิลีนต่อความสามารถในการเก็บประจุไฟฟ้า

2. สารเคมี อุปกรณ์และวิธีการทดลอง

2.1 สารเคมี

ท่อนาโนคาร์บอนชนิดหลายชั้น (MWNTs) จากมหาวิทยาลัยเชียงใหม่

พอลิเอนิลีน (Emeraldine base polyaniline, PANi)

Poly(vinylidene fluoride) (PVF)

N-Melhyl-2-pyrrolidinon (NMP)

กรดซัลฟิวริก

2.2 อุปกรณ์ที่ใช้

Hot plate

ตู้อบ

แผ่นสแตนเลส (stainless steel , หนา 0.5 mm)

อุปกรณ์สำหรับวัดค่าความจุไฟฟ้า

คอมพิวเตอร์

2.3. วิธีการทดลอง

2.3.1 การออกแบบและสร้างวงจรสำหรับวัดค่าความจุไฟฟ้า

วงจรที่ใช้ในการวัดค่าความจุไฟฟ้าจะถูกควบคุมผ่านทางคอมพิวเตอร์กับโปรแกรมที่เขียนเอง วงจรนี้ประกอบไปด้วยตัวต้านทาน (1 kΩ) ต่อเข้ากับตัวจ่ายไฟที่ควบคุมด้วยเครื่องคอมพิวเตอร์ แล้วต่อเข้ากับตัวเก็บประจุที่ต้องการวัดดังแสดงในรูปที่ 1 จากนั้นจะให้กระแสไฟฟ้าคงที่ค่าหนึ่ง ไหลผ่านตัว R ไปยังตัว C เรียกกระบวนการนี้ว่าการอัดประจุ (charge) ส่วนในกรณีการคายประจุ (discharge) วงจรนี้จะควบคุมให้กระแสไหลออกจากตัว C ในปริมาณที่คงที่ ซึ่งทั้งสองกรณีเราจะทำการวัดค่าความต่างศักย์ที่ตกคร่อมบนตัวเก็บประจุเทียบกับเวลาที่ทำการอัดหรือคายประจุเพื่อนำไปคำนวณหาค่าความจุไฟฟ้า (C) ตามความสัมพันธ์ข้างล่าง

$$C = \frac{\Delta Q}{\Delta V} \qquad (1)$$

เมื่อ $\Delta Q = I \times \Delta t$

จะได้ $$C = \frac{I \times \Delta t}{\Delta V} \qquad (2)$$

เมื่อ I คือ ค่ากระแสไฟฟ้า (A)

ΔQ คือ ขนาดประจุไฟฟ้าในตัวเก็บประจุ (C)

Δt คือ เวลาในการอัดประจุหรือคายประจุ (s)

ΔV คือ ความต่างศักย์ที่ตกคร่อมบนตัวเก็บประจุ (V)

2.3.2 ขั้นตอนการประดิษฐ์ขั้วเก็บประจุไฟฟ้า

เตรียมสารละลายที่มีส่วนผสมของท่อนาโนคาร์บอนและท่อนาโนคาร์บอนผสมพอลิเอนิลีน โดยมีพอลิเมอร์ poly(vinylidene fluoride) (PVF) เป็นตัวช่วยยึด (binder) และ N-Melhyl-2-pyrrolidinon (NMP) เป็นตัวทำละลาย ที่อัตราส่วนต่างๆ ดังแสดงในตารางที่ 1 นำสารละลายคาร์บอนนี้ไปเคลือบบนแผ่นสแตนเลสขนาดประมาณ 3 cm × 1.5 cm ที่ผ่านการทำความสะอาดแล้ว หลังจากนั้นนำฟิล์มไปอบที่อุณหภูมิ 90 ºC เป็นระยะเวลา 12 ชั่วโมง

2.3.3 ขั้นตอนการทดสอบค่าความจุไฟฟ้าและลักษณะผิวของฟิล์ม

ฟิล์มคาร์บอนจะถูกปิดทับด้วยเทปใสที่มีรูขนาด 0.196 cm^2 การติดเทปใสบนฟิล์มก็เพื่อควบคุมพื้นที่ในการเกิดปฏิกิริยาเคมีระหว่างฟิล์มกับสารอิเล็กโทรไลต์ ในกระบวนการอัดและคายประจุฟิล์มคาร์บอนสองแผ่นจะถูกแช่ในสารละลายอิเล็กโทรไลต์ (0.5 M H_2SO_4) และต่อเข้ากับวงจร

อัดคายประจุดังรูปที่ 1 แล้วทำการวัดค่าการเก็บประจุไฟฟ้าที่กระแส 1 mA ลักษณะผิวของฟิล์มจะถูกวิเคราะห์ด้วยกล้องจุลทรรศน์อิเล็กตรอนแบบส่องกราด (scanning electron microscope, SEM)

3. ผลการวิจัยและอภิปรายผล

3.1ผลการวิเคราะห์ลักษณะผิวของฟิล์มด้วยกล้องจุลทรรศน์อิเล็กตรอน (SEM)

จากภาพถ่าย SEM ดังรูปที่ 2 และ 3 จะเห็นว่าท่อนาโนคาร์บอนมีการกระจายตัวอย่างสม่ำเสมอและฟิล์มมีลักษณะเป็นรูพรุน การที่ฟิล์มมีรูพรุนมากนั้นจะเป็นประโยชน์อย่างมากต่อความสามารถในการเก็บประจุไฟฟ้าเพราะว่าอิเล็กโทรไลต์สามารถที่จะซึมเข้าไปในฟิล์มได้เป็นปริมาณมาก ส่งผลให้ฟิล์มมีพื้นที่ผิวสัมผัสกับสารอิเล็กโทรไลต์มากและทำให้ได้ค่าเก็บประจุไฟฟ้าที่สูงตามไปด้วย นอกจากนั้นจะเห็นว่าบนผิวท่อนาโนคาร์บอนมีก้อนบางอย่างคลุมอยู่คิดว่าเป็นพอลิเมอร์ PVF สำหรับฟิล์มที่มีส่วนผสมของพอลิเอนิลีนขนาดของก้อนจะใหญ่กว่าที่พบบนฟิล์มท่อนาโนคาร์บอน ทั้งนี้น่าจะเนื่องมาจากการกระจายตัวที่ไม่ดีของพอลิเอนิลีน

3.2.ผลการวัดค่าความจุไฟฟ้าของตัวเก็บประจุมาตรฐาน (4,700 μF, บริษัท Samsung)

รูปที่ 4 แสดงผลความต่างศักย์ที่ตกคร่อมบนตัวเก็บประจุมาตรฐาน ในช่วงการอัดและคายประจุที่กระแสคงที่ 1 mA กับเวลา จะเห็นว่ากราฟมีลักษณะเป็นรูปสามเหลี่ยมซึ่งช่วงที่มีความชันเป็นบวกจะเป็นช่วงการอัดประจุ แต่ในช่วงที่มีความชันเป็นลบจะเป็นช่วงของการคายประจุ เมื่อนำความสัมพันธ์ระหว่างความต่างศักย์ที่วัดได้กับเวลาในช่วงการอัดประจุไปทำการวิเคราะห์หาค่าความจุไฟฟ้า ตามสมการที่ 2 จะได้ค่าความจุไฟฟ้าต่อรอบดังแสดงในรูปที่ 5 จะเห็นว่าผลการวัดค่าความจุไฟฟ้าของตัวเก็บประจุมาตรฐาน (4,700 μF) จำนวน 300 รอบ ได้ค่าความจุไฟฟ้าอยู่ในช่วง 4,600 ถึง 5,100 μF ซึ่งมีค่าใกล้เคียงกับค่าที่ระบุไว้ ดังนั้นเทคนิคนี้มีความแม่นยำเพียงพอที่จะใช้วิเคราะห์หาค่าความจุไฟฟ้าของตัวเก็บประจุที่ต้องการทราบค่า

3.3 ผลการวัดค่าความจุไฟฟ้าของฟิล์มท่อนาโนคาร์บอนและฟิล์มท่อนาโนคาร์บอนผสมพอลิเอนิลีน

การเก็บประจุของฟิล์มท่อนาโนคาร์บอนและฟิล์มท่อนาโนคาร์บอนผสมพอลิเอนิลีนจะใช้สองกระบวนการด้วยกันคือ

1. กระบวนการ double layer effect

ท่อนาโนคาร์บอนจะใช้หลักการ double layer effect ในการเก็บประจุ [7] โดยมีขั้นตอนการเก็บประจุดังนี้ ท่อนาโนคาร์บอนที่อยู่บนฟิล์มที่ต่อเข้ากับขั้วลบจะดึงดูดประจุบวก (H^+) เข้ามาล้อมรอบผิวของท่อคาร์บอนไว้ ส่วนท่อคาร์บอนที่อยู่บนฟิล์มที่ต่อเข้ากับขั้วบวกจะดึงประจุลบ (SO_4^{2-}) เข้ามาล้อมผิวท่อคาร์บอนไว้ จึงเสมือนว่ามีการเก็บสะสมของประจุบวกและประจุลบไว้ที่แต่ละฟิล์ม

2. กระบวนการ redox reaction

พอลิเอนิลีนจะใช้ปฏิกิริยา redox reaction ในการเก็บหรือคายประจุ สำหรับกรณีการอัดประจุพอลิเอนิลีนบนขั้วลบจะรับอิเล็กตรอนจากแบตเตอรี่แล้วเกิดปฏิกิริยากับ H^+ กลายเป็น leucoemeraldine พอลิเอนิลีน ส่วนในกรณีการคายประจุพอลิเอนิลีนจะปล่อยอิเล็กตรอนและ H^+ คืนให้กับอิเล็กโทรไลต์เพื่อกลับไปเป็น emeraldine พอลิเอนิลีน [8] ดังแสดงในสมการเคมีข้างล่าง

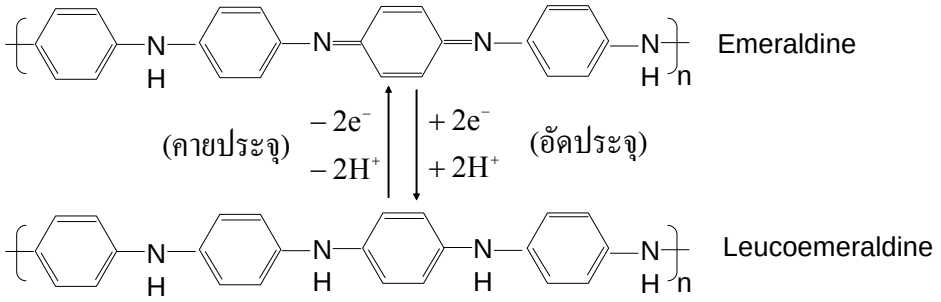

ผลการทดลองการอัดและคายประจุที่กระแส 1 mA พบว่าค่าความจุไฟฟ้าจำเพาะของฟิล์มที่มีส่วนผสมของพอลิเอนิลีนจะมีค่าสูงกว่าฟิล์มท่อนาโนคาร์บอน ดังแสดงในรูปที่ 6 และตารางที่ 2 การที่พอลิเอนิลีนช่วยเพิ่มค่าความจุไฟฟ้าเป็นเพราะว่าพอลิเอนิลีนสามารถเกิดปฏิกิริยากับไฮโดรเจนไอออน (H^+) ดังสมการเคมีข้างต้นร่วมกับการเก็บประจุแบบ double layer effect ของท่อนาโนคาร์บอน ที่อัตราส่วน MWCNTs : PANi (0.4 g : 0.2 g) ได้ค่าความจุสูงสุดถึง 47 F/g แต่เมื่อเพิ่มอัตราส่วนพอลิเอนิลีนมากขึ้นผลพบว่าค่าความจุไฟฟ้าจำเพาะลดลงเหลือ 20 F/g การลดลงของค่าความจุไฟฟ้าเมื่อเพิ่มปริมาณของพอลิเอนิลีนน่าจะเนื่องมาจากการกระจายตัวที่ไม่สม่ำเสมอของพอลิเอนิลีน ดังเห็นในภาพ SEM (รูปที่ 3) และอาจจะเนื่องมาจากการลดลงของค่าการนำไฟฟ้าของฟิล์มเพราะพอลิเอนิลีนนำไฟฟ้าได้ไม่ดีเท่าท่อนาโนคาร์บอน

4. สรุปผลการทดลอง

งานวิจัยนี้ได้สร้างวงจรอัดและคายประจุที่ควบคุมผ่านทางคอมพิวเตอร์ ผลการวัดค่าความจุไฟฟ้าของตัวเก็บประจุมาตรฐานพบว่าได้ค่าที่ใกล้เคียงกับค่าที่ระบุไว้ การวิเคราะห์ลักษณะผิวฟิล์มด้วย SEM พบว่าฟิล์มมีลักษณะเป็นรูพรุนและพอลิเอนิลีนมีการจับตัวกันเป็นกลุ่ม ค่าความจุไฟฟ้าจำเพาะของฟิล์มที่มีส่วนผสมของพอลิเอนิลีนจะมีค่าสูงกว่าฟิล์มคาร์บอนเพราะว่าฟิล์มที่มีส่วนผสมของพอลิเอนิลีนใช้สองกระบวนการ double layer effect และ redox reaction ในการเก็บประจุ ที่อัตราส่วน 0.4 g MWCNTs : 0.2 g PANi ได้ค่าความจุไฟฟ้าจำเพาะที่สูงสุดประมาณ 47 F/g

เกียรติกรรมประกาศ

ขอขอบคุณนางสาวสุมารินทร์ อินทจักร์ ที่ช่วยทำงานวิจัยและงานวิจัยนี้ได้รับการสนับสนุนจากสำนักงานกองทุนสนับสนุนการวิจัย (สกว.) เลขที่ MRG5080226

เอกสารอ้างอิง

1. W. Qin, J.-L. Li, G. Fei, W.-S. Li, K.-Z. Wu, X.-D. WANG "Activated carbon coated with polyaniline as an electrode material in supercapacitors" New Carbon Materials, 23(3) (2008) 275–280.
2. C.-C. Hu, W.-Y. Li and J.-Y. Lin "The capacitive characteristics of supercapacitors consisting of activated carbon fabric–polyaniline composites in $NaNO_3$" Journal of Power Sources 137 (2004) 152–157.
3. W.-C. Chen, T.-C. Wen and H. Teng "Polyaniline-deposited porous carbon electrode for supercapacitor" Electrochimica Acta 48 (2003) 641-649.
4. V. Khomenko1, E. Raymundo-Piñero, E. Frackowiak and F. Bėguin1 "High-voltage asymmetric supercapacitors operating in aqueous electrolyte" Appl. Phys. A 82 (2006) 567–573.
5. M. Mastragostino, C. Arbizzani and F. Soavi "Polymer-base supercapacitors" Journal of Power Sources 97-98 (2001) 812-815.
6. C. Peng, S. Zhang, D. Jewell and G. Z. Chen "Carbon nanotube and conducting polymer composites for supercapacitors" Progress in Natural Science 18 (2008) 777–788.
7. C. Du and N. Pan "Supercapacitors using carbon nanotubes films by electrophoretic deposition" Journal of Power Sources 160 (2006) 1487–1494.
8. E. T. Kang, K. G. Neoh and K. L. Tan "Polyaniline: a polymer with many interesting intrinsic redox states" Prog. Polym. Sci, 23 (1998) 211-324.

รูปภาพ

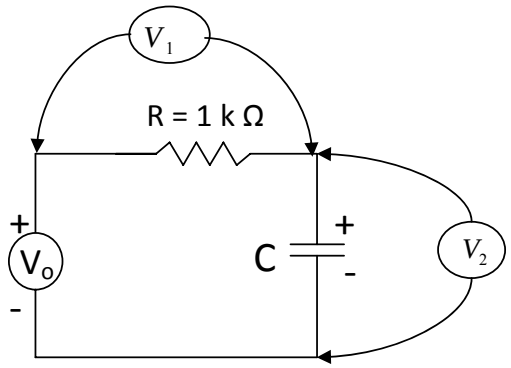

รูปที่ 1 ลักษณะวงจรที่ใช้ในการอัดและคายประจุของตัวเก็บประจุ เมื่อ V_0 คือโวลต์ที่ออกจากแหล่งจ่ายไฟ V_1 คือความต่างศักย์ตกคร่อมบนตัวต้านทาน และ V_2 คือความต่างศักย์ที่ตกคร่อมบนตัวเก็บประจุ

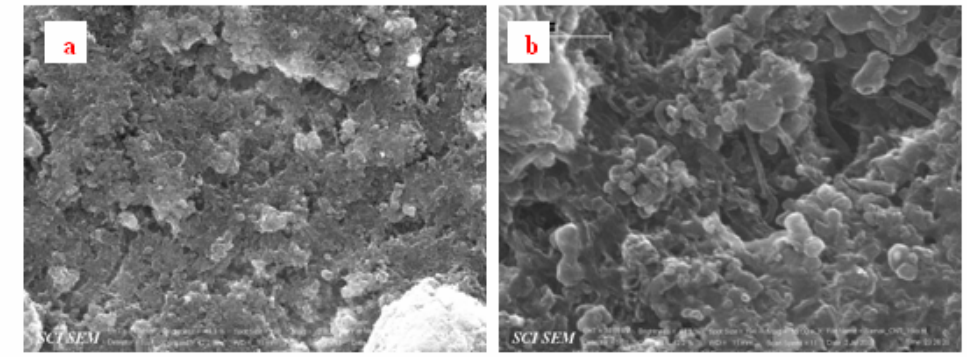

รูปที่ 2 ภาพถ่าย SEM ของฟิล์มท่อนาโนคาร์บอน a) ที่กำลังขยาย 2,000 เท่า b) ที่กำลังขยาย 15,000 เท่า

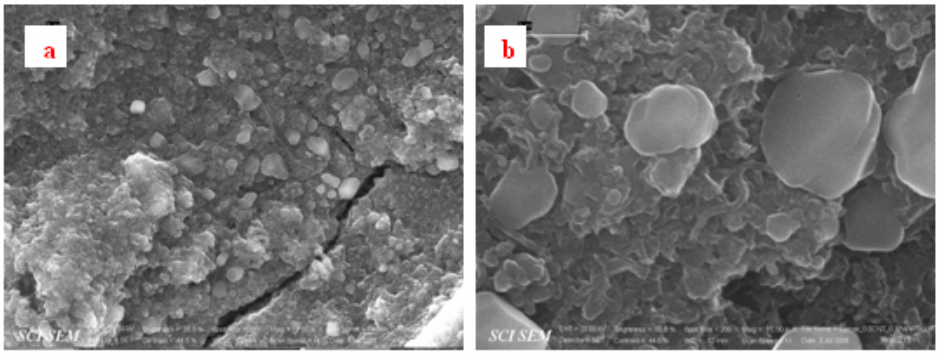

รูปที่ 3 ภาพถ่าย SEM ของฟิล์มท่อนาโนคาร์บอนผสมพอลิเอนิลีน ที่เงื่อนไข 0.5 g MWCNTs : 0.1 g พอลิเอนิลีน a) ที่กำลังขยาย 2,000 เท่า และ b) ที่กำลังขยาย 15,000 เท่า

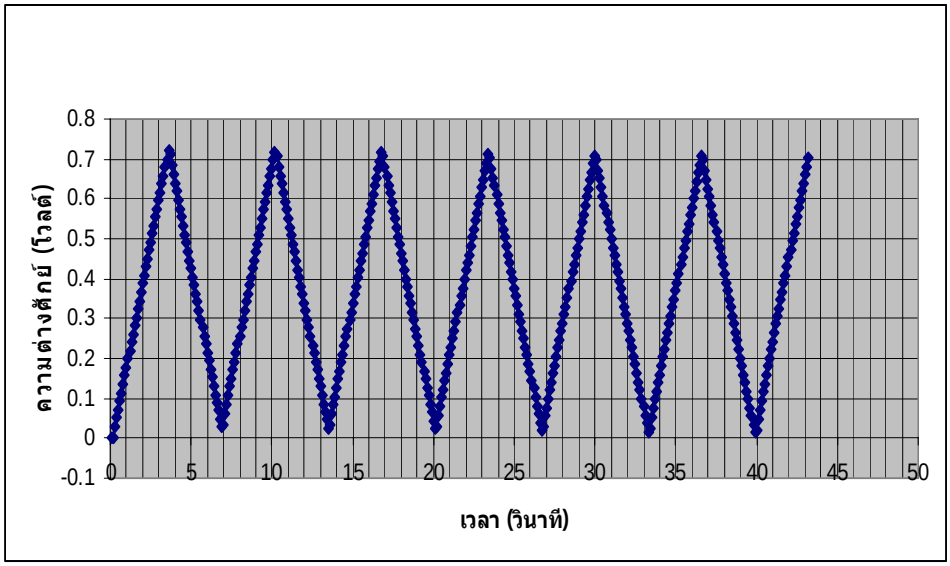

รูปที่ 4 กราฟแสดงความสัมพันธ์ระหว่างความต่างศักย์บนตัวเก็บประจุมาตรฐาน 4,700 μF กับเวลา (V-t) ในกระบวนการอัดประจุและคายประจุที่กระแส 1 mA

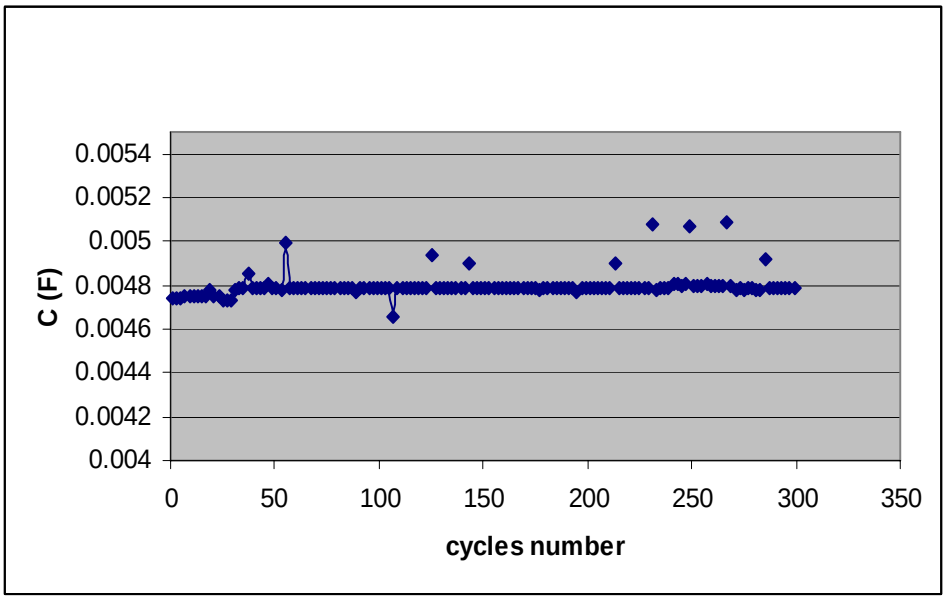

รูปที่ 5 ค่าความจุไฟฟ้าที่แต่ละรอบของการอัดประจุที่กระแส 1 mA ของตัวเก็บประจุมาตรฐาน 4,700 µF

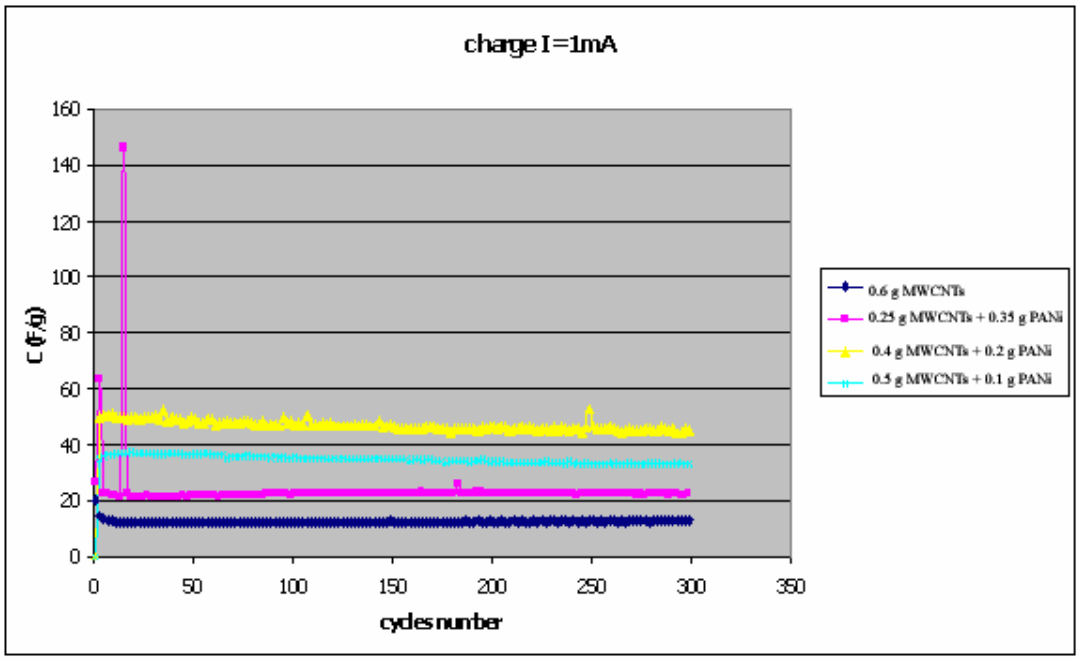

รูปที่ 6 กราฟแสดงค่าความจุไฟฟ้าจำเพาะของตัวเก็บประจุแต่ละชนิด ในช่วงการอัดประจุที่กระแสไฟฟ้า 1 mA

ตาราง

MWCNTs (mg)	**PANi (mg)**	**PVF (mg)**	**NMP (ml)**
0.6	0	0.1	3
0.5	0.1	0.1	3
0.4	0.2	0.1	3
0.25	0.35	0.1	3

ตารางที่ 1 อัตราส่วนของท่อนาโนคาร์บอน (MWCNTs) พอลิเอนิลิน (PANi) PVF และ NMP ที่ใช้ในการเตรียมฟิล์มเก็บประจุไฟฟ้า

ชนิดของฟิล์มเก็บประจุ	**ค่าความจุไฟฟ้าจำเพาะ (C, F/g)**
ท่อนาโนคาร์บอน (0.6 g MWCNTs)	12
ท่อนาโนคาร์บอนผสมพอลิเอนิลีน (0.25 g MWCNTs : 0.35 g PANi)	20
ท่อนาโนคาร์บอนผสมพอลิเอนิลีน (0.4 g MWCNTs : 0.2 g PANi)	47
ท่อนาโนคาร์บอนผสมพอลิเอนิลีน (0.5 g MWCNTs : 0.1 g PANi)	35

ตารางที่ 2 สรุปค่าความจุจำเพาะไฟฟ้าของตัวเก็บประจุฟิล์มท่อนาโนคาร์บอนและฟิล์มท่อนาโนคาร์บอนผสมพอลิเอนิลีน

Appendix IV

(In preparation for submitting to **Carbon**)

Enhancing dye-sensitized solar cell performance of multiwall carbon nanotube counter electrode by acid modification

Wasan Maiaugree[a], Samuk Pimanpang[a,*], Wirat Jarernboon[b], Santi Maensiri[a] and Vittaya Amornkitbamrung[a]

[a]*Department of Physics, Faculty of science, Khon Kaen University, Khon Kaen, Thailand, 40002*

[b]*College of KMITL Nanotechnology, King Mongkut's Institute of Technology Ladkrabang, Chalongkrung Rd., Ladkrabang, Bangkok 10520, Thailand and ThEP Center, CHE, 328 Si Ayutthaya Rd., Bangkok 10400, Thailand*

Abstract

Modified and non-modified carbon nanotubes are coated on the conductive glass and the conductive plastic by the slurry paste and are used as the counter electrode of dye-sensitized solar cells (DSSCs). Scanning electron microscopes indicate the well deposition of the modified and non-modified carbon nanotubes on the conductive glass, while only the modified carbon nanotubes are well deposited on the plastic substrate. The efficiency of the non-modified and modified carbon nanotube glass DSSCs is ~2.73% and ~3.46%, respectively, and the efficiency of the non-modified and modified carbon nanotube flexible DSSCs is ~0.80% and ~1.79%, respectively. The low performance of the flexible DSSCs is attributed to the low indium tin oxide conductivity and the thin TiO_2 film. The voltammogram results

suggest that the superiority of the modified carbon nanotube DSSCs is attributed to the higher catalytic activity of the modified carbon nanotube films than the non-modified carbon nanotube films.

Key words: Dye-sensitized solar cell; Multiwall carbon nanotube**;** Flexible solar cell

*Corresponding author: samukpi@kku.ac.th

1. Introduction

Dye-sensitized solar cell (DSSC) has been intensively studied because of its simple structure, low fabrication cost, promising light harvesting efficiency and environmental friendliness. DSSC is thought as the next generation solar cell, which exhibits a potential replacement to the conventional silicon solar cell. The high energy conversion efficiency of dye-sensitized solar cells is accomplished through the use of a high porous semiconductor film coated with a monolayer dye-sensitizer as the working electrode, which was developed by O'Regan and Grätzel in 1991 [1]. TiO_2 nanoparticle is commonly used semiconductor because it delivers the highest energy conversion efficiency among semiconductors (ZnO, Nb_2O_5, WO_3, In_2O_3, SnO_2) [2-5]. TiO_2 nanoparticles server as the electron-transporting medium between dye-sensitizers and the electron collector (transparent conductive substrate). Electrons from the electron collector will flow through the external load reaching the counter electrode, and undergo the reduction with tri-iodide ($I_3^- + 2e^- \rightarrow 3I^-$) by help of the catalyst film. Therefore, the catalyst film (counter electrode) is an important component of the DSSC device, which directly manipulates the cell performance.

Platinum (Pt) film is commonly used as the DSSC counter electrode because of its good catalytic activity, but Pt is an expensive material. Other cheaper materials have been studied as the alternative DSSC catalyst such as carbon black, carbon nanotubes or conductive polymers [6-10]. Carbon nanotubes are considered used as the DSSC counter electrode because of its unique properties such as good catalytic activity, good conductivity, high thermal stability, high aspect ratio and comparatively lower price than Pt. Thus, by switching to carbon nanotube counter electrode, the DSSC production cost should be minimized.

It is reported that the acid treatment can introduce functional groups: hydroxyl group or carboxylic group, on the carbon nanotube surface. The presence of these functional groups is found to enhance nanotubes' catalytic activity [11-13]. Thus, by using acid-treated carbon nanotube film as the DSSC counter electrode, the tri-iodide reduction rate and the solar cell efficiency should be optimized. Carbon nanotube films are fabricated by various methods such as chemical vapor deposition, arc discharge, electrophoretic deposition or slurry paste [14-20]. The slurry paste is a simple method in preparing the low temperature carbon film by using polymers, Polyvinyl Fluoride (PVF) or Polyvinylidene Fluoride (PVDF), as binders. There are not many studies characterizing the slurry pasted carbon nanotube film as the DSSC counter electrode. In this present work, we explore the possibility of using the slurry pasted carbon nanotube film as the DSSC counter electrode and the effect of the acid treatment on the cell performance. Additionally, the suitability in applying carbon nanotube films coated on the conductive plastic as the flexible DSSC counter electrode is also investigated. To verify the factors influencing the DSSC performance, scanning electron microscope, UV-visible spectrometer and cyclic voltammetry are performed, and the detail analysis is discussed in this work.

2. Experimental

2.1 Modification of MWCNTs

Multiwall carbon nanotubes (MWCNTs) were purchased from Chiang Mai University, Thailand. MWCNTs were modified by the mixed acids (H_2SO_4 : HNO_3 at a volume ratio of 3 : 1) for 30 min at room temperature prior to use in order to generate a carboxylic group on the carbon nanotube surface. Then, the modified

carbon nanotubes were rinsed with deionized water for three times, filtered with filter paper and dried at 80˚C at the ambient conditions.

2.2 Preparation of TiO_2 and MWCNT films

2.2.1 TiO_2 film coated on the conductive glass substrate (TiO_2/FTO)

The conductive glass (Fluoride doped Tin Oxide glass, FTO, sheet resistance of 15 Ω/sq, Solaronix), was used as a substrate for coating TiO_2 films. The dense TiO_2 layer was span on the conductive glass from the Titanium diisoproxide bis(acetylacetonate) solution, 1 mL of Titanium diisopropoxide ($C_{16}H_{28}O_6Ti$ 75 wt.% in isopropanol) in 20 mL isopropanol. The porous transparent TiO_2 film was coated on the dense TiO_2 film by a doctor blade technique using the TiO_2 paste PST-18NR (CATALYSTS & CHEMICALS IND. CO., LTD). A scattered TiO_2 layer was coated on the porous TiO_2 film by the doctor blade using PST–400C (CATALYSTS & CHEMICALS IND. CO., LTD). TiO_2 films were annealed at 500 °C for 1 h at the ambient conditions, and the post annealed TiO_2 films were immersed in the dye solution, *cis*-bis(isothiocyanato) bis(2,2′-bipyridyl-4,4′-dicarboxylato)-ruthenium(II)-bis-tetrabutylammonium (N719, Solaronix, 5×10^{-4} M in Acetonitrile : tert-Butanol at a volume ratio of 1:1) for 24 h at room temperature in the dark.

2.2.2 TiO_2 films coated on the conductive plastic substrate (TiO_2/ITO/PEN)

The indium tin oxide coated on polyethylene naphthalate (ITO/PEN, sheet resistance of 60 Ω/sq, Peccell Technologies, Inc.) was used as the conductive flexible substrate. The TiO_2 slurry, mixture of 5 g TiO_2 (P25, 20 nm, Degussa, Germany) in 20 ml isopropanol, was carefully pasted on the ITO/PEN substrate and let it dry in the air. Then, TiO_2 films were pressed by the hydraulic pressure (Model HP–10, T.M.C. INDUSTRIAL CO.,LTD.) at the compression pressure ~510 MPa, called *pressed TiO_2* film. The pressed TiO_2 films were immersed in the N719 dye solution, 5×10^{-4}

M in Acetonitrile : tert-Butanol at a volume ratio of 1:1, for 24 h at room temperature in the dark.

2.2.3 MWCNTs films

MWCNT film was deposited on the conductive glass (MWCNT/FTO) and the conductive plastic (MWCNT/ITO/PEN) substrates by the slurry paste. The carbon slurry was a mixture of 0.6 g MWCNTs and 0.1 g PVF in 3 ml N-Methyl-2-pyrrolidion (NMP). The carbon slurry was stirred by the magnetic stirrer for 30 minutes. The slurry was pasted on the conductive glass and plastic by a glass rod as using scotch tapes as the thickness controller, and then films were dried at 80 °C for 6 h.

2.3 DSSC assemble

The glass dye-sensitized solar cell was assembled by using dye-TiO_2/FTO film as the working electrode and MWCNT/FTO film as the counter electrode with the cell active area of 0.7 cm × 0.7 cm. These two electrodes were sandwiched together with three layers of a 60-μm thick Surlyn polymer film (Solaronix) as a plastic sealant and a cell spacer. Three Surlyn film layers were applied because of the thick carbon film. A liquid electrolyte was filled into the cell through the drilled hole on the counter electrode. After electrolyte filling, the hole was sealed by a Surlyn polymer film cover with a small piece of the glass slide.

In case of the flexible DSSCs, the dye-pressed-TiO_2/ITO/PEN films and the MWCNT/ITO/PEN films were used as the working electrode and the counter electrode, respectively, with the cell active area of 0.7 cm × 0.7 cm. The performance of the flexible solar cells was measured at the open cell condition (unsealed condition) because of the sealing difficulty. From our experience, we encountered many cells shorting after the cell sealant. Three layers of a 60-μm thick Surlyn polymer film

were used as a cell spacer. The liquid electrolyte, mixture of 0.6 M MPI (1-Methyl-3-popylimidazolium iodide), 0.1 M LiI (Lithium iodide anhydraus), 0.05 M I_2 (Iodide), 0.5 M TBP (tert-Butylpyridine) and 0.0025 M $LiCO_3$ (Lithium carbonate) in Acetonitrile, was used as the electrolyte for both glass and flexible DSSCs. The cell performance was measured with a super solar simulator (WACOM, Class A) system under 1 sun at an air mass (AM) of 1.5 and a light intensity of 100 $mW.cm^{-2}$.

2.4 Film characterization

The film morphology and the film thickness were characterized by scanning electron microscopy (SEM, LEO, SEM 1450VP, UK). The amount of adsorbed dye was estimated with a UV-visible spectrometer (UV-160A, SHIMADZU) by desorbing dye of TiO_2 films in 10 mL (in case of TiO_2/FTO films) and 5 mL (in case of TiO_2/ITO/PEN films) of a mixed 0.1 M NaOH and ethanol at a volume ratio 1:1. The cyclic voltammetry (CV) was measured in a three-compartment cell with Autolab system at a scan rate of 20 mV/s. The Pt plate (area ~0.385 cm^2) and the Ag/AgCl electrode were used as the counter electrode and the reference electrode, respectively. The Pt and carbon films were taped with an insulating tape with an open area of 0.073 cm^2 prior to the CV scan.

3. Results and discussion

3.1 Glass DSSCs

The surface morphology of TiO_2 and carbon nanotube films coated on the conductive glass is characterized by SEM, and images are presented in Fig. 1 and 2, respectively. The SEM results show that TiO_2 and carbon nanotube films are porous structures. The cross-section image of TiO_2 film (Fig. 1b) clearly shows three different layers: 1) a dense-TiO_2 layer ~0.5 μm, 2) a porous transparent TiO_2 layer

~5.5 μm and 3) a scattered TiO_2 layer ~3.2 μm. The amount of dye molecules adsorbed on the TiO_2 films, a TiO_2 area of 0.49 cm^2, was analyzed by the UV-visible spectrometer. Figure 3(a) shows the absorbance spectra of three desorbed dye solutions of TiO_2/FTO samples. All three absorbance spectra exhibit close absorbance value; implying that the TiO_2 thickness should be close to one another. The amount of dye loaded on the TiO_2 films is calculated via the following equations:

$$A_\lambda = \varepsilon_\lambda c l, \qquad (1)$$

and $$M = cV. \qquad (2)$$

Where, A_λ and ε_λ are the absorbance value and the specific absorbance ($M^{-1}\cdot cm^{-1}$) as a function of wavelength, respectively. c is the desorbed dye concentration (M), l is the thickness of the standard cuvette glass (1 cm), V is the volume of the dye solution (10 ml), and M is the amount of dye molecules adsorbed on the TiO_2 films (mol). By using the specific absorbance at λ = 300 nm, $\varepsilon_{300} = 5.7\times10^4$ $M^{-1}cm^{-1}$, the amount of dye molecules is about 10.86×10^{-8}, 10.71×10^{-8} and 9.92×10^{-8} mol/cm^2 (average $10.50\times10^{-8} \pm 0.51\times10^{-8}$ mol/cm^2). Hence, it can be inferred that the consistence TiO_2 thickness is possible prepared by the doctor blade technique.

The thickness of the MWCNT film coated on the conductive glass (MWCNT/FTO) estimated from the cross-section SEM images (Fig. 2) is ~33-65 μm. Owing to the high CNT aspect ratio and the high film porosity, the interfacial area between the electrolyte and the counter electrode should be large, which subsequently elevates the solar cell efficiency. The DSSC performance was analyzed with the solar simulator, and the photocurrent density (J)-photovoltage (V) curves are presented in Fig. 4(a). The short-circuit current density (J_{sc}), open-circuit voltage (V_{oc}), fill factor (FF) and efficiency (η) are extracted from the J-V curves and are listed in Table 1. As shown in Table 1, the Pt DSSC generates the highest energy conversion efficiency

(3.9%), while the non-modified and modified DSSCs deliver ~2.73% and ~3.46%, respectively. The larger efficiency of the Pt DSSC should be attributed to the better catalytic activity of the Pt film over the carbon nanotube films.

It has been reported that the presence of carboxylic groups on carbon nanotubes' surface strengthens the nanotube reactivity [11-13]. Therefore, the emergence of functional groups on the modified carbon nanotubes may be an explanation to the superior cell performance of the modified carbon DSSC. In justifying this point, the cyclic voltammetry (CV) was conducted in a potential range from -0.4 V to 1.0 V in the acetonitrile solution of 10 mM LiI, 1 mM I_2 and 0.1 M $LiClO_4$ at the scan rate of 20 mV/s, and the CV result is illustrated in Fig. 5(a). The voltammogram of the Pt film exhibits two oxidation peaks at 0.33 V and 0.66 V, and two reduction peaks at 0.14 V and 0.53 V. Whereas, the carbon films do not manifest any clear oxidation and reduction peak. Surprising, the voltammogram of Pt film is lower than that of the carbon nanotube films, which contradicts to its superior performance. Huang et. al. and Li et. al. also observed the larger CV current density and the lower cell efficiency of the carbon film than the Pt film [21-22]. One reasonable explanation to this is attributed to the excellent charge storing characteristic of the carbon nanotube films as reported by many researchers [23-25]. The square-like shape of the carbon CV curves is an evident to the coexistence of the electrochemical capacitance on the carbon nanotube films. Thus, the high current density of the carbon nanotube films is likely due to the ions storing on the electrode surface by the double layer effect rather than the redox reaction. The large electrode capacitance will suppress electrons interacting with tri-iodide resulting in the lower solar cell efficiency than the Pt DSSC, as seen in Table 1.

3.2 Flexible DSSCs

In section 3.1, we are successfully employing the low temperature slurry pasted carbon nanotube films coated on the conductive glass (MWCNT/FTO) as the DSSC counter electrode. Thus, it should be possible to apply the carbon nanotube film coated on the conductive plastic (MWCNT/ITO/PEN) as the counter electrode. By altering the substrate to the plastic type, the lower production cost, the lighter weight and the flexibility DSSCs should be gained. However, the TiO_2 paste (PST-18NR and PST-400C) is not appropriated in coating the TiO_2 film on the plastic substrate because it contains polymers, which have to be removed at high annealing temperature (400 °C – 500 °C). But, the plastic cannot sustain such a high temperature. Grinis et. al.[26] and Yamaguchi et. al.[27] reported that by compressing TiO_2 film under a high compression pressure, the TiO_2 nanoparticle connectivity is improved resulting in the low TiO_2 film resistance and the high DSSC performance without a high temperature annealing. Fredin et. al.[28] simulation also confirms the increase of the electron diffusion coefficient and the photocurrent upon the reduction of the TiO_2 film porosity. Hence, the compression technique should be a suitable approach in depositing TiO_2 film on the conductive plastic substrate. The free polymer TiO_2 slurry, consisted of 5 g TiO_2 (P25) in 20 ml isopropanol, is pasted on the conductive plastic and pressed by the hydraulic pressure at the pressure ~510 MPa.

Figure 6(a) and 6(b) show the optical images of the un-pressed and pressed TiO_2 films, respectively. It observes that the pressed TiO_2 film is clearer than the un-pressed film, which is contributed to the denser of TiO_2 nanoparticles. The top and cross-section morphologies of the pressed TiO_2 films are shown in Fig. 6(c) and 6(d), respectively. The thickness of the pressed TiO_2 film estimated from the cross-section SEM is ~1.6 μm. It is worth mentioning that with too much TiO_2 slurry pasted on the

plastic surface, the TiO_2 film is not well adhered to the plastic, and it is easily peeled of the substrate after the compression. With an appropriate amount of TiO_2 slurry pasted on the plastic substrate, the pressed TiO_2 film is well attached to the plastic surface.

The amount of dye loaded on the pressed films is analyzed by UV-visible spectrometer, and the result is presented in Fig. 3(b). Three absorbance spectra show the close absorbance value; meaning that the thickness of three TiO_2/ITO/PEN samples are about the same. Hence, with a carefully paste, the consistence TiO_2 thickness is possible coated on the plastic. Note that the solution volume in desorbing dye of the TiO_2/ITO/PEN films is 5 ml, which is a half of a volume of the TiO_2/FTO films (10 ml). Thus, the absorbance spectra in Fig. 3(a) and 3(b) cannot be directly compared. By using equations (1) and (2), and $\varepsilon_{300} = 5.7\times10^4\ M^{-1}cm^{-1}$, the average amount of dye coated on the pressed TiO_2/ITO/PEN films is $\sim 5.69 \times 10^{-8} \pm 0.41 \times 10^{-8}$ mol/cm^2. As expected, the amount of dye loaded on the TiO_2/ITO/PEN films is much less than the TiO_2/FTO films by ~46% because of the thinner TiO_2 film. In case of the MWCNT/ITO/PEN films, there are prepared by same method as the MWCNT/FTO films. The carbon film morphologies are characterized and shown in Fig. 7. Interestingly, the low magnification images of the non-modified and modified carbon nanotube films, Fig. 7(a) and 7(c), display the very different structures. The modified CNTs are well spread on the ITO/PEN surface, whereas the non-modified CNTs form the island-like structures on the ITO/PEN surface. The well depositing of the modified CNTs on the ITO/PEN surface should be attributed to the strong interaction between the functional groups of the nanotube surface and the ITO/PEN surface [29-30].

The performance of the flexible DSSCs, using dye/pressed-TiO_2/ITO/PEN film as the working electrode and MWCNT/ITO/PEN film as the counter electrode, are tested, and the result is shown in Fig. 4(b). J_{sc}, V_{oc}, FF and η are analyzed and summarized in Table 1. Similar trend to the glass solar cell is observed as the efficiency of the Pt cell is larger than the CNT cells. This further supports the better catalytic activity of the Pt film over the carbon film. The efficiency of the flexible solar cells is lower than the glass DSSCs for all three counter electrodes. Three reasonable factors in limiting the flexible DSSC performance are: 1) the higher sheet resistance of the conductive plastic (60 Ω/sq) than the conductive glass (15 Ω/sq), 2) the thinner TiO_2/ITO/PEN film (~1.6 μm) than the TiO_2/FTO film (~5.5 μm, transparent layer) and 3) the less amount of dye adsorbed on the TiO_2/ITO/PEN film (~5.69×10^{-8} mol/cm^2) than the TiO_2/FTO film (~10.50×10^{-8} mol/cm^2).

The efficiency of the modified carbon nanotube flexible DSSC (~1.79%) is higher than the non-modified carbon nanotube flexible DSSC (~0.80%). To identify the factors in strengthening the modified carbon performance, the cyclic voltammogram is conducted and the result is shown in Fig. 5(b). The voltammogram curves present the larger current density of the modified carbon films than the non-modified nanotube films. The Pt film yields the lower voltammogram curve than the carbon films even though it produces the highest conversion efficiency. This could be explained by the excellent charge storage characteristic of the carbon nanotubes inducing ions storing at the electrode surface rather than the redox reaction. Two oxidation peaks and two reduction peaks are detected on the Pt/ITO/PEN curve at 0.47 V and 0.85 V, and -0.06 V and 0.50 V, respectively. The modified and non-modified carbon nanotube films have no clear oxidation and reduction peaks, as seen in Fig. 5(b). The current density of the non-modified CNT films is detained by two

reasons: 1) a low amount of carbon nanotubes coated on the ITO/PEN substrate and 2) no carboxylic groups formed on the MWCNT surface. The low amount of MWCNTs coated on the plastic substrate should be the main issue attenuating the oxidation/reduction current and the cell performance of the non-modified CNT films. Hence, the presence of the functional groups promotes the flexible DSSC performance through increasing the adhesion strength between nanotubes and indium tin oxide.

4. Conclusion:

The low temperature carbon nanotube film coated on the conductive glass and the conductive plastic substrates are able to use as the DSSC counter electrode. The efficiency of the modified carbon nanotube DSSCs is larger than the non-modified carbon nanotube DSSCs for both glass and plastic substrates. This is because the modified carbon nanotubes are surrounded by the active carboxylic groups and the better deposited on the substrates. The modified carbon nanotubes are well coated on the ITO/PEN surface, whereas the non-modified carbon nanotubes form island-like structure on the ITO/PEN surface. The efficiency of the modified carbon nanotube glass and plastic solar cells are ~3.46% and ~1.79%, respectively.

Acknowledgement:

Authors would like to thank Narapond Munmee for helping with the lab work and associate professor Werasak Surareungchai for the Autolab system. This work is supported by Thai Research Fund (TRF, grant number MRG5080226), Center of Excellence in Physics, and the Integrated Nanotechnology Research Center (INRC), Khon Kaen University.

Reference:

[1] O'Regan B, Grätzel M. A low-cost, high-efficiency solar cell based on dye-sensitized colloidal TiO_2 films, Nature 1991; 353: 737-40.

[2] Grätzel M. Conversion of sunlight to electric power by nanocrystalline dye-sensitized solar cells, J. Photochem. Photobiol. A 2004; 164(1-3): 3-14.

[3] Tennakone K, Kumara G.R.R, Kottegoda I.R.M, Perera V.S.P. An efficient dye-sensitized photoelectrochemical solar cell made from oxides of tin and zinc, Chem. Commun. 1999; 1(1): 15-6.

[4] Sayama K, Sugihara H, Arakawa H. Photoelectrochemical Properties of a Porous Nb_2O_5 Electrode Sensitized by a Ruthenium Dye, Chem. Mater. 1998; 10(12): 3825-32.

[5] Fukai Y, Kondo Y, Mori S, Suzuki E. Highly efficient dye-sensitized SnO_2 solar cells having sufficient electron diffusion length, Electrochem. Commun. 2007; 9(7): 1439-43.

[6] Kay A, Grätzel M. Low cost photovoltaic modules based on dye sensitized nanocrystalline titanium dioxide and carbon powder , Sol. Energy. Mater. Sol. Cell 1996; 44(1): 99-117.

[7] Imoto K, Takahashi K, Yamaguchi T, Komura T, Nakamura J, Murata K. High-performance carbon counter electrode for dye-sensitized solar cells, Sol. Energy Mater. Sol. Cell 2003; 79(4): 459-69.

[8] Murakami T.N, Grätzel M. Counter electrodes for DSC: Application of functional materials as catalysts, Inorg. Chim. Acta 2008; 361(3): 572-80.

[9] Suzuki K, Yamamoto M, Kumagai M, Yanagida S. Application of Carbon Nanotubes to Counter Electrodes of Dye-sensitized Solar Cells, Chem. Lett. 2003; 32(1): 28-9.

[10] Balraju P, Kumar M, Roy M.S, Sharma G.D. Dye sensitized solar cells (DSSCs) based on modified iron phthalocyanine nanostructured TiO_2 electrode and PEDOT:PSS counter electrode, Synthetic Met. 2009; 159(13): 1325–31.

[11] Yang S, Li X, Zhu W, Wang J, Descorme C. Catalytic activity, stability and structure of multi-walled carbon nanotubes in the wet air oxidation of phenol, Carbon 2008; 46(3): 445-52.

[12] Yang S, Zhu W, Li X, Wang J, Zhou Y. Multi-walled carbon nanotubes (MWNTs) as an efficient catalyst for catalytic wet air oxidation of phenol, Catal. Commun. 2007; 8(12): 2059–63.

[13] Lu C, Su F, Hu S. Surface modification of carbon nanotubes for enhancing BTEX adsorption from aqueous solutions, Appl. Surf. Sci. 2008; 254(21): 7035–41.

[14] Kuan H.C, Ma C.C.M, Chang W.P, Yuen S.M, Wu H.H, Lee T.M. Synthesis, thermal, mechanical and rheological properties of multiwall carbon nanotube/waterborne polyurethane nanocomposite, Compos. Sci. Technol. 2005; 65(11-12): 1703–10.

[15] Chen W, Tao X, Xue P, Cheng X. Enhanced mechanical properties and morphological characterizations of poly(vinyl alcohol)–carbon nanotube composite films, Appl. Surf. Sci. 2005; 252(5): 1404–9.

[16] Dhand C, Arya S.K, Singh S.P, Singh B.P, Datta M, Malhotra B.D. Preparation of polyaniline/multiwalled carbon nanotube composite by novel electrophoretic route, Carbon 2008; 46(13): 1727-35.

[17] Boccaccini A.R, Cho J, Roether J.A, Thomas B.J.C, Minay E.J, Shaffer M.S.P. Electrophoretic deposition of carbon nanotubes, Carbon 2006; 44(15): 3149–60.

[18] Gohel A, Chin K.C, Lim K.Y, Tay S.T, Liu R, Chen G.S, et al. Selective area growth of aligned carbon nanotubes by ion beam surface modification, Chem. Phys. Lett 2003; 371 (1-2): 131–5.

[19] Dong B, He B.L, Li H.L. Preparation and electrochemical characterization of polyaniline/multi-walled carbon nanotubes composites for supercapacitor, Mat. Sci. Eng. B 2007; 143(1-3): 7-13.

[20] Gupta V, Miura N. Polyaniline/single-wall carbon nanotube (PANI/SWCNT) composites for high performance supercapacitors, Electrochim. Acta 2006; 52 (4): 1721-6.

[21] Huang Z, Liu X, Li K, Li D, Luo Y, Li H, et al. Application of carbon materials as counter electrodes of dye-sensitized solar cells, Electrochem. Commun 2007; 9(4): 596-8.

[22] Li P, Wu J, Lin J, Huang M, Huang Y, Li Q. High-performance and low platinum loading Pt/Carbon black counter electrode for dye-sensitized solar cells, Sol. Energy 2009; 83(6) : 845-9.

[23] Frackowiaka E, Béguin F. Electrochemical storage of energy in carbon nanotubes and nanostructured carbons, Carbon 2002; 40(10): 1775–87.

[24] Zhang J, Kong L.B, Wang B, Luo Y.C, Kang L. In-situ electrochemical polymerization of multi-walled carbon nanotube/polyaniline composite films for electrochemical supercapacitors, Synthetic Met. 2009; 159(3-4): 260–6.

[25] Pandolfo A.G, Hollenkamp A.F. Carbon properties and their role in supercapacitors, J. Power Sources 2006; 157(1): 11–27.

[26] Grinis L, Dor S, Ofir A, Zaban A. Electrophoretic deposition and compression of titania nanoparticle films for dye-sensitized solar cells, J. Photochem. Photobiol. A 2008; 198(1): 52-9.

[27] Yamaguchi T, Tobe N, Matsumoto D, Nagai T, Arakawa H, Sol. Energy Mater. Sol. Cell 2010; doi:10.1016/j.solmat.2009.12.029.

[28] Fredin K, Nissfolk J, Hagfeldt A. Brownian dynamics simulations of electrons and ions in mesoporous films, Sol. Energy. Mater. Sol. Cell 2005; 86(2): 283-97.

[29] Oh S.J, Cheng Y, Zhang J, Shimoda H, Zhou O. Room-temperature fabrication of high-resolution carbon nanotube field-emission cathodes by self-assembly, Appl. Phys. Lett. 2003; 82(15): 2521-3.

[30] Shimoda H, Oh S.J, Geng H.Z, Walker R.J, Zhang X.B, McNeil L.E, et. al. Self-assembly of carbon nanotubes, Adv. Mater. 2002; 14(12): 899-901.

Table captions:

Table 1: Summary of the open-circuit (V_{oc}), short-circuit (J_{sc}), fill-factor (FF) and efficiency (η) of the DSSCs as using the Pt, non-modified and modified carbon nanotube films as the counter electrode.

Figure captions:

Fig. 1: (a) The top and (b) the cross-section SEM images of TiO_2/FTO film.

Fig. 2: (a) The low and (b) the high magnification SEM images of the non-modified carbon nanotube film coated on the conductive glass (N-CNT/FTO). (c) The low and (d) the high magnification SEM images of the modified carbon nanotube film coated on the conductive glass (M-CNT/FTO).

Fig. 3: The absorbance spectra of the desorbed dye solutions of (a) the TiO_2/FTO films in the 10 ml of 0.1 M NaOH and ethanol at volume ratio of 1:1 and (b) the pressed TiO_2/ITO/PEN films in the 5 ml of 0.1 M NaOH and ethanol at volume ratio of 1:1.

Fig. 4: Plot of the photocurrent density (J) versus the photovoltage (V) of (a) the Pt/FTO, non-modified (N-CNT/FTO) and modified carbon nanotube (M-CNT/FTO) glass DSSCs, and (b) the Pt/ITO/PEN, non-modified (N-CNT/ITO/PEN) and modified carbon nanotube (M-CNT/ITO/PEN) flexible DSSCs.

Fig. 5: The cyclic voltammograms of (a) the FTO, Pt/FTO, N-CNT/FTO and M-CNT/FTO and (b) the ITO/PEN, Pt/ITO/PEN, N-CNT/ITO/PEN and M-CNT/ITO/PEN in the acetonitrile solution of 10 mM LiI, 1 mM I_2 and 0.1 M $LiClO_4$ at the scan rate of 20 mV/s.

Fig. 6: The optical image of (a) the un-pressed TiO_2/ITO/PEN film and (b) the pressed TiO_2/ITO/PEN film. (c) The top and (d) the cross-section SEM images of the pressed TiO_2/ITO/PEN film.

Fig. 7: (a) The low and (b) the high magnification SEM images of the non-modified MWCNT/ITO/PEN film. (c) The low and (d) the high magnification SEM images of the modified MWCNT/ITO/PEN film.

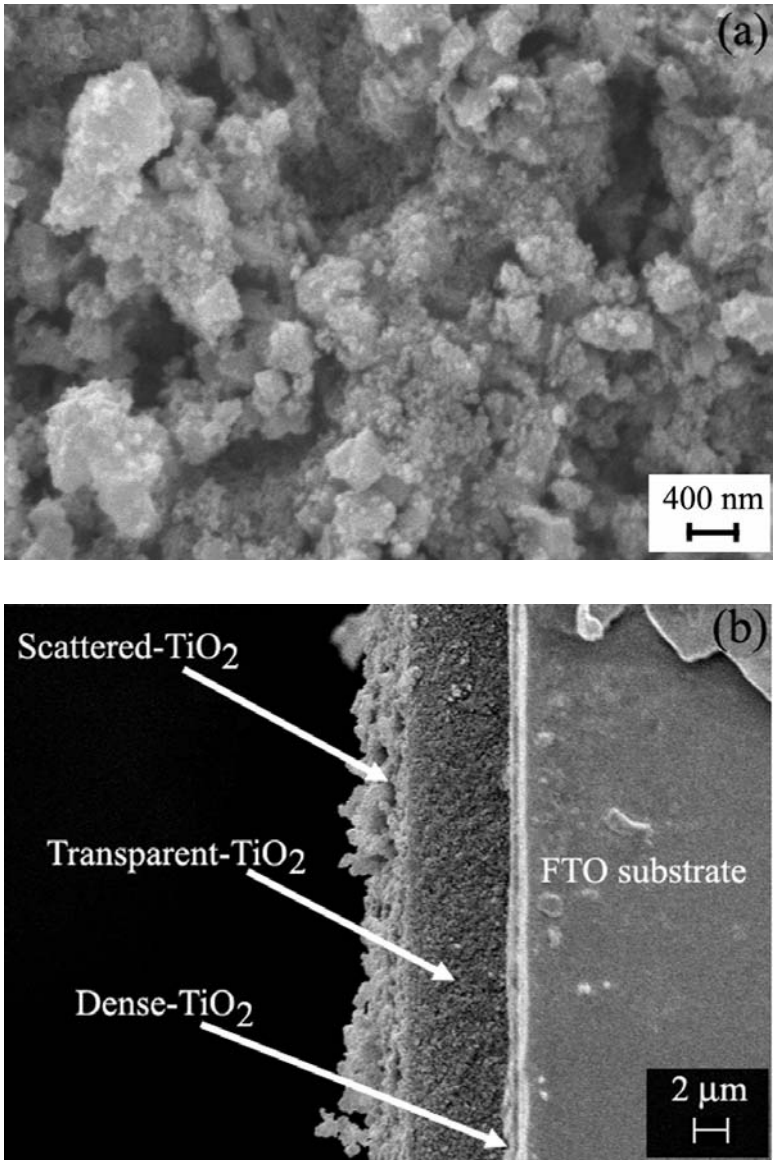

Fig. 1: Wasan Maiaugree et. al.

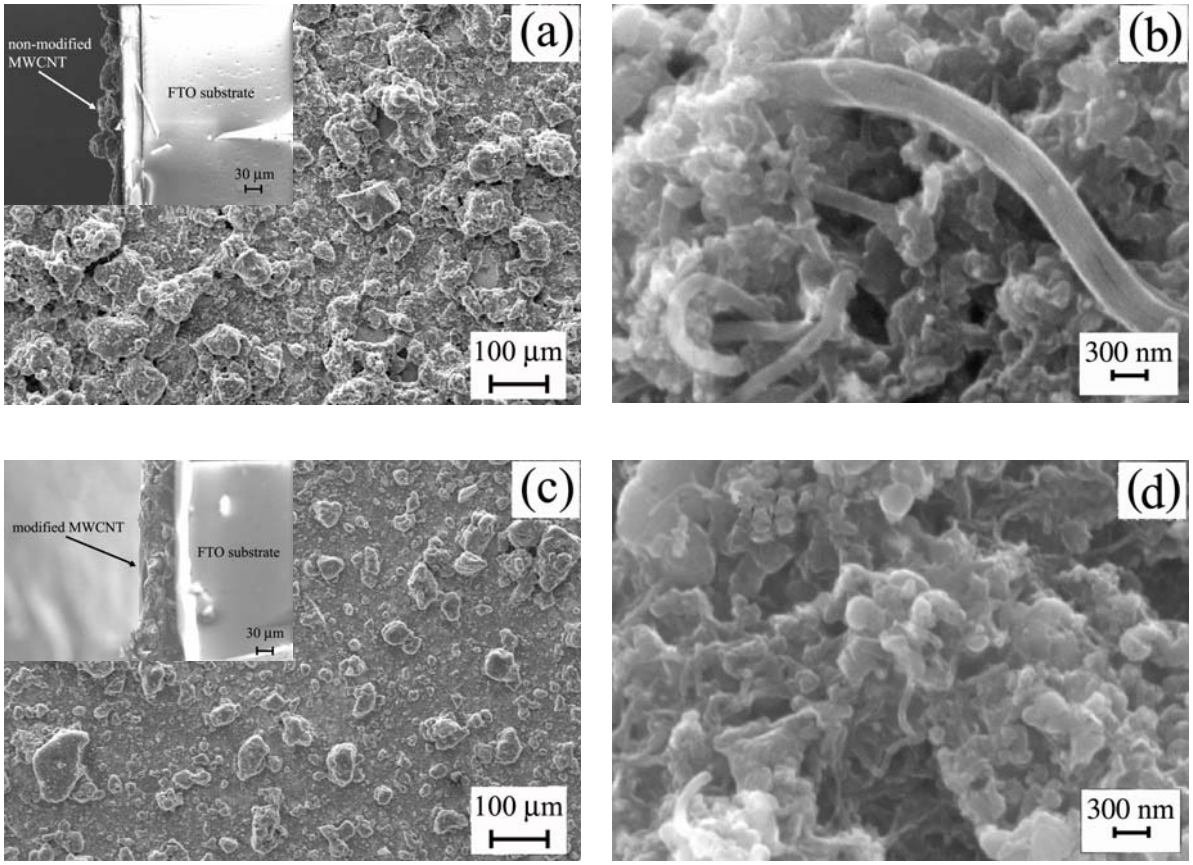

Fig. 2: Wasan Maiaugree et. al. .

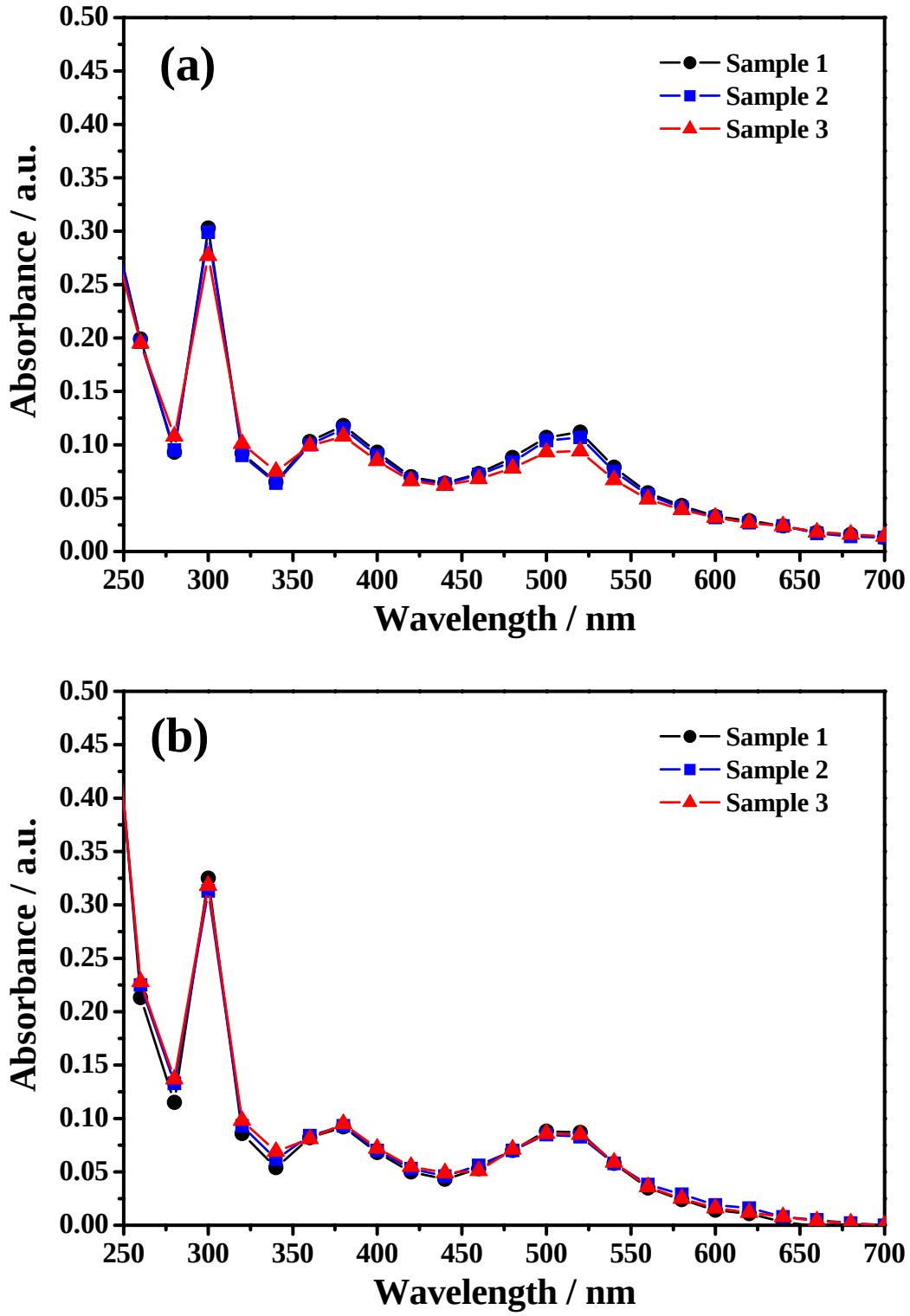

Fig. 3: Wasan Maiaugree et. al.

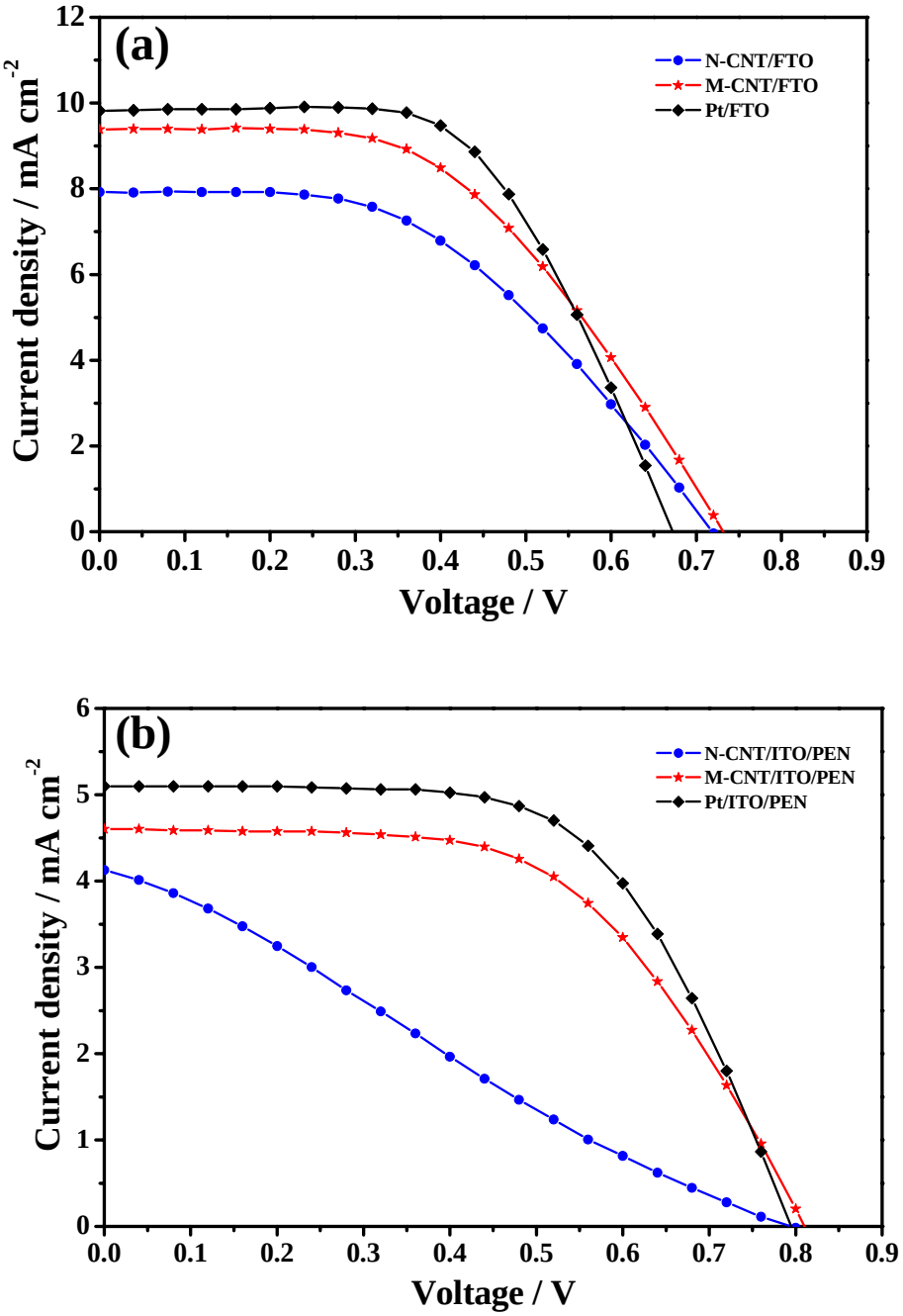

Fig. 4: Wasan Maiaugree et. al.

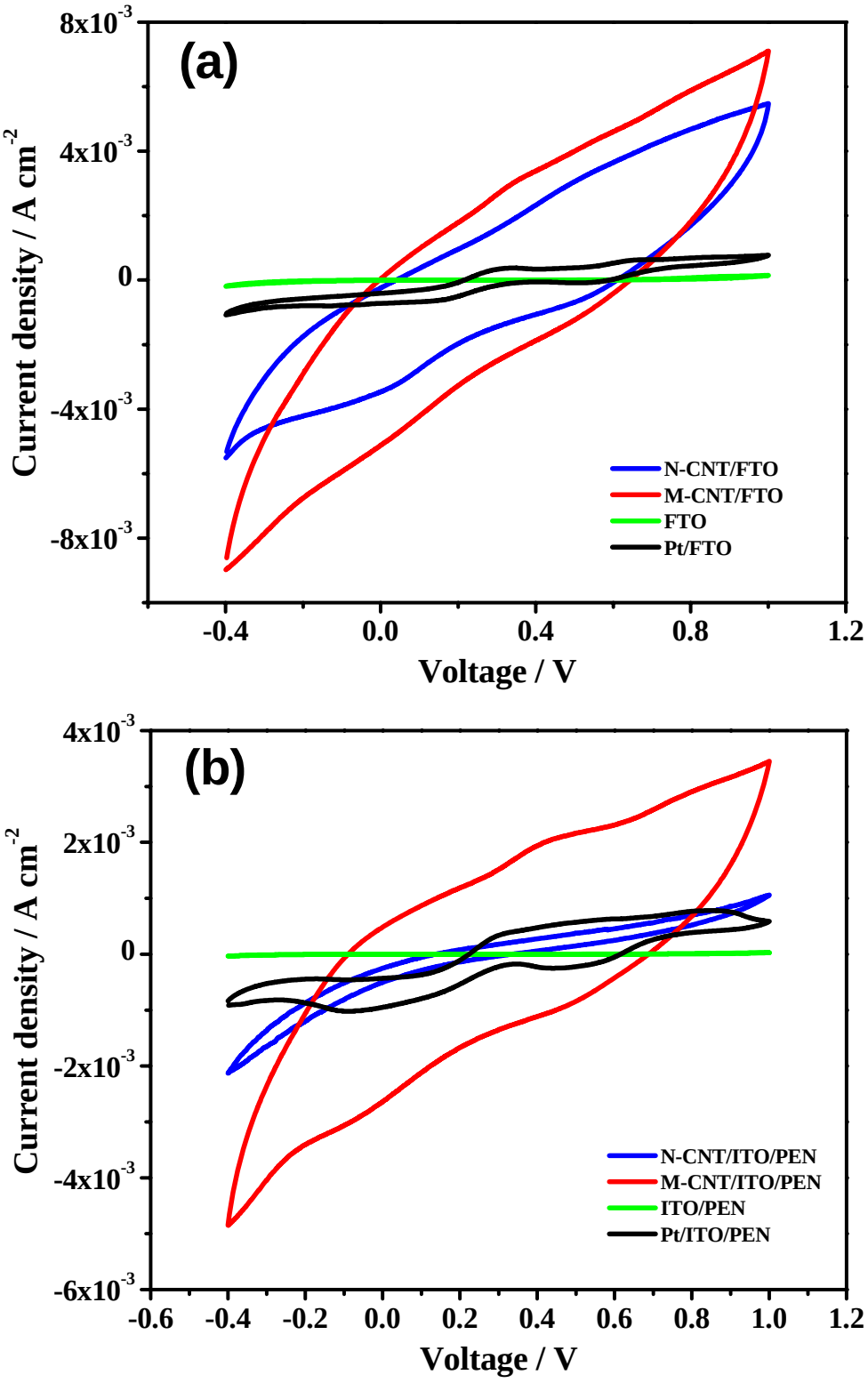

Fig. 5: Wasan Maiaugree et. al.

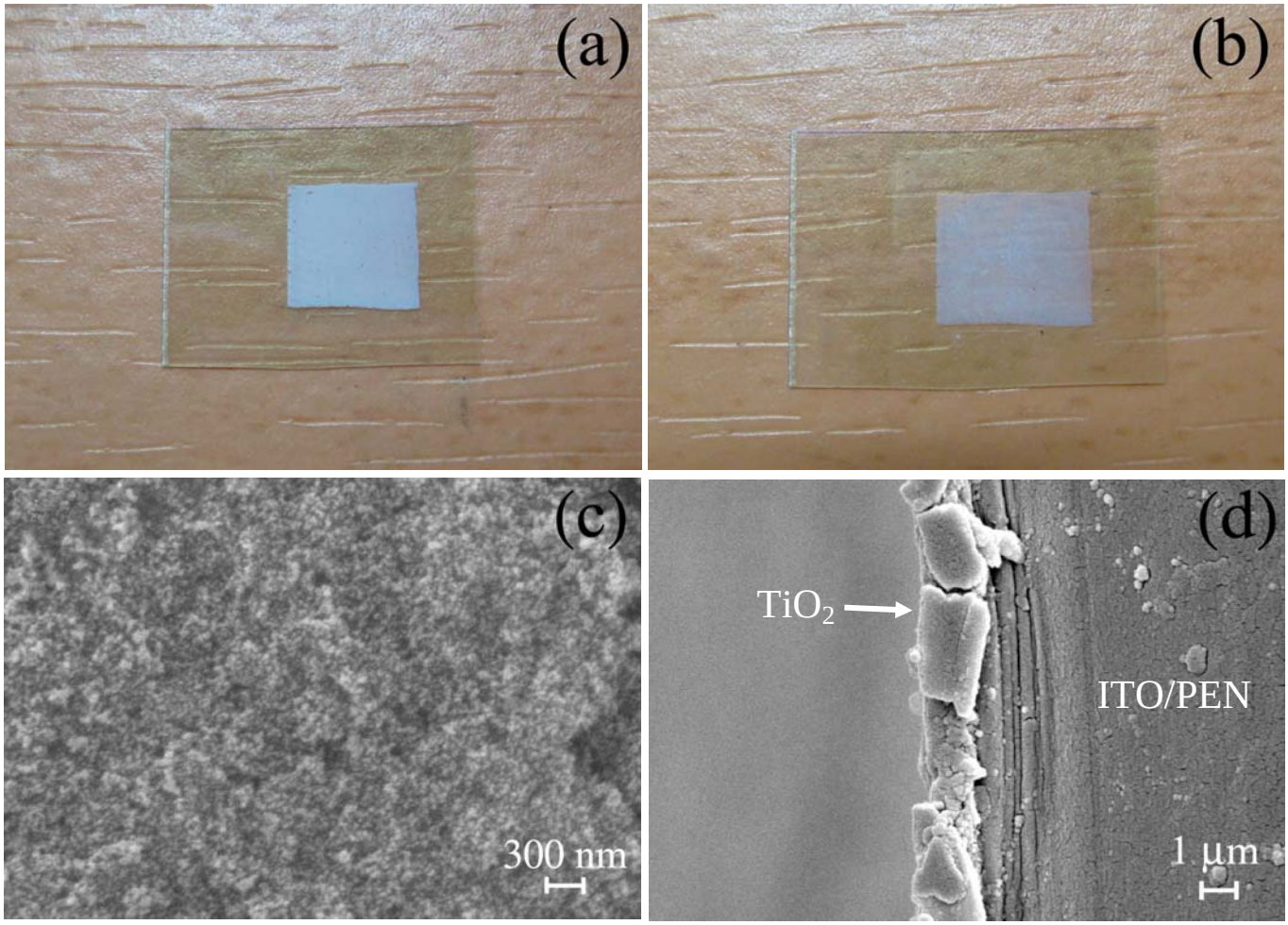

Fig. 6: Wasan Maiaugree et. al.

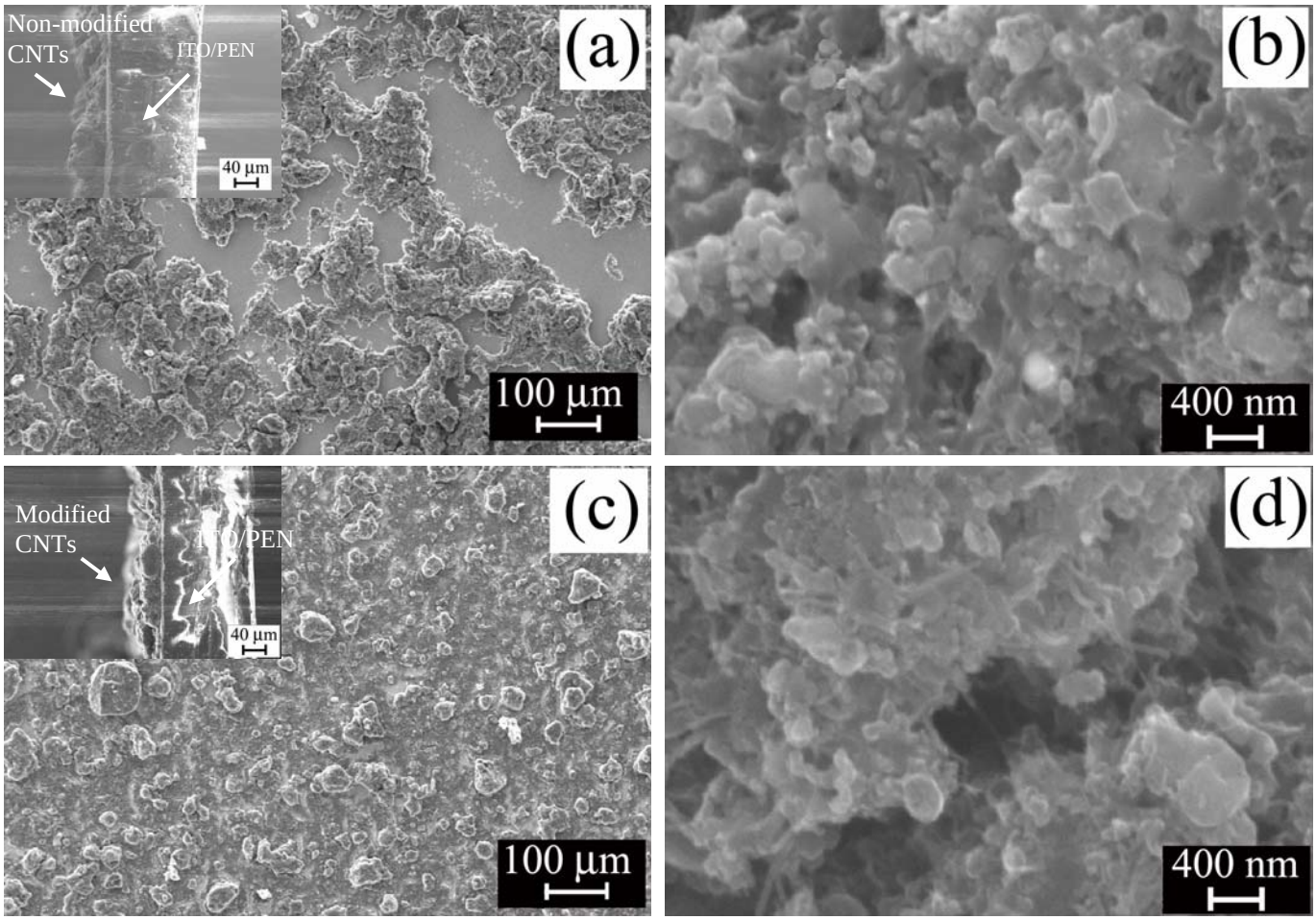

Fig. 7: Wasan Maiaugree et. al.